ASSESSMENT OF IMPACTS OF LAND USE AND LAND COVER CHANGES ON RUNOFF IN THE LUVUVHU CATCHMENT AREA

A thesis submitted to the University of the Western Cape in the fulfilment of the degree of Master of Science

By:

MABUDA MPHO OSCAR

Department of Earth Sciences

Faculty of Natural Sciences

Supervisor

Prof D. Mazvimavi

Co-supervisor

Prof T. Dube

JUNE 2023

ABSTRACT

This study aims to assess the impacts of land use and land cover (LULC) changes on runoff in the Luvuvhu catchment in Limpopo, South Africa. To achieve this aim, the study had two specific objectives. The first objective was to determine past and future spatial trends of LULC change, using remote sensing data. To determine the past spatial trends of LULC, Landsat images from 1990 to 2020 were classified using the Support Vector Machine (SVM). The results revealed that there were significant LULC changes in the Luvuvhu catchment during the selected study period. The results of the LULC classification showed that built-up area increased by 4.8% from 1990 to 2020. Plantation and natural vegetation decreased by 0.3% and 18.9%, respectively. Bare land and waterbodies increased by 15.2% and 0.4%, respectively. Agricultural land decreased from 4.7% to 3.5%. The classification results showed high overall accuracies (93% to 98%) and Kappa coefficients (>0.9). These results showed good classification. The artificial neural networks-cellular automata (ANN-CA) based simulation model was implemented to predict future LULC in 2025 and 2030. The predicted LULC for 2025 shows that the built-up area will increase by approximately 120 km^2, plantation by 17 km^2, agricultural land by 51 km^2 and bare land by 168 km^2. Natural vegetation may lose up to 356 km^2 in 2025. Meanwhile, a waterbody may lose close to 2 km^2 by 2025. The trends observed in 2025 are expected to continue until the year 2030. The second objective was to establish the response of runoff to LULC changes, using a process-based semi-distributed approach. The study adopted the Soil and Water Assessment Tool (SWAT) model for the simulation of the hydrological response of the Luvuvhu catchment. The calibration and validation for monthly flow between the observed and simulated data showed a good relationship. Model performance for the calibration and validation for both the 1990 LULC and 2020 LULC period show satisfactory results. On average, overall surface runoff increased by 7.3% from 169.14 mm to 181.49 mm between 1990 and 2020. The results show that the surface runoff of the Luvuvhu catchment was altered due to the significant LULC changes in bare land and natural vegetation with a 15.2% increase and an 18.9% decrease, respectively. Therefore, these changes contributed significantly to the runoff response of the Luvuvhu catchment. This study provides baseline information on the impacts of LULC changes on surface runoff within the Luvuvhu catchment in Limpopo, South Africa.

Keywords: Hydrological modelling; LULC changes; Luvuvhu catchment; Remote sensing; Support vector machine; Surface runoff; SWAT model; SWAT-CUP.

Table of Contents

LIST OF FIGURES

LIST OF TABLES

ABBREVIATIONS

ANN	Artificial Neural Networks
ARC	Agricultural Research Council
CA	Cellular Automata
CE	Commission Error
CVA	Change vector analysis
DEM	Digital Elevation Model
DWA	Department of Water and Affairs
DWS	Department of Water and Sanitation
FAO	Food and Agriculture Organisation
GIS	Geographic Information Systems
HRUs	Hydrological Response Units
JMD	Jeffries-Matusita Distance
LH	Latin Hypercube
LR	Logistic Regression
LULC	Land Use Land Cover
MC	Markov Chain
MCE	Multi-criteria Evaluation
ML	Maximum Likelihood
MLP	Multi-Layer Perception
MOLUSCE	Modules of Land Use Change Evaluation
NSE	Nash-Sutcliffe efficiency
OA	Overall Accuracy
OE	Omission Error

PA	Producer's Accuracy
PBIAS	Percentage Bias
ROIs	Regions of Interest
SRTM	Shuttle Radar Topography Mission
SUFI-2	Sequential Uncertainty Fitting
SVM	Support Vector Machine
SWAT	Soil and Water Assessment Tool
SWAT-CUP	SWAT Calibration Uncertainty Procedure
TCC	True Colour Composite
TD	Transformed Divergence
TOPMODEL	Topography-based hydrological model
UA	User's Accuracy
USGS	United States Geological Survey
UTM	Universal Transverse Mercator
WGS	World Geodetic System
WoE	Weights of Evidence

DECLARATION

I, Mabuda Mpho Oscar, declare that this full dissertation, entitled '**Assessment of impacts of land use and land cover changes on runoff in the Luvuvhu catchment area'** is my own work, and has not been submitted before for any degree or examination at any other university. Complete references indicate and acknowledge all the sources used or quoted in this full dissertation.

Full names: Mabuda Mpho Oscar

Signature: …….. Date: …….

ACKNOWLEDGEMENTS

First, I would like to thank the Lord Almighty in whom I believe for the guidance, protection, and wisdom he has given me in all the days of my life. Grateful for his love, grace, and mercy for guiding me through this academic journey.

Secondly, I would like to thank my Supervisor Prof. D. Mazvimavi and my Co-supervisor Prof. T. Dube for the best supervision, guidance, and encouragement. Their tireless efforts and willingness to extract the finest for this thesis are highly appreciated. Through their supervision, I have learnt several things, and among them, the most important is to be critical and independent.

I want to express my sincere appreciation to the National Research Foundation (NRF) for the financial support for my entire study.

Furthermore, I am grateful to the Agricultural Research Council (ARC) for providing the meteorological data, which was important during the analysis.

I would also like to express my deepest gratitude to Miss Netshikulwe Khuliso who supported me emotionally, socially, and academically. Thank you for all the time you invested in advising and assisting me, without your efforts, I would not be this far.

To Nkosi Mary, thank you for introducing me to SWAT modelling and teaching me everything related to it. Your dedication during the time of modelling was priceless, I appreciate the time and effort you committed.

I also extend my gratitude to Mr Musumuvhi Ndamulelo who enlightened me in various aspects of remote sensing your guidance cannot be left unmentioned.

Finally, I want to thank my entire family: my mother, Ms Naledzani Mercy Tomane, my grandparents Mr and Mrs Tomane, my sister Zwoluga Mangalani Tomane and Mr Nemasetoni for the profound love, support, and encouragement they showed during this academic journey.

DEDICATION

This thesis is dedicated to my mother Ms Naledzani Mercy Tomane, the late Mrs Netshikulwe L.B, my sister Mangalani Zwoluga Tomane and the entire Tomane family.

Jeremiah 29:11

"For I know the plans I have for you, plans to prosper you and not harm you, plans to give you hope and future".

CHAPTER 1: INTRODUCTION

1.1 Background of the study

The Earth provides humans with everything they require to survive; as a result, humans modify and use the land to meet their daily needs. Land use and land cover (LULC) change is a key factor that affects the Earth's system (Lambin et al., 2001). The evolving human population, climate change and natural occurrences drive successive LULC changes. LULC changes occur to primarily support the increasing human population (Getahun & Haj, 2015; Yadav, 2019). Agriculture and urbanisation are the most destructive anthropogenic activities for biodiversity (Gessesse et al., 2014; Affessa et al., 2022). The increasing need for food, water, fuel, fibre, and shelter for the growing population causes the expansion and intensification of agricultural and urban activities (Griscom et al., 2009; Warburton et al., 2012). The land cover reflects ecological and hydrological processes within a catchment. Therefore, changes in a catchment will significantly affect the hydrological and terrestrial ecosystems of that area (Maviza & Ahmed, 2020).

Anthropogenic activities affect the ecological and hydrological cycle by changing the physical structure of the landscape and water fluxes (Turner et al., 2003). Furthermore, LULC changes affect the water cycle by changing the magnitude and timing of runoff (Sterling et al., 2012), due to changes in evapotranspiration, infiltration, and the rate of runoff generation (Guo et al., 2020; Anand et al., 2018). Similarly, Peng & Wang (2012) stated that LULC changes and rainfall patterns affect the intensity and frequency of surface runoff. Factors such as rainfall intensity, slope steepness and change of energy influence runoff generation (Gessesse et al., 2014; Ozdemir and Elbas, 2014). The increase in surface runoff often leads to flooding and increased annual discharge (Ntanganedzeni & Nobert, 2020). Therefore, understanding the relationship that exists between LULC changes, hydrologic processes, and the hydrological response of catchments, for better land use planning and management of catchments is crucial.

Hydrological modelling has become popular for assessing LULC change (Devia et al., 2015; Sidle, 2021). Previous studies that assessed how LULC change affected the hydrological response in the Luvuvhu catchment have reported comparable results although they used different hydrological modelling approaches. These studies show an increase in peak discharges in the Luvuvhu catchment due to deforestation (Warburton et al., 2012; Mathivha et al., 2016; Thavhana et al., 2018). While different studies investigated the impacts of LULC

change, it is quite important to investigate potential future impacts. Further investigations of these impacts of land cover will aid in land restoration.

The assessment of LULC change in catchment hydrology requires remote sensing and geographic information systems (GIS). The importance of remote sensing has been emphasized in previous studies (Jewitt et al., 2004; Griscom et al., 2009; Warburton et al., 2012; Zhang et al., 2014; Mathivha et al., 2016). Remotely sensed and GIS data provide the spatial and temporal information needed for modelling (Dwarakish & Ganasri, 2015). Different modelling approaches are used based on the size, type, and rate of LULC change in the study area (Dwarakish & Ganasri, 2015; Sidle, 2021). The selection of the hydrological modelling approach requires knowledge of the catchment. This study incorporates the use of remotely sensed data and the physical-conceptual semi-distributed modelling approach to examine runoff response due to LULC change in the Luvuvhu catchment.

1.2 Problem Statement

Population growth in South Africa raises a cause for concern about the sustainability of the environment and pressure tolerance capacity of various catchments. The South African population increased from 44.8 million to 55.6 million from 2011 to 2016 and the estimates show persisting growth of up to 60.6 million in 2022 (Statistics South Africa, 2022). However, population growth is a worldwide crisis. The removal of natural vegetation cover to accommodate the growing population leads to sedimentation and increased discharge (Xu et al., 2013). The impacts of increased runoff include flooding of surrounding areas (Ntanganedzeni and Nobert, 2020), while increased velocities in surface runoff may lead to erosion of riverbanks or stream channels due to high peak flow rate (Mazibuko et al., 2021). The potential impacts of LULC change on hydrological processes in the Luvuvhu catchment were established by Mathivha et al. (2016), using an empirical hydrological modelling approach and a few selected storm events. Although numerous studies have been conducted on LULC change in the Luvuvhu catchment, there have been limited SWAT-based hydrological studies that quantify the runoff response of different LULC scenarios. Therefore, evaluating the impacts of LULC change using a larger number of rainfall data and a physically-based hydrological modelling approach for different LULC periods is still imperative. Furthermore, previous studies that assessed the impacts of LULC change on runoff did not consider the heterogeneity of the catchment characteristics. Therefore, this study will give a holistic view of the extent of LULC change and its implications on runoff in the Luvuvhu catchment. This

approach establishes the impacts of LULC change on surface runoff at catchment scales using parameters related to the physical catchment properties. In addition, given the advancement in LULC modelling and prediction approaches, and the continuous development in the catchment it is important to measure and monitor LULC changes for better accuracy and management. Therefore, further evaluation of the spatial distribution of LULC change and its impacts on surface runoff is necessary to track LULC changes and their implication on runoff response in the catchment.

1.3 Objectives of the study

This study aims to assess the impacts of LULC changes on runoff in the Luvuvhu catchment in Limpopo, South Africa.

1.3.1 Specific objectives:

i. To determine past and future spatial trends of LULC change.
ii. To establish the response of runoff to LULC changes.

1.4 Research questions

i. What has been the spatial distribution of LULC change in the Luvuvhu catchment?
ii. What are the potential LULC change patterns of Luvuvhu catchment in the near future?
iii. What are the effects of LULC change on runoff in the Luvuvhu catchment?

1.5 Research outline

Chapter 1: This chapter introduces the study and outlines the problem statement. In addition, this presents research questions, the main aim, and the objectives of the study. Lastly, the chapter provides an outline of the thesis layout of the study.

Chapter 2: Provides a detailed review of the driving forces of LULC change, their impacts on the ecology and hydrological processes, different LULC modelling methods, various hydrological modelling approaches, their strengths and limitations, remote sensing as a tool for LULC monitoring.

Chapter 3: Gives a brief description of the study area (location, hydrology, topography, geology, climate, and vegetation). This chapter also outlines the methods used to collect,

prepare, and analyse data to achieve the objectives of the study. It further provides information on the application of software packages used during analysis.

Chapter 4: Presents the results of LULC classifications, LULC future prediction and runoff simulations. This chapter attempts to highlight the extent of historical and potential future LULC patterns change and assess runoff response to historical LULC changes.

Chapter 5: Provides the summary of the main findings and provides recommendations for water resource managers, land use planners, policymakers and future research.

CHAPTER 2: LITERATURE REVIEW

2.1 Introduction

The terms “land use” and “land cover” are closely related concepts that are often used interchangeably; however, they have quite different meanings. Land cover refers to the physical condition of the earth’s surface that constitutes layers of soil, topography, plants, and animals (Sousa-Neto et al., 2018). Land use in contrast is the exploitation and transformation of the land surface due to human activities such as buildings, agricultural land, and pastures (Nagendra et al., 2004; Verburg et al., 2009; Sousa-Neto et al., 2018). Early research established that LULC changes result from both natural and anthropogenic activities. Increasing population, economic activities, and improved livelihoods often drive the anthropogenic activities (Ramankutty & Foley, 1999). Natural occurrences such as climate change, floods, and earthquakes may accelerate changes in land cover. Many of the environmental problems associated with LULC changes gradually affect different environmental settings including water resource quality and quantity which has become a severe problem in South Africa. Shrestha et al. (2020) outlined that land cover change may affect the natural occurrence of surface runoff. Land use change also influences atmospheric elements of the hydrological cycle such as temperature and evapotranspiration that affect the hydrology of a catchment (Takamatsu et al., 2013). LULC change monitoring is therefore essential in providing the knowledge needed for better comprehension of environmental changes and modelling of the hydrological response of catchments. This chapter aims to review the concept of the hydrological response of catchments because of LULC change. Therefore, this chapter highlights the drivers of LULC change and the impacts of LULC change on surface runoff at a local, regional, and global scale. The use of remote sensing techniques for land cover classification, as well as models used for monitoring and measuring LULC change in catchments. Different hydrological modelling approaches were also reviewed to determine the most appropriate model for runoff simulation. The evaluation of these methods aided in determining the approach used to achieve the objectives of the study.

2.2 Evaluation of driving forces of LULC Change

The examination of LULC change driving forces at local and global levels is necessary particularly in solving environmental issues such as land degradation (Munthali et al., 2019). Identifying the driving forces of LULC change enables the prediction of future LULC impacts

(Kindu et al., 2015). Evaluating the impact of LULC change on the earth's system requires past, present, and future knowledge about land use response to different driving forces (Jingan et al., 2005). Humans often respond to signals from the environment and their sociocultural framework and are inclined to improve their economic and sociocultural stance (Verburg et al., 2004). Hence, the two main categories of LULC change drivers are socioeconomic and biophysical factors (Verburg et al., 2004; Tizora et al., 2018). Biophysical factors comprise characteristics and processes occurring in the physical environment (e.g., climate variation, topography, landform, geomorphic processes etc.), while socioeconomic factors include demographic, social, economic, institutional, political factors etc. (Briassoulis, 2020). Many biophysical factors indirectly alter land cover and have an impact on how land is used (Verburg et al., 2004). However, the core drivers of LULC change vary from one point to another (Kindu et al., 2015; Munthali et al., 2019). LULC driving factors may be categorised as proximate and underlying factors (Tizora et al., 2018). Geist & Lambin (2002) established a framework for analysing the proximate and underlying causes of LULC changes (Figure 2.1). Proximate factors are human-related activities that occur on land at a local scale (e.g., individual farms, households, or communities) which directly affect forest cover (Lambin et al., 2003). There are three broad classes of proximate factors, which include infrastructure expansion, agricultural expansion, and wood extraction (Geist & Lambin, 2002) (Figure 2.1). Underlying factors are fundamental socioeconomic forces such as human population growth or agricultural practices that strengthen the proximate causes of land cover change (Lambin et al., 2003). The underlying factors comprise demographic, economic, technological, institutional and cultural factors (Geist & Lambin, 2002) (Figure 2.1). Underlying factors originate from national or global level (e.g., districts, provinces, or country) and may result from interactions between socioeconomic and biophysical variables which have indirect impacts on land cover (Geist & Lambin, 2002; Lambin et al., 2003; Tizora et al., 2018).

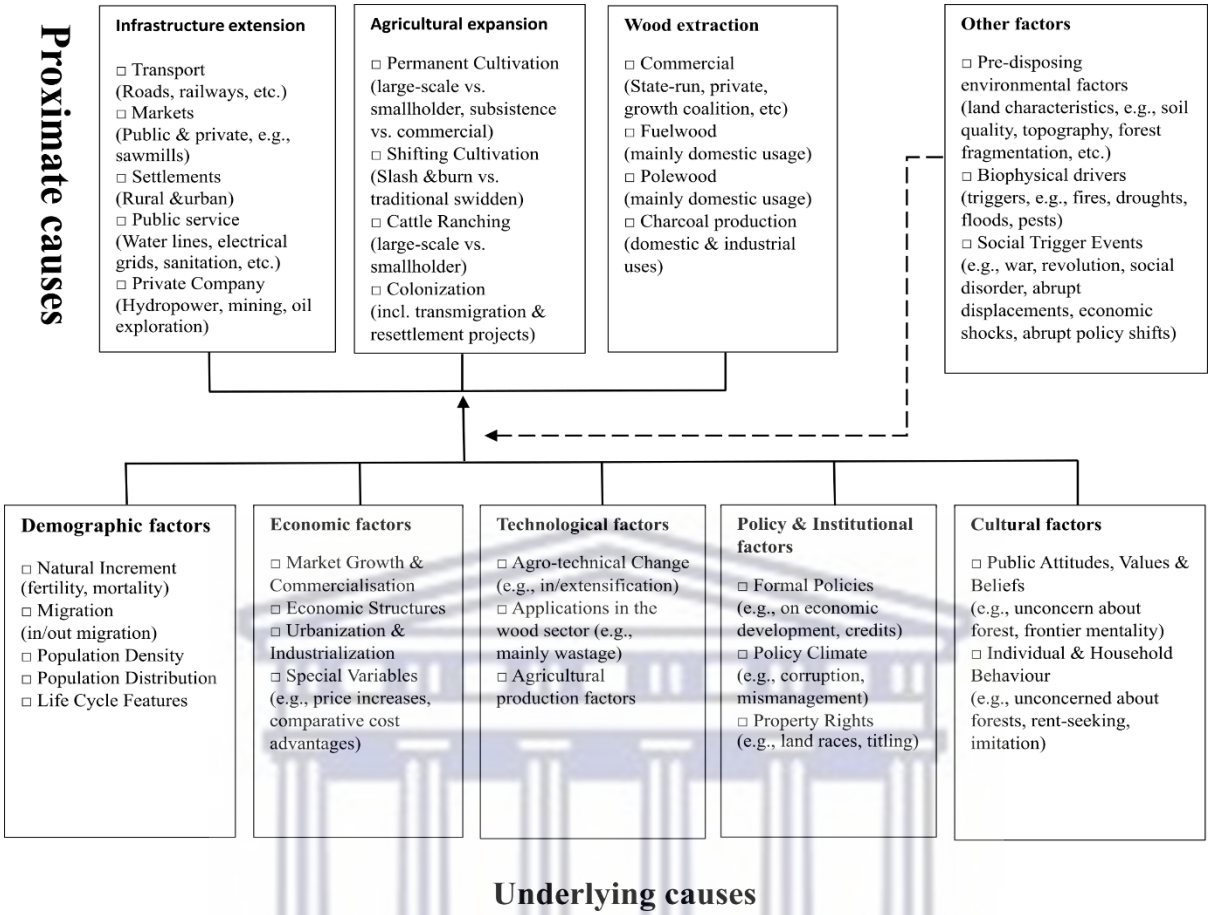

Figure 2. 1: Proximate and underlying causes of LULC change (Geist & Lambin, 2002).

Early researchers were more attentive to biophysical causes when assessing LULC change drivers and neglected the interaction between socioeconomic and environmental factors (Lo & Yang, 2002). The lack of spatially explicit data and methodologies caused the negligence in linking the biophysical and social data (Veldkamp & Lambin 2001; Jingan et al., 2005). Modern research has started to integrate both biophysical and socioeconomic data for LULC assessment (Sohl & Sleeter, 2012). However, acquiring information about LULC change for the integration of these drivers is challenging due to the varying spatial scales of biophysical processes and socioeconomic decision-making (Lo & Yang, 2002). Most integration models are specific to a particular type of land use at a certain scale and do not consider the entire land system (Dang & Kawasaki, 2017). For example, the International Institute for Applied Systems Land Use Change (IIASA-LU), the International Model for Policy Analysis of Agricultural Commodities and Trade (IMPACT), and the Integrated Model to Assess the Global Environment (IMAGE) are specific to agriculture at national or global scales (Dang & Kawasaki, 2017). LULC drivers are still the subject of contentious debate; therefore, there is still a need for further research about the LULC drivers at local, regional, and global scales.

2.3 Ecological response to LULC change

LULC changes have significant effects on the earth's system (Lambin et al., 2001). This study focuses on LULC change effects on the hydrological response of the Luvuvhu catchment. Although LULC change contributes significantly to economic growth and has many social benefits, its adverse effects on environmental quality, productivity and biodiversity cannot be ignored (Wang et al., 2014). Lambin et al. (2001) stated that LULC change has direct impacts on soil degradation, local climate, and global warming. Furthermore, LULC change alters ecological systems and their ability to support human and animal life (Lambin et al., 2001; Falcucci et al., 2006).

Turner et al. (2003) outlined that LULC change leads to habitat loss and fragmentation of the environment. The ecological system within the converted areas tends to degrade due to factors such as nitrate flux, impaired water quality, sedimentation, and other nonpoint pollutants (Strayer et al., 2003; Wang et al., 2014). The degradation of the environment affects the functioning of the local ecological system leading to loss of habitats for animal and plant species (Turner et al., 2003). Industrial and urban pollutants such as heavy metals and nutrients wash out as runoff into receiving water bodies (Tang et al., 2005; Wang & Kalin, 2018). Intensive agriculture i.e., cotton and rice growing affects water quality due to high nitrate concentration from fertilizers, pesticides, herbicides, and land drainage (Jingan et al., 2005). Phosphorus and nitrate flux in water bodies leads to eutrophication, thus giving out hostile odour and taste (Jingan et al., 2005). Mazvimavi et al. (2007) added that rivers may lose the ability to support biodiversity due to the diversion and storage of water and pollutants loading. Jingan et al. (2005) and Cunjak et al. (2013) stated when water flow patterns and water quality change, there tends to be a decline in animal and plant abundance (biological degradation).

Early research has documented many effects of LULC change on ecology. However, the precise inter-relationships between LULC change and ecological responses are difficult to establish in a specific catchment (Cunjak et al., 2013). According to Lambin et al. (2001) and Strayer et al. (2003), the disregard for the intensity of land use, types of land use, rates of transformation, and spatial patterns of LULC change cause difficulty in relating LULC change to the ecological response of catchments. In addition, the relationship between LULC changes and ecology in different regions is not constant and varies over space and time due to the difference in catchment characteristics and sources of pollution. Furthermore, a lag also exists between ecological responses and physical habitat modifications (Strayer et al., 2003).

Therefore, to fully understand the ecological response of land to LULC change, more studies are required.

2.4 Impacts of land cover change on hydrological components

The impact of LULC change on hydrological characteristics and catchment processes is a widely studied concept. Rural areas in South Africa are associated with five primary drivers of LULC changes namely, commercial afforestation, woody encroachment, urbanization, increased dry land cultivation and rangeland degradation (Gibson et al., 2018). The major effects associated with LULC change are the alteration of hydrological processes influencing water yield within a catchment (Tena et al., 2019). Precipitation is a key input in catchment hydrology; it affects different hydrological processes such as interception, evapotranspiration, infiltration, and groundwater recharge, and thus determines runoff generation (Li et al., 2017). However, the hydrological response of a catchment depends on vegetation, changes in drainage networks and the duration of the changes (Owuor et al., 2016). Therefore, it is crucial to understand the effects of LULC change on catchment hydrology to

(i) help identify alterations of hydrological processes,
(ii) assess the availability of water resources under increasing population and
(iii) formulate appropriate land use management projection (Tena et al., 2019).

Studies conducted in the Luvuvhu catchment show LULC changes due to agricultural practices and urbanization (Warburton et al., 2012; Mathivha et al., 2016). Some LULC changes may not affect the hydrology of the catchment immediately due to the time lag between these changes and their effect on the water balance (Warburton et al., 2012), however, their impact on hydrological components is inevitable. Vegetation intercepts water by capturing rainfall on leaf surface areas throughout the canopy and through the litter it deposits on the ground. Plantation forests tend to transpire more water than indigenous vegetation, hence reducing runoff and groundwater recharge (Chemura et al., 2020). The removal of such dense vegetation cover reduces canopy interception and leads to more surface runoff (Matheussen et al., 2000; Livesley et al., 2014). However, the impacts of interception on surface runoff are distinctive during small precipitation storms and show no major effect during large storms and flood occasions (Hosseini and Ashraf, 2015).

LULC changes also affect evapotranspiration, one of the key components of the hydrological cycle. LULC change affects evapotranspiration by changing the underlying surface properties

such as surface roughness, vegetation cover and surface reflectance (Liu & Hu, 2019). Evapotranspiration links the water cycle with land surface energy and carbon cycles (Liu et al. 2013). Evapotranspiration returns approximately 60% of precipitation from land back to the atmosphere (Odongo et al., 2019). Furthermore, evapotranspiration is higher in natural forests than on land cover with sparse vegetation (Owuor et al., 2016). Forest clearance may reduce evapotranspiration and increase rates of streamflow (Matheussen et al., 2000). An increase in evapotranspiration may result in variations in the hydrological cycle, as precipitation evaporates back into the atmosphere, less surface runoff is accumulated (Chemura et al., 2020). Reduced runoff will pose significant effects on hydrologic, economic, and ecological functions (Chemura et al., 2020). The reduction of evapotranspiration rates on the other hand alters water yield due to excess water, thus increasing aquifer recharge and surface runoff (Owuor et al., 2016; Odongo et al., 2019). It is important to evaluate the extent of change in the rate of evapotranspiration given the continuous patterns of LULC changes in catchments.

Infiltration is also an important process of the water cycle which is influenced by vegetation, root density, soil type and soil texture (Angelaki et al., 2018). LULC changes have considerable impacts on the rate of infiltration and groundwater recharge. Soil hydro-physical properties such as soil texture, bulk density, porosity, and hydraulic conductivity determine how soil captures and retains precipitation (Owuor et al., 2016). The distribution of LULC changes over a catchment influences major changes in the physical properties of soil (Sun et al., 2018). Some of the significant changes in soil properties are the loss of organic matter and an increase in bulk density, which lowers infiltration rates (Sun et al., 2018), and affects groundwater recharge. In East African Watersheds, Mengistu et al. (2022) evaluated the impacts and implications of LULC dynamics on groundwater recharge and surface runoff, and the results from the calibrated model show a decline in groundwater recharge and an increase in surface runoff. According to Mathivha et al. (2021), the evaluation of the relationship between groundwater levels and hydrological extremes in the Luvuvhu catchment also shows a declining rate of groundwater recharge. LULC change may have also contributed to the decrease in groundwater level and increased volume of runoff across the Luvuvhu catchment.

2.5 Implications of LULC on surface runoff response

Complex natural and anthropogenic factors occurring at the catchment scale influence the runoff characteristics of a catchment (Xu et al., 2014; Sajikumar & Remya, 2015). Many studies that have focused on the impacts of LULC change on surface runoff reveal an increase

in surface discharge over space and time (Griscom et al., 2009; Mathivha et al., 2016; Wang et al., 2017; Guzha et al., 2018; Mengistu et al., 2022). However, factors that affect surface runoff may depend on the land cover type, climate and topography which may result in varying runoff responses (Wang et al., 2017; Guzha et al et al., 2018). Prolonged or intense rainy seasons, deforestation, and urbanisation are the major factors that result in increased surface runoff (Griscom et al., 2009; Petchprayoon et al., 2010; Mathivha et al., 2016). Frequent precipitation results in saturated soil which leads to higher runoff generation, while afforestation has strong effects on peak flows, and reduction of base flows during drought seasons (Robinson et al., 2003). The effects of LULC change and climate change vary from one catchment to another given the difference in catchment characteristics. Guzha et al. (2018) argued that the well-known basics of forests and water relations do not include catchments located within tropical regions, therefore implying that there are variations in the effects of LULC change between tropical regions and other non-tropical regions. Studies by Serpa et al. (2015) and Wang et al. (2017) showed that deforested lands have higher runoff than forest areas. Clearing woodlands and forests due to population growth rapidly increases surface runoff which results in high peak flows (Hassaballah et al., 2017). Wang et al. (2017) stated that LULC change has "increased global runoff by 0.08 mm per year and accounts for 50% of the change in global runoff over the last century", and its contribution to changes in runoff patterns is larger compared to climate changes. Forested catchments are characterised by lower peak flows and higher base flows; therefore, afforestation helps reduce floods and support base flows (Robinson et al., 2003). LULC changes occurring rapidly due to compact indigenous forest, plantation and agriculture within a small-scale catchment may also result in reduced streamflow and baseflow (Hassaballah et al., 2017); however, more research is needed to support this claim.

In many cases, seasonal increase in surface discharge may result from both LULC change and climatic conditions (Serpa et al., 2015; Wang et al., 2017). Human activities that influence change in catchment hydrology include different land use types, vegetation cover and alteration of soil properties (Hu et al., 2005; Tomer & Schilling, 2009). Therefore, anthropogenic activities adversely alter the frequency, patterns, quantity, and quality of river regimes (Getahun & Haj, 2015). Rising temperatures, changes in rainfall patterns, forest loss and forest plantation changes in streamflow patterns (Zhang et al., 2006). A Study by Tomer & Schilling, (2009) shows that climate change and LULC changes resulted in the increase in runoff in the Midwest catchments. In some catchments, the quantity of low flows depends on groundwater recharge through infiltration during or after precipitation events (Smakhtin, 2001). Lørup et al.

(1998) also stated that LULC change may have adverse effects on the rates and volume of rivers resulting in reduced low flows and increased flood rates. Smakhtin (2001); Robinson et al. (2003) and Li et al. (2018) concluded that LULC change causes a significant decrease in low flows. To improve understanding of streamflow and its future characteristics, historical LULC change impacts in a particular catchment must be considered (Tadele & Förch, 2007). Effective ways of studying low flows and peak flows involve the use of remote sensing, precipitation data and previous catchment maps (Petchprayoon et al., 2010). Many studies that focused on LULC impacts and runoff response utilize remote sensing data and hydrological modelling for detecting change in LULC and runoff response assessment, respectively.

2.6 LULC change models

To support land use planning and policies, land use change models are used to evaluate the impacts of land cover change on biophysical processes (Veldkamp & Lambin 2001; Verburg et al., 2004). Land use models explain the causes (why), locations (where) and the rate (when) of LULC change (Lambin et al., 2000). Models have different strengths in applicability; some models can capture the spatial complexity of catchments, while other models have weaknesses in expressing spatial details (Jingan et al., 2005). According to Veldkamp & Lambin (2001) and Jingan et al. (2005), a modelling approach that is conducted in a spatially explicit, integrated, and multi-scale manner, is an effective method that provides different ways for conducting research experiments that challenge current knowledge of the major processes in land use change. There are a variety of models that analyse LULC change; however, these models vary in perspectives, methodological approaches, data availability and modelling goals. Categories of land use change models include empirical-statistical models, stochastic models, optimization models, dynamic simulation models and integrated models (Lambin et al., 2000; Lambin, 2004). According to Lambin et al. (2000) and Lambin (2004), Table 2.1 summarises categories of land use change models and their characteristics.

Empirical-statistical models identify the main driving variables that cause LULC changes by using the multivariate statistical analysis of the possible exogenous contribution to empirically derived rates of change (Lambin, 2004; Jingan et al., 2005). The empirical-statistical models make use of multiple regression techniques to model land use change patterns (Lambin et al., 2000). Stochastic models describe processes that move through a set of states sequentially, from one land use category to another (Jingan et al., 2005). These models describe the state of the system for land use change as the quantity of land experiencing various land uses (Lambin

et al., 2000). Stochastic models make use of transition probability models such as Markov chain, spatial diffusion models and cellular automata (Lambin, 2004). Optimization models adopt a farm analysis at the microeconomic level using linear programming, or at the macroeconomic level using general equilibrium models (Lambin et al., 2000). Optimization models are comprised of different socioeconomic models that focus on supply and demand (Aspinall, 2004). Dynamic simulation models evaluate the patterns of land cover change that occur due to the interaction between biophysical and socioeconomic processes in space and time (Lambin, 2004). These models make use of simulation models (e.g., process flow, cellular automata, agent-based models) to highlight the interaction between biophysical and socioeconomic processes (Lambin et al., 2000). Integrated models make use of independent models that were initially designed to function on their own and combine different modelling techniques to answer specific research questions (Lambin et al., 2000). However, these models vary in detail and the complexity they represent (van Delden et al., 2011). Schaldach & Priess (2008) reviewed different integrated models that simulate the functioning of the land system.

Table 2. 1: Land use model categories adapted from studies by Lambin et al. (2000) & Lambin (2004).

Model category	**Model strengths and weaknesses**	**Modelling method**
Empirical-statistical models	**Advantages:** • Determine the specific causes of land use changes. • Predict patterns of land use change patterns. • Predict changes in land use intensity where such changes have been measured in the recent past. **Disadvantages:** • Regression models are not spatial. • Do not establish a causal relationship between the causes and consequences of the land use dynamic. • Regression models perform poorly outside the region of the variable space. • Cannot be applied for a wide-ranging extrapolation	Multiple linear regression models

Stochastic models	**Advantages:** • Mathematical and operational simplicity. • Requires data for current land use only. • Predict when changes in land use might occur in the near future, under a strict assumption of stationarity of the process. • Can be used without information on the driving forces and mechanisms of land use changes. **Disadvantages:** • Are limited in their application of land use intensification as they only use transition observed in the recent past.	Transition probability models
Optimization models	**Advantages:** • Allows investigation of the influence of various policy measures on land allocation. **Disadvantages:** • Models of urban and peri-urban land allocation are much more developed than their rural counterparts. • Optimization models suffer limitations, such as the arbitrary definition of objective functions and non-optimal behaviour of people e.g., differences in values, attitudes, and cultures. • The applicability of these models for projections is limited due to unpredictable fluctuation of prices and demand factors and the role of non-economic drivers of changes.	Linear programming Land rent theory of von Thünen and Ricardo
Dynamic(process-based) simulation models	**Advantages:** • They condense and aggregate complex ecosystems into a small number of differential equations in a stylized manner. • Are based on a priori understanding of the forces driving change in a system.	Simulation models Dynamic spatial simulation

	• Allow exploration of probable effects of the continuation of current land use practices or changes in cultural or ecological parameters. • These models allow testing of scenarios on future land use changes. **Disadvantages:** • They are difficult to translate to land use patterns due to the need to incorporate the economic or social mechanisms driving land-use transitions. • The scale issue is difficult in dynamic simulation models and can be parameterised based on local observations of decision-making.	
Integrated (Hybrid) models	**Advantages:** • Allows integration of different modelling techniques to answer specific research questions. **Disadvantages:** • The level of integration is not always high.	They differ due to the integrated models

2.7 Remote sensing as a tool for LULC change monitoring

The use of remotely sensed data and geographical information systems (GIS) has gained popularity and has become crucial in the analysis of land cover, its uses and the changes that occur on land (Liping et al., 2018). Remote sensing encompasses the use of sensory devices that measure electromagnetic radiation that is emitted by the earth and its features (Aplin, 2004). The use of remote sensing is often associated with GIS (Liping et al., 2018; Mallupattu & Sreenivasula, 2013). GIS is an integrated system of hardware and software that may be used to acquire, save, retrieve, alter, and display geographical information to order to organise and present data as maps (Mallupattu & Sreenivasula, 2013). The LULC data obtained using GIS is essential for land use management. The rapid LULC change due to population growth and development needs advanced methods for catchment planning and environmental management (Herold et al., 2002). However, the complexity of LULC change classification requires multidisciplinary exploration (Veldkamp & Lambin, 2001).

Over the years, remote sensing and GIS have advanced to allow LULC monitoring and prediction (Dewan & Yamaguchi, 2008; Liping et al., 2018). LULC change monitoring requires two images acquired at separate times for comparison (Aplin, 2004). Monitoring and measuring LULC change involves the use of old images of an area compared to recent images of the same area. According to Mallupattu & Sreenivasula (2013) and Veldkamp & Lambin (2001), GIS simplifies the retrieval of images stored from previous years, therefore making comparison of past and current land cover possible. However, there are various sources and different methods of retrieving remotely sensed data. Given the differences in resolution and spectral properties, atmospheric correction to remove distortions caused by clouds, haze and atmospheric scattering is important in remote sensing (Aplin, 2004; Liping et al., 2018). After all the atmospheric corrections, clear images make the comparison possible and simple (Veldkamp & Lambin, 2001). The use of remote sensing and GIS is popular because they are cost-effective and efficient methods for LULC change monitoring (Dewan & Yamaguchi, 2008).

2.8 LULC change detection approach

Singh (1989) defined change detection as a technique of finding variations in the state of an object or phenomenon by monitoring it over time. A process of assessing temporal changes using multi-temporal datasets, with geographic data as the major source and typically in digital (satellite images), analogue (aerial pictures), or vector format (feature maps) (Théau, 2017). Satellite remote sensing can deliver rapid, accurate and consistent information about the earth's surface for reasonable environmental change monitoring costs. This knowledge is crucial for sustainable development, decision-making, the management of natural resources, and the preservation of ecosystems and biodiversity (Ban & Yousif, 2016).

The underlying idea behind using satellite remotely sensed data is to ascertain that LULC changes result in radiance value changes to radiance variations caused by LULC changes that occur over time (Singh, 1989). Multi-temporal/multi-date satellite image classification is necessary before to change detection analysis. Image classification is defined as a method of grouping pixels in the image into classes or categories given their content. Classification of images can be either supervised or unsupervised classification. Unsupervised image classification is achieved through statistics, classifying pixels in a dataset without user-defined training classes. On the other hand, supervised classification is the process of classifying image pixels in a dataset into classes based on user-defined training data (Richards & Jia, 2005). The

basis of both classification methods entails that LULC-type data should be in proximity with each other in measurement space, while data from various classes should be relatively well separated (Babykalpana & ThanushKodi, 2010). Although supervised classification can be considerably more accurate, it is highly dependent on the LULC training classes, the image-processing experience of the user, and the spectral dissimilarities of the classes (Richards & Jia, 2005). Researchers have used both classification methods in LULC mapping (Babykalpana & ThanushKodi, 2010), with the supervised method being the most applied (Islam et al., 2018; Janiola & Puno, 2018; Vivekananda et al., 2020) and achieving better classification accuracies (Kafi et al., 2014).

The change detection of LULC using multi-temporal remote sensing images is multifaceted due to uncertainty in the measured phenomena, restrictions on the remote sensor's ability to measure LULC changes, inherent noise during the imaging process, compatibility of pictures from various sensors, uncertainty in the change detection process, as well as phenology, sun angles, etc. (Ban & Yousif, 2016). Such aspects along with the unique properties of remotely sensed images such as noise, image distortion and resolution are considered during the selection of the change detection method. Due to the difficulty in selecting a change detection method, there is no single approach that can manage all change detection issues (Ban & Yousif, 2016) and as a result, several researchers have applied different change detection methods. However, each technique focuses on various aspects of change detection for example, unsupervised change detection (e.g., Bovolo & Bruzzone, 2007), image differencing (e.g., Muavhi, 2021), post-classification comparison (e.g., Vivekananda et al., 2020), vegetation index differencing (e.g., Muavhi, 2021). One of the commonly used satellite image data for remote sensing LULC change detection is the freely available, Landsat imagery (Islam et al., 2018; Janiola & Puno, 2018; Vivekananda et al., 2020). With a geographic resolution appropriate for tracking LULC changes, Landsat offers one of the longest and most reliable satellite recordings of the terrestrial surface (Townshend and Justice, 1988).

Simulation and modelling of future LULC trends are growing rapidly owing to the importance of identifying the effects of humans on the environment. As a result, many approaches and software packages for LULC modelling and prediction are available (Mas et al., 2014). The Markov Chain (MC) model is the most applied method in modelling and simulating future LULC changes (Singh et al., 2015; Khawaldah, 2016). The MC-based simulation is a stochastic model that uses transition probability to predict future states based on the current state (Lambin et al., 2000; Huang et al., 2020). According to Bell & Hinojosa (1977) and Rendana et al.

(2015), the MC-based simulation has been identified as the most appropriate model for short-term projections with only a one-way transition. Researchers attribute the ability of MC-based simulation to the principle of operation of MC, which is independent and unaffected by the state of cells around the cell under observation (Ghosh et al., 2017). Consequently, MC modelling alone may not adequately analyse certain LULC scenarios, because it does not account for the spatial distribution of each category. Thus, obtaining the right direction may be challenging, although the magnitude of change is accurately predicted (Boerner et al., 1996; Ghosh et al., 2017). The Cellular Automata (CA) model therefore accounts for the spatial attribute and the direction of the change (Ghosh et al., 2017). Previous research has confirmed that combining the stochastic MC model and the CA model can simply simulate multi-directional LULC changes and provide better accuracies (Ozturk, 2015; Yuan et al., 2015). Modules of Land Use Change Evaluation (MOLUSCE) plugin, which is a QGIS-based tool, was recently introduced to analyse and predict future LULC scenarios. The MOLUSCE plugin can formulate a transition probability matrix using the integrated CA-MC approach and perform simulations based on models such as Weights of evidence (WoE), logistic regression (LR), artificial neural networks (ANN) and multi-criteria evaluation (MCE) (Kafy et al., 2021).

2.9 Hydrological modelling approaches

Researchers from various fields study the hydrologic cycle and different hydrologic occurrences to ascertain the responses of hydrological systems. Researchers make use of different methods to evaluate the potential impacts of LULC change on hydrology. These methods are classified into three categories, namely, hydrological modelling, multivariate statistics, and paired catchment studies (Woldesenbet et al., 2017). Numerous hydrological models are used to study the effects of LULC change, climate change and, soil properties on water resources. Models represent basic real-world features and predict system behaviours (Devia et al., 2015). All models are unique with different characteristics and capabilities, and it is important to learn which models work best for various studies. Common inputs used by different hydrological models include meteorological data, soil characteristics, topography, vegetation, and hydrogeology.

Over the years, hydrological modelling has gained popularity in the field of hydrology and has become the most appropriate way of studying different hydrological regimes. However, debates on which hydrological modelling approaches are best persist. Hydrological modelling has evolved and has become multifaceted due to the increase in possible computations (Sidle,

2021). Hydrological models require comprehensive knowledge of catchment features, catchment properties and the physics of underlying hydrological settings (Devia et al., 2015). Furthermore, these models are spatially and temporally distributed due to remote sensing data availability (Devia et al., 2015; Sidle, 2021). Different modelling approaches allow applicability in both gauged and ungauged basins, and the classification of hydrological models may be somehow complicated. According to Sidle (2021), hydrological approaches are classified into three groups, namely, empirical models, conceptual models, and physically-based models. The division of the three general groups is based mostly on the description of the hydrological processes (Dwarakish & Ganasri, 2015). The hydrologic models are further divided into three categories that describe the distribution of random variables in space and the temporal difference, with the spatial structure of hydrological models being the most important; these include lumped, semi-distributed, and fully distributed models (Dwarakish & Ganasri, 2015; Sidle, 2021). These are also known as deterministic modelling approaches. Xu (1999) classified the modelling approaches into four categories based on the level of complexity and temporal representation; the categories were "Empirical models (annual base); Water-balance models (monthly base); Conceptual lumped-parameter models (daily base); Process-based distributed-parameter models (hourly base)". However recent studies (Devia et al., 2015; Dwarakish & Ganasri, 2015; Sidle, 2021) have separated the classification of hydrological models into stochastic, deterministic, and hydrological process descriptions, this is more understandable and easier to comprehend.

2.9.1 Process-based modelling approach

Hydrological models vary widely and can help in solving many catchment problems. Depending on the specifics of the model, they may help in water quality appraisal, appropriate water resource management, flood estimation, LULC change, sedimentation, nutrients, and pesticide circulation. Empirical or statistical models are data-driven models that rely on the availability of hydrological data, and do not consider the features and the physical hydrological processes within a catchment (Devia et al., 2015; Dwarakish & Ganasri, 2015; Sidle, 2021). According to Mathivha et al. (2016), the curve number approach is an example of an empirical model . Other examples include artificial neural networks and fuzzy regression, which establish relationships that exist between precipitation and runoff (Devia et al., 2015). Empirical models may be useful for ungauged catchments, where data is acquired from other gauged catchments with similar hydrologic properties within the same vicinity (Dwarakish & Ganasri, 2015). The data requirement of the empirical modelling approach is quite favourable; however, the

approach has inaccuracies due to the absence of spatial and temporal depiction (Sidle, 2021). Therefore, many researchers have not recommended the use of an empirical approach for hydrological prediction in catchments experiencing complex LULC changes.

The conceptual modelling approach uses simple efficient semi-empirical algorithms and accounts for some hydrological catchment parameters (Sidle, 2021). Conceptual modelling entails types of reservoirs that represent the water exchange processes such as runoff, rainfall, infiltration, and evaporation within the catchment (Devia et al., 2015; Beven et al., 2020). The TOPMODEL is the most popular of the conceptual approach models. Conceptual modelling requires a large amount of data and thus calibration is important for accurate results (Nourani et al., 2011; Beven et al., 2020). The calibrating process entails curve fitting, which creates difficulty in the interpretation of results, and therefore assessing the effects of LULC changes using this approach may be challenging (Devia et al., 2015; Sidle, 2021).

The physically based modelling approach also referred to as process-based models, is the most effective of the three approaches and utilizes numerical principles to depict the true physical characteristics that drive hydrological processes within a catchment (Sidle, 2021). Therefore, process-based models can represent the spatial and temporal differences of significant catchment properties (i.e., topography, slope, vegetation, soil properties, precipitation, temperature, and evapotranspiration) (Dwarakish & Ganasri, 2015). These models depict real-world features and apply to a wide range of hydrological problems. The ability to incorporate physical characteristics into computations makes the process-based approach more complex than the others (Sidle, 2021). The physically based modelling approach also requires enormous amounts of data which makes it undesirable but efficient (Arnold et al., 1998; Dwarakish & Ganasri, 2015; Sidle, 2021). Examples of models using physically based principles include the SWAT and MIKE SHE models (Arnold et al., 1998; Zhang et al., 2008; Devia et al, 2015). These models predict hydrological response in catchments experiencing immense LULC changes and non-stationary climate conditions (Sidle, 2021). Studies such as (Dixon & Earls, 2012; Anand et al., 2018; Thavhana et al 2018; Mengistu et al., 2019; Afonso De Oliveira Serrão et al., 2022) have made use of the physically-based approach effectively (i.e., SWAT model).

2.9.2 Deterministic modelling approach

According to Dwarakish & Ganasri (2015) and Sidle (2021), further classification of hydrological models shows that the models may also be classified according to the spatial structure of the hydrological models. Therefore, the spatial setting of hydrological models may be lumped, semi-distributed, and fully distributed (Sidle, 2021). Dwarakish & Ganasri (2015) consider the three approaches as deterministic and spatial discretization. The lumped model approach interprets the catchment as a homogeneous unit, therefore disregarding the heterogeneity of the catchment (Sidle, 2021), and requires less amount of data for modelling purposes. Lumped models simulate different hydrological responses in single points within a basin without dimension (Dwarakish & Ganasri, 2015), and are not applicable in large complex catchments (Sidle, 2021). The lumped model approach generally aligns with the empirical approach, which also requires less data for smaller catchments.

The semi-distributed approach considers the spatial uniqueness of each point within a catchment and thus divides the catchment into small grid units known as Hydrologic Response Units (HRUs) (Dwarakish & Ganasri, 2015). The HRUs are divided according to the LULC types, soil properties, and geomorphology, therefore the hydrological response simulated in each HRU is unique to the properties of that unit (Arnold et al. 1998; Dwarakish & Ganasri, 2015; Sidle, 2021). Semi-distributed models include the conceptual TOPMODEL as well as other physically based models such as the SWAT model (Beven et al., 2020; Sidle, 2021). Semi-distributed models may require large data for calibration purposes. Fully distributed models are complex and require extensive amounts of data because the hydrological processes are specified in small grids within the catchment (Sidle, 2021). The functions of spatial structures define the model variables; however, the spatial structures contain nonlinear interactions (Zhang et al., 2008; Dwarakish & Ganasri, 2015). Examples of fully distributed models include the MIKE-SHE and VELMA models (Zhang et al., 2008; Devia et al., 2015; Sidle, 2021). These models investigate the hydrological response of catchments to climate and LULC changes at numerous spatial and temporal scales (Zhang et al., 2008; Sidle, 2021).

Selecting a model for assessing LULC change impacts can be challenging, however, these approaches scale down the most appropriate model for each specific study. Model selection may depend on the availability of data, since some models may be useful in gauged and ungauged catchments (Devia et al., 2015). The selection of models also depends on the type of catchment; large catchments with complex LULC activity will require models with the

capacity to manage large data, while smaller catchments which are more concerned with the availability of meteorological data (Sidle, 2021) would make do with simple model formations. Therefore, it is of significance to take note of the respective applications of different models during selection.

2.10 Conclusion

The assessment of LULC change impacts is important and recognised globally. The effects of LULC changes on evapotranspiration, interception, evaporation, and infiltration have significant implications for the earth's energy and water balance. Therefore, hydrological modelling has become extremely significant in assessing and predicting the effects of LULC on ecology and hydrology. Hydrological modelling and remote sensing techniques assess many of the challenges associated with extensive LULC changes and growing populations. The gaps in understanding the impacts or influence of LULC changes on hydrology may be due to the complexity of comprehending the spatial distribution of the changes. Researchers in related fields have spent years trying to account for the spatial distribution of land use in hydrological models. However, remote sensing and GIS have been of great significance in hydrological modelling and in studying and monitoring surface land patterns. Effective hydrological models make use of spatially distributed data to increase modelling accuracy. Remotely sensed hydrological datasets have become the most reliable source for researchers. Data needed for hydrological applications can be estimated remotely. Several remote sensing systems provide data imperative to hydrological modelling. For example, Digital elevation models (DEMs) such as Advanced Space-borne Thermal Emission Reflection Radiometer (ASTER) and Shuttle Radar Topography Mission (SRTM) account for surface water flow and its interaction with groundwater. Furthermore, advancements in technology have made it possible to derive spatial variable data such as temperature, rainfall and LULC using Moderate Resolution Imaging Spectro-radiometer and Landsat images with high spatial and temporal resolution. Aerial photos were the primary source of LULC data before the development of satellite imaging. The accuracy of remotely sensed hydrological datasets is of utmost importance during hydrological modelling. Model representation of hydrological processes and catchment characteristics often determines the accuracy of the model output; thus, it is important to accurately estimate input values. Variations in the accuracy of LULC data may lead to varying interpretations of results during hydrological modelling. Furthermore, DEM resolution is important in hydrological modelling, for empirical, conceptual, and physically based modelling approaches. Remote sensing and GIS are relevant during the simulation of LULC impacts on

catchment and therefore these tools work hand in hand to produce advanced hydrological response results. There is a need for continued research to advance modelling through recent technology, to achieve the best hydrological surface response monitoring, measuring and prediction techniques.

CHAPTER 3: MATERIALS AND METHODS

3.1 Research approach

The study determined the impacts of LULC change on surface runoff in the Luvuvhu catchment. A multi-temporal analysis of satellite images and field observations was used to analyse LULC changes and their influence on surface runoff. Mathematical models including Cellular Automata (CA), Markov Chain (MC) model and the semi-distributed Soil Water Assessment Tool (SWAT) model were used to analyse the collected data sets.

3.2 Description of the study area

The Luvuvhu catchment is situated in the Limpopo Province, South Africa. This catchment is situated in the Luvuvhu/Letaba Water Management Area. The Luvuvhu catchment is located between latitudes 22°17'57"S and 23°17'31"S and longitudes 29°49'16"E and 31°23'02"E and covers an area of approximately 5941 km² (Figure 3.1). The Luvuvhu catchment is under the governance of the Vhembe District municipality. The Luvuvhu catchment shows various LULC patterns influenced by the seasonal and socio-cultural practices of the local communities (State of Rivers Report, 2001). The catchment mainly consists of rural settlements, commercial agriculture, and the Kruger National Park, with three major urban centres, which are Thohoyandou, Louis Trichardt, and Malamulele (Hope et al., 2004, Odiyo et al., 2012). Odiyo et al. (2015) outlined that land use activities in the Luvuvhu catchment are commercial forestry, commercial agriculture, commercial irrigation agriculture, rangeland, conservation areas and urban areas. The upper region of Luvuvhu catchment consists of narrow, steep small rivers that drain into the Luvuvhu River. Rivers that drain into the Luvuvhu River include Sterkstroom, Latonyanda, Dzindi, Mukhase, Mbwedi, Mutshundudi, Mutale and Tshinane (State of Rivers Report, 2001; Nkuna and Odiyo, 2011). The Luvuvhu River and all its tributaries are perennial rivers (State of Rivers Report, 2001) with the Mutshundudi and Dzindi Rivers having large waterfalls. Furthermore, the Luvuvhu catchment has three major dams namely, Vondo Dam, Albasini Dam and Nandoni Dam (Hope et al., 2004) (Figure 3.1). The catchment also has small dams, which include the Phiphidi Dam, Mambedi Dam and Damani Dam (State of Rivers Report, 2001).

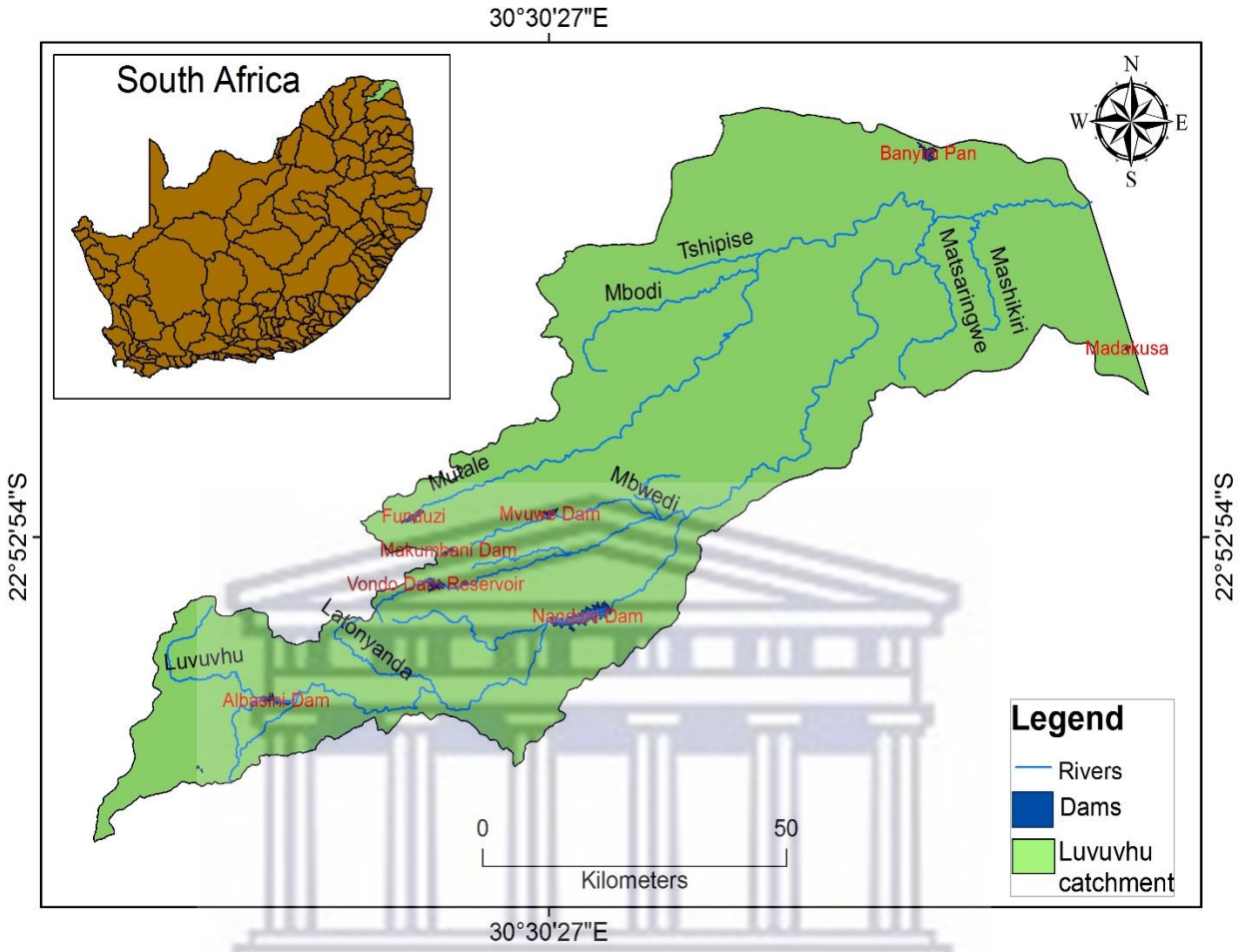

Figure 3. 1: Location of the Luvuvhu catchment in Limpopo, South Africa

- **Topography**

The Luvuvhu River originates from the southeastern slopes of the Soutpansberg Mountain and flows through Kruger National Park into the Limpopo River (Claassen, 1996). The catchment is situated at 1312 m above sea level (Ntanganedzeni and Nobert, 2020). The general terrain is mostly flat with few protruding ridges extending in the east-west direction with a mean ridge height of approximately 800 m to 1200 m, while the highest peak is above 1500 m (Odiyo et al., 2012). The landscape of Luvuvhu catchment results in shallow water storage dams, which expose a significant amount of surface water to evaporation giving rise to shallow water storage dams, which entail large water surfaces exposed to evaporation. Figure 3.2 shows the elevation map of the Luvuvhu catchment.

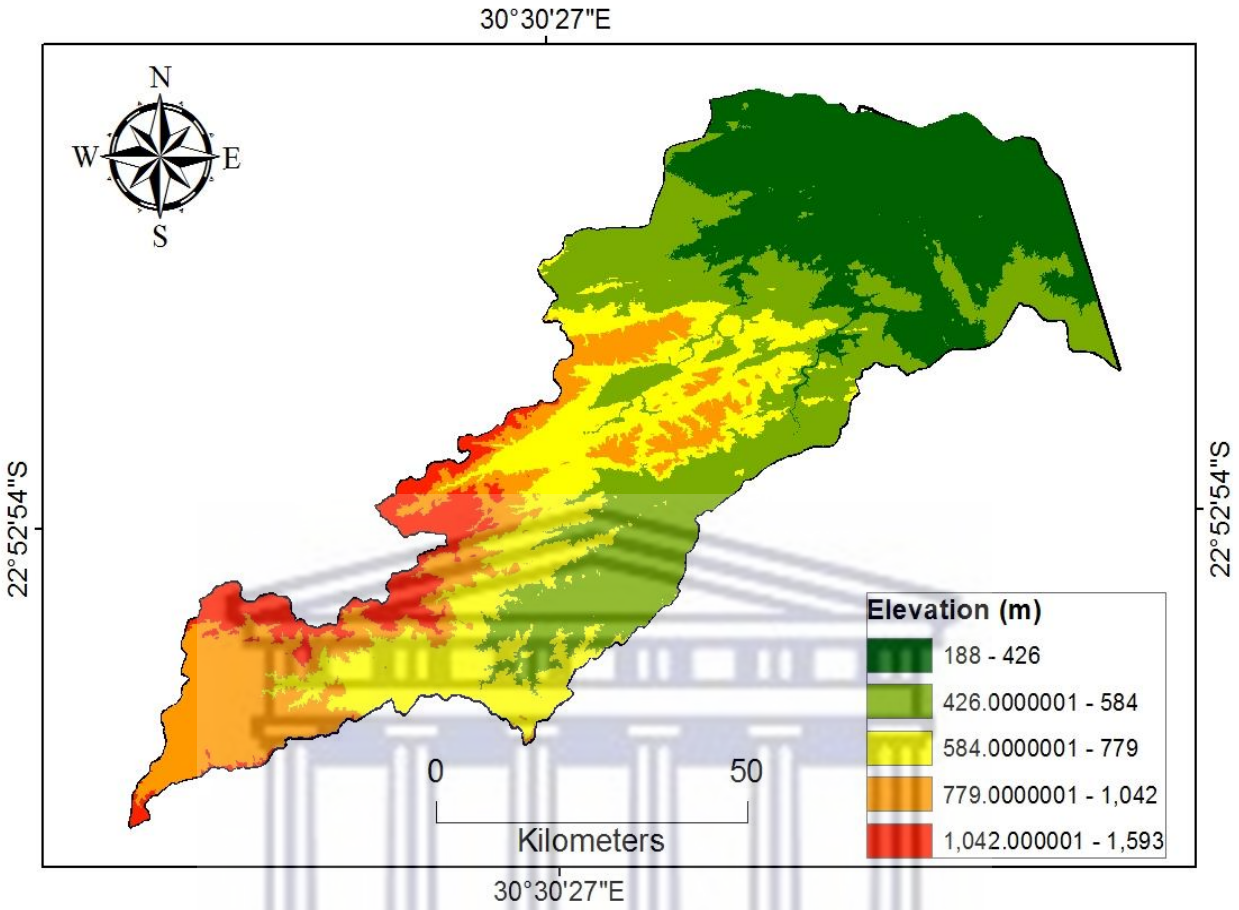

Figure 3. 2: Luvuvhu catchment elevation map

- **Geology**

The geology in the Luvuvhu catchment consists of different geological units, the dominant geological formations are granite, granite gneiss, and volcanic and sedimentary rocks of the Karroo Supergroup which underlies most of the catchment (Bristow and Venter, 1986). However, the most important geological units in the catchment include the Barberton, Drakensberg, and Soutpansberg groups (Claassen, 1996). The study area also consists of granite-greenstone terrain of the north-easterly part of the Kaapvaal Craton and highly metamorphosed rocks of the Southern Marginal zone of the Limpopo Mobile Belt. The volcanic succession of the Soutpansberg formations is the most dominant of all the formations or geological units. The Soutpansberg Mountains predominantly consist of volcanic basalt and quartzite rocks (Mathivha et al., 2021). The variety of the geological formations gives rise to the four main soil classes in the Luvuvhu catchment, namely, Glenrosa, Hutton, Mispah and Shortland (Claassen, 1996). Figure 3.3 shows the geological map of the Luvuvhu catchment.

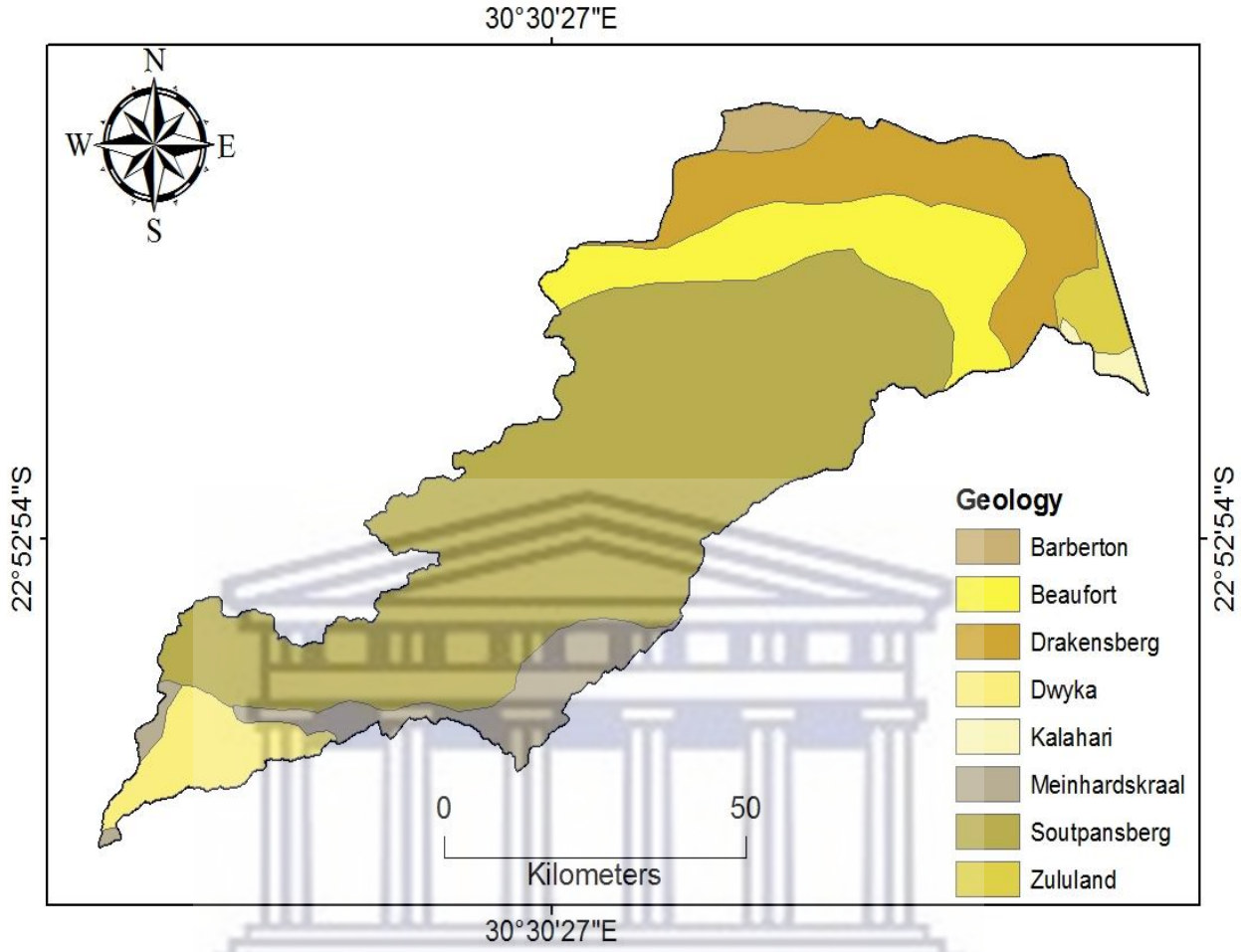

Figure 3. 3: Geological map of the Luvuvhu catchment

- **Climate**

The climate in the Luvuvhu catchment varies from humid sub-tropical to semi-arid climates. The western part of the Luvuvhu catchment is characterised by a dry, hot semi-arid climate, while the eastern part is more humid with subtropical temperatures (Hope et al., 2004). Temperature variations occurs due to seasonal changes, with elevated temperatures experienced between October to February and low temperatures between May to July. The mean annual temperature ranges from 18°C in the southwest region to 24°C in the north-eastern plains of the catchment (Odiyo et al., 2012). Precipitation in the Luvuvhu catchment varies greatly due to the undulating topographic features ranging from 200 m to 1300 m (Thavhana et al., 2018). The catchment has a mean annual precipitation of 608 mm/year, rising from 300 mm/year in the dry lower areas of the catchment to 1870 mm/year in the mountainous upper areas of the catchment (Odiyo et al., 2012). Rainfall is strongly seasonal and occurs mainly during the summer months (October to April).

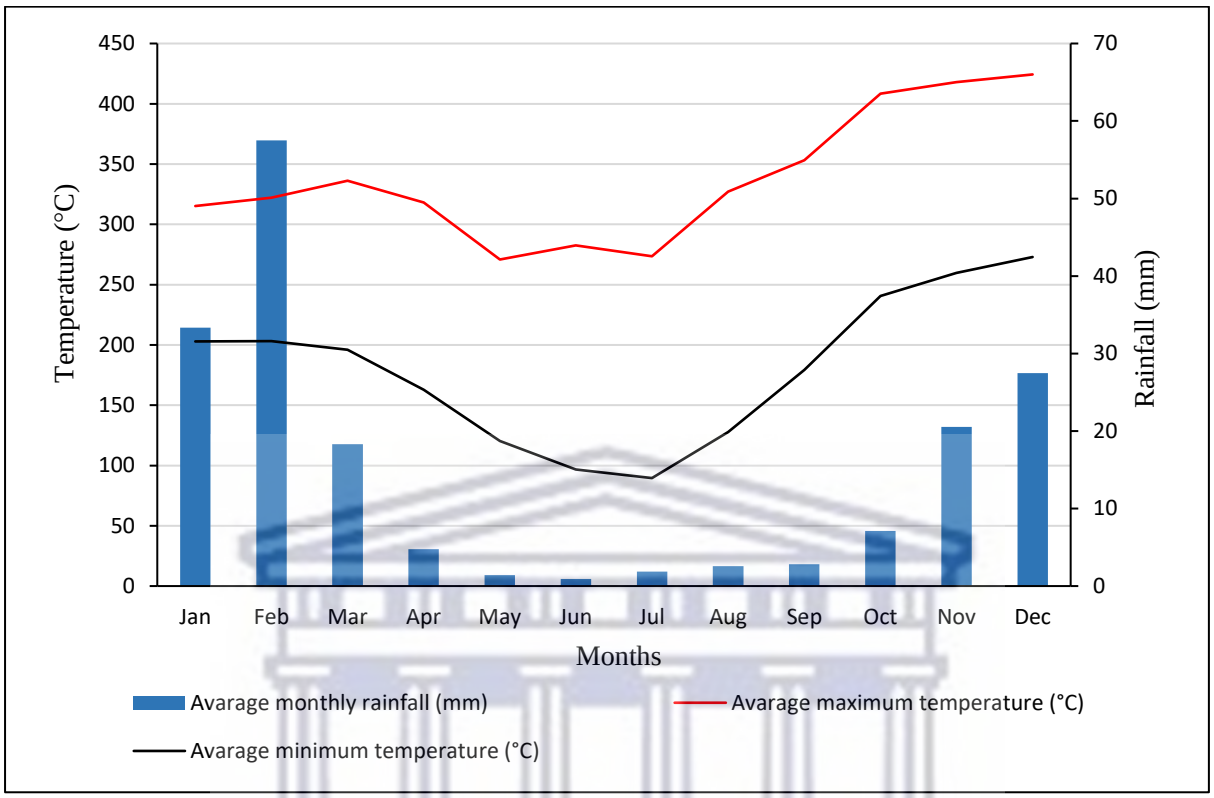

Figure 3. 4: Average monthly climate data recorded in the Pafuri weather station from 1992-2020

- **Vegetation**

The riparian vegetation categorised as large trees, shrubs, and reeds is dominant in the Luvuvhu catchment (Kundu et al., 2013). Riparian area zones are the boundaries between land and rivers that are composed of aquatic ecological units that play a significant role in environmental functions (Götze et al., 2003). Examples of such vegetation include acacia woodland species. However, most acacia species in the Luvuvhu catchment have been removed to accommodate crop production. Alien species such as eucalypts, poplars and Mauritius thorn have invaded the riparian vegetation, thus resulting in dense vegetation downstream of the Luvuvhu River (State of Rivers Report, 2001). Other alien vegetation invading the Luvuvhu catchment include Peanut butter cassia, mulberry, lantana, bug weed, guava, syringa and castor-oil plant (State of Rivers Report, 2001). Vegetation in the Luvuvhu catchment protects the river's network by acting as a barrier to erosion through the stabilisation of banks, thus reducing the impacts of floods (State of Rivers Report, 2001; Hope et al., 2004).

3.3 Data collection methods

3.3.1 LULC datasets

Landsat imagery (Landsat 5 TM and Landsat 8 OLI) was used to determine LULC change in the study area. This study made use of Landsat imagery because it is freely accessible, and has optimal ground resolution and spectral band efficiency. Furthermore, Landsat imaging was considered due to its long-term existence as it covers the study period. The image acquisition dates were selected based on data quality, data availability, and limited or absence of cloud cover (Table 3.1). All images were acquired between June and October, which is a dry season in the area (Muavhi, 2020). Nine Landsat images covering 30 years (1990 to 2020), with a five-year interval, along WRS path 169 and row 075/076, were acquired from the United States Geological Survey (USGS) website (https://earthexplorer.usgs.gov/). Bands 1, 2, 3, 4, 5 and 7 of Landsat 5 TM and bands 2, 3, 4, 5, 6 and 7 of Landsat 8 OLI (Table 3.2) were selected based on spectral and spatial resolution and ability to map LULC as demonstrated in previous studies (e.g., Islam et al., 2018; Janiola & Puno, 2018; Vivekananda et al., 2020).

Table 3. 1: Details of Landsat datasets used in this study.

Scene ID	Acquisition Date	WRS Path/Row	Cloud Cover
LT05_L2SP_169076_19901006_20200915_02_T1	1990/10/06	169/076	0-1%
LT05_L2SP_169076_19950801_20200912_02_T1	1995/08/01	169/076	0-1%
LT05_L2SP_169075_19950801_20200912_02_T1	1995/08/01	169/075	0-1%
LT05_L2SP_169076_20000830_20200906_02_T1	2000/08/30	169/076	0-1%
LT05_L2SP_169076_20050913_20200901_02_T1	2005/09/13	169/076	0-1%
LT05_L2SP_169076_20100506_20200824_02_T2	2010/05/06	169/076	0-1%
LT05_L2SP_169075_20100506_20200825_02_T2	2010/08/06	169/075	0-1%
LC08_L2SP_169076_20150808_20200908_02_T1	2015/08/08	169/076	0-1%
LC08_L2SP_169076_20200504_20210508_02_T1	2020/05/04	169/076	0-1%

Table 3. 2: Characteristics of Landsat imageries used in this study.

Landsat Type	Band ID	Bandwidth (μm)	Spatial resolution
Landsat 5	Band 1 (Blue)	0.45-0.52	30 m
	Band 2 (Green)	0.52-0.60	30 m
	Band 3 (Red)	0.63-0.69	30 m
	Band 4 (Near-infrared)	0.76-0.90	30 m
	Band 5 (Shortwave Infrared)	1.55-1.75	30 m
	Band 7 (Shortwave Infrared)	2.08-2.35	30 m
Landsat 8 OLI	Band 2 (Blue)	0.43-0.45	30 m
	Band 3 (Green)	0.53-0.59	30 m
	Band 4 (Red)	0.64-0.67	30 m
	Band 5 (Near Infrared)	0.85-0.88	30 m
	Band 6 (Shortwave Infrared)	1.57-1.65	30 m
	Band 7 (Shortwave Infrared)	2.11-2.29	30 m

3.4 LULC data analysis methods

3.4.1 Pre-processing of remotely sensed images

Landsat images were geo-referenced to the Universal Transverse Mercator (UTM) zone 36S with World Geodetic System (WGS) 1984 projection in the ArcGIS environment. Mosaicking of 1995 and 2010 Landsat image scenes (Table 3.1) was also conducted in the ArcGIS. The mosaicked and/or geo-referenced images were exported in Geo-Tiff format for further analysis using ENVI Version 5.0 software. In the ENVI environment, Landsat bands for each period (1990, 1995, 2000, 2005, 2010, 2015 and 2020) were stacked in layers to create a multiband image and then subset to cover the study area.

3.4.1.1 Atmospheric correction

The solar radiation reflected by the earth's surface passes through the atmosphere prior to its retrieval by the sensor. As a result, the images collected by the sensor include information about

both the atmosphere and the earth's surface. Therefore, atmospheric correction is implemented to compensate for atmospheric effects such as aerosols, and water vapour, which may interfere with accurate mapping of surface objects (Research Systems Inc, 2008).

Various models for correcting atmospheric effects have been developed (Research Systems Inc., 2008). The first-principles atmospheric correction modelling (FLAASH) is considered as one of the most accurate atmospheric correction tools (Research Systems Inc., 2008; Janiola & Puno, 2018; Ngondo et al., 2021). The FLAASH tool corrects wavelengths in the visible through near-infrared to shortwave infrared spectral regions, up to 2.5 μm; thus, covering the wavelengths of the six Landsat bands considered for this study (Table 3.2). Contrary to several other atmospheric correction tools that interpolate radiation transfer properties from a pre-calculated database of modelling results, FLAASH incorporates the MODTRAN4 radiation transfer code and converts radiance to reflectance by considering various parameters. These parameters include (i) a digital elevation model of the region, (ii) sensor altitude, (iii) data acquisition time, (iv) atmospheric models (v) aerosol models, (vi) scene centre coordinates, etc. (Research Systems Inc, 2008).

To implement FLAASH, the multiband image generated from the stacking of six Landsat bands was converted to BIL "band interleaved by line" image format which is compatible with FLAASH. Figure 3.5 shows the parameters which were used to derive surface reflectance images. The rural aerosols model was selected since the study area is not highly affected by industrial or urban sources. The tropical atmospheric model was considered owing to the geographical aspect and surface temperature of the region. A 2-Band (K-T) method was used to retrieve aerosol. The tropical atmospheric model is suitable for satellite sensors with wavelength channels around 0.66 μm and 2.10 μm (Research Institute Inc., 2008), like Landsat (Table 3.2). In case of initial visibility, the clear weather condition of 50 km (Research Institute Inc., 2008) was used. The option selected for water retrieval option was 'no' since the Landsat sensor lacks wavelength channels (around 0.82 μm, 0.94 μm and 1.135 μm) appropriate for water retrieval (Research Institute Inc., 2008) (Table 3.2). The option selected uses a constant water vapour amount for all pixels in the image (Research Institute Inc., 2008). In summary, the model input parameters were selected by considering the characteristics of both the study area (Muavhi and Mutoti, 2021) and the sensor used (Table 3.2).

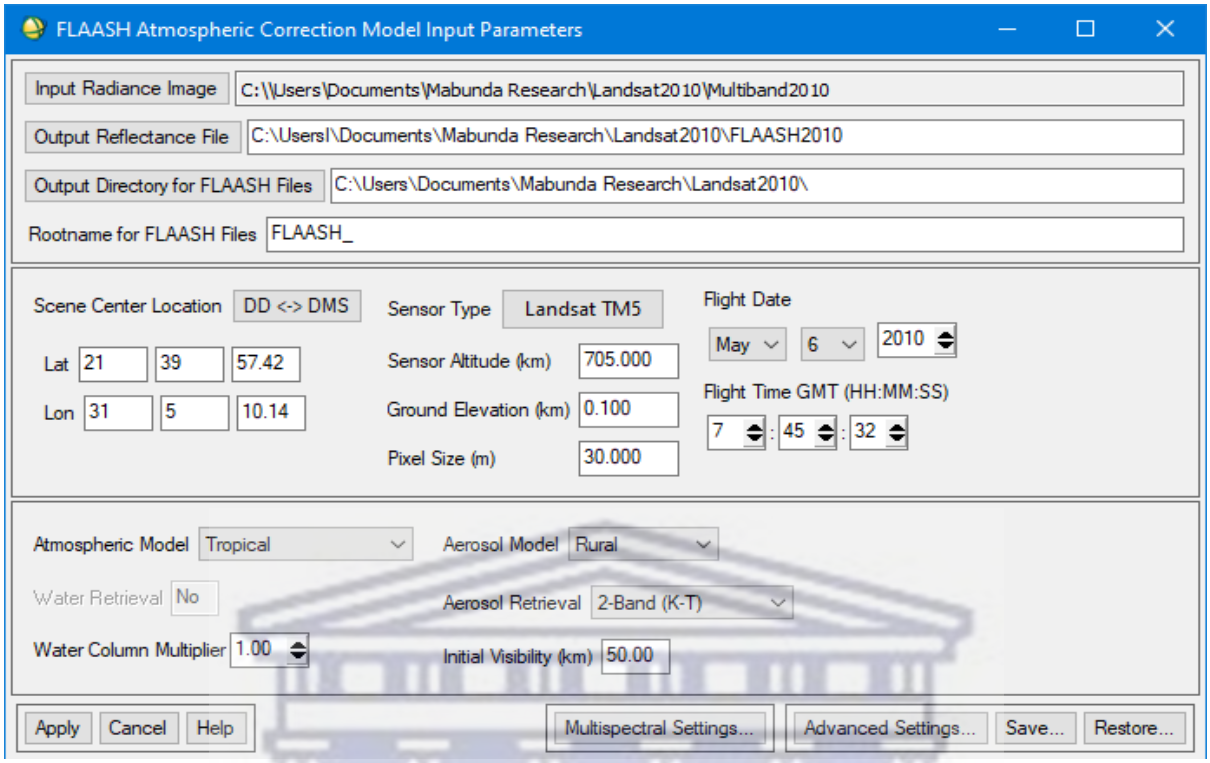

Figure 3. 5: FLAASH image from ENVI software showing the parameters utilized to generate surface reflectance image.

3.4.1.2 Selection of training samples

For Landsat 5 TM images, bands 3, 2 and 1 in red, green blue, respectively were combined to create a true colour composite (TCC) image of the area. Meanwhile, bands 4, 3 and 2 in red, green, and blue, respectively were combined to create TCC images for Landsat 8 OLI images. The advantage of a TCC image is that the features in this composite image appear in their true natural colour forms, which simplifies visual interpretability and selection of training samples (Muavhi, 2021). TCC images were thoroughly studied to gather representative samples of the six LULC types considered in this study (Table 3.3). Depending on the availability of Google Earth images acquired during or close to the acquisition dates of the Landsat images, Google Earth Pro was used as an additional tool for gathering LULC samples. Google Earth Pro was used because it can go back in time and zoom in on areas of interest at high spatial resolutions, which is crucial in the accurate selection of representative samples of LULC for multi-temporal analysis (Muavhi, 2020). The only drawback of using Google Earth as the sole source of gathering representative samples of LULC for multi-temporal analysis is that some periods (dates/years) of interest may not possess Google Earth images; hence it was important to use Google Earth as an additional tool to TCC images where possible.

Table 3. 3: Major LULC characterizing the study area.

LULC	Description
Waterbody	Natural and man-made surface water bodies (rivers, streams, dams, etc.)
Built-up	Settlements, public utilities, industrial and commercial complexes, roads, etc.
Bare Land	Unoccupied and virgin land either characterized by soils and/or rocks
Plantation	These were mainly planted commercial trees
Natural vegetation	Forest, trees, shrubs, bushes, and grass of natural origin (sparse and dense), aquatic plants
Agricultural Land	This includes cumulative land occupied by different crops

Representative samples of LULC classes were extracted as regions of interest (ROIs), which were then examined for class separability using Transformed Divergence (TD) and Jeffries-Matusita Distance (JMD). Separability measures between different LULC classes are necessary for the evaluation of the quality of the sample's representative of the LULC classes to avoid misclassification or unreliable LULC classification in the final output (Powell et al., 2004; Dabboor et al., 2014). TD is a measure of the statistical distance between class pairs of interest and provides information about their separability (Swain & Davis, 1978; Richards & Jia, 2005; Manoj et al., 2013). This separability measure can be calculated by utilizing the equation below (Swain & Davis, 1978):

$$TD_{ij} = 2000(1 - \exp\left(\frac{-D_{ij}}{8}\right)) \quad (3.\ 1)$$

where ,

$$D_{ij} = \frac{1}{2}tr((C_i - C_j)(C_i^{-1} - C_j^{-1})) + \frac{1}{2}tr((C_i^{-1} - C_j^{-1})(\mu_i - \mu_j)\left((\mu_i - \mu_j)^T\right)) \quad (3.\ 2)$$

Where, i and j are the two classes being compared, C_i is the covariance matrix of class i, μ_i is the mean vector of class i, tr is the trace function which calculates the sum of the elements on the main diagonal, T is the transpose of the matrix.

On the other hand, JMD is a function of class separability which behaves more like probability of accurate classification (Swain et al., 1971). The probability density of the spectral vectors, S_1 and S_2 for the bands (l = 1, 2,..., L) is p_l and q_l, and the JM distance (Swain et al., 1971; Chang, 2003; Richards & Jia, 2005; Padma & Sanjeevi, 2014) is given as:

$$JMD(S_1S_2) = \sqrt{\sum_{l=1}^{L}[\sqrt{p_l} - \sqrt{q_l}]} \quad (3.\ 3)$$

If the p_l and q_l are of normal distribution, then the JMD is represented as:

$$JMD(S_1S_2) = 2(1 - e^{-B}) \quad (3.\ 4)$$

Where Bhattacharya distance *(B)* measuring the mean *(M)* and variance *(V)* of the spectral vectors is defined as:

$$B(S_1S_2) = \frac{1}{8}(M_{S1} - M_{S2})^T \left[\frac{V_{S1}+V_{S2}}{2}\right]^{-1} + \frac{1}{2} In \left[\frac{|V_{S1}+V_{S2}/2|}{\sqrt{|V_{S1}||V_{S2}|}}\right] \quad (3.\ 5)$$

TD and JMD separability measures provide indirect estimation of the likelihood of correct classification between the samples of different LULC classes (Manoj et al., 2013). The TD and JMD separability measures of class pairs indicate how well the classes separate and are reported as values in the range of 0-2; where 2 indicates perfect separation of the two classes and 0 shows complete overlap between the spectral signatures of two classes (Richards & Jia, 2005; Research Systems Inc, 2008), while ≥1.5 indicates acceptable separability between classes (Latty & Hoffer, 1980). In general, values greater than 1.9 between two classes indicate excellent separability (Richards & Jia, 2005). The LULC classes in this study achieved TD separability measures from 1.86 up to 2.00. Built-up areas attained relatively low separability measures particularly with bare land (Figure 3.6); while waterbody generally attained relatively high separability measures with five LULC classes. The difficulty in separating built-up and bare land can be attributed to spectral similarities of certain roofing materials (clay tiles) and bare soils (ferromagnesian soils). Muavhi (2020) demonstrated the difficulty in separating these two LULC classes, in a study conducted in the same provincial region.

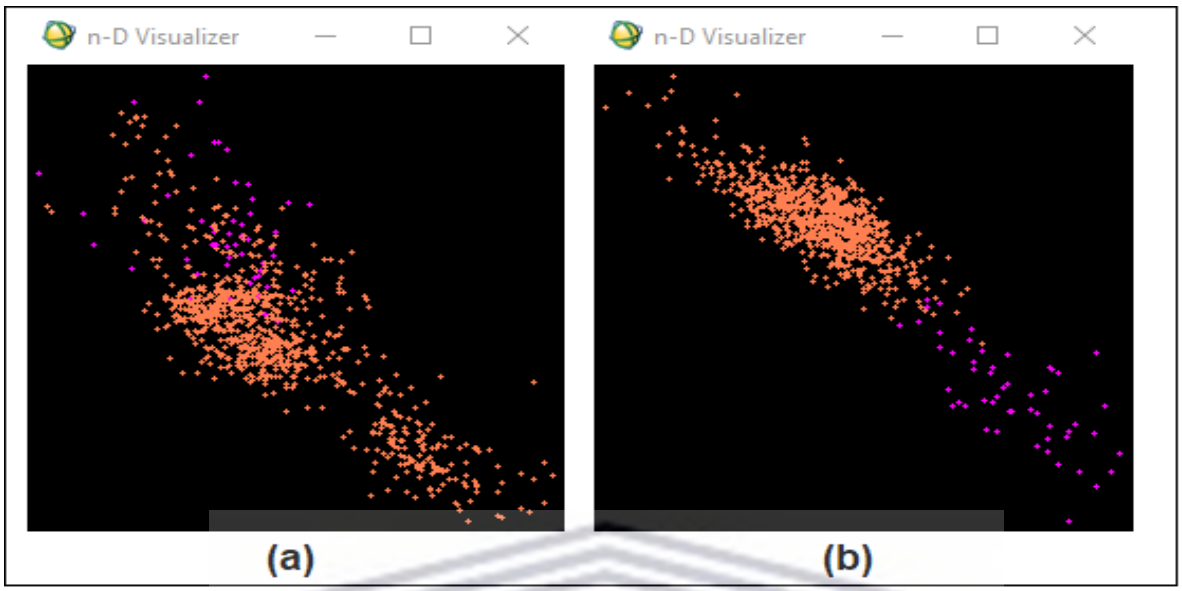

Figure 3. 6: n-D Visualizer images showing the separability of built-up (magenta) and bare land (coral). (a) Demonstrates difficulty in separating the two classes. In such cases, separability was improved by either selecting a new ROIS or editing the original ROIs (b).

Each separable LULC class was exported to n-D Visualizer, which is an interactive tool which can be used to select groups of pixels into classes (Research Systems Inc, 2008). Two subclasses from each class were randomly created in the n-D Visualizer and then exported to be utilized as a training dataset for image classification and another subclass as a testing dataset for accuracy assessment (Figure 3.7).

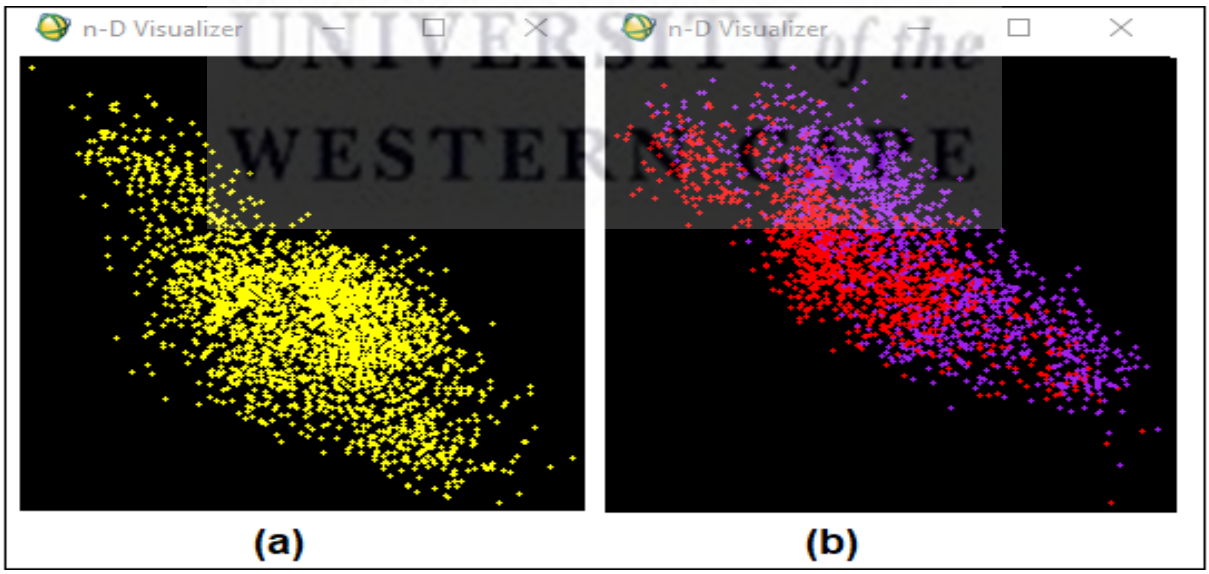

Figure 3. 7: n-D visualizer images showing (a) a class (other vegetation) and (b) randomly created subclasses: training (red) and testing (purple) dataset.

3.4.2 Image classification

Supervised image classification was selected to classify the Landsat image pixels into six LULC types using the generated training dataset. Several supervised classification algorithms are available for classifying various satellite images (Richards & Jia, 2005). Despite its drawback of assuming a normal distribution of spectral signatures of classes, the Maximum Likelihood (ML) algorithm remains one of the most popular and widely applied supervised image classification techniques (Swain & Davis 1978; Richards & Jia, 2005; Kafi et al., 2014; Janiola & Puno, 2018; Mazhar & Fadia, 2019; Vivekananda et al., 2020). However, of recent Support Vector Machine (SVM) has been proposed as one of the machine-learning algorithms capable of overcoming the inherent drawback of the parametric classification algorithm such as ML and other non-parametric algorithms such as Neural Network (NN) machine learning algorithm (Manoj et al., 2013). In addition, the SVM algorithm appears to be incredibly dependable when dealing with heterogeneous classes when the number of training samples is limited or small (Lothar et al., 1999).

The superior performance of the SVM in LULC mapping was demonstrated in the study of Muavhi (2020) which was conducted in the same region. The SVM was compared to seven algorithms i.e., ML, Minimum Distance, Mahalanobis Distance, NN, Parallelepiped, Spectral Angle mapper and Spectral Information Divergence. SVM achieved better overall accuracies and class individual accuracies than the other seven algorithms (Muavhi, 2020). Huang et al. (2002) compared SVM to ML, NN and Decision Tree algorithms using Landsat imagery and reported that SVM produced relatively high accuracies among the three supervised classification techniques. Manoj et al. (2013) also conducted the LULC classification using ML and SVM algorithms and SVM attained better overall classification accuracy compared to ML.

3.4.2.1 Support Vector Machine

Support Vector Machine (SVM) supervised classification algorithm is a non-parametric machine-learning algorithm. In other words, this technique does not assume a normal distribution of spectral signatures of classes (Richards & Jia, 2005). Vapnik and co-workers formulated SVM as a binary classification method in the late 1970s and it was further developed in the 1990s (Vapnik, 1998).

The basic idea behind the SVM is to construct an n-1 dimensional separating hyperplane to discriminate two classes in an n-dimensional space. The SVM achieves this by choosing

extreme data points referred to as support vectors to create the hyperplane. In cases where some data points in the two classes might fall into a "grey," it is difficult to separate them. SVM solves this problem by

(1) permitting some data points to the wrong side of the hyperplane by introducing a user-defined parameter that specifies the trade-off between the maximization of the margin and the minimization of the misclassifications; and

(2) utilizing kernel functions such as linear, polynomial, sigmoid, and radial basis functions (RBF) to add extra dimensions to enable the separability of the two classes in high n-dimensional space (Chang & Lin, 2001; Yu et al., 2010).

The selection of kernel functions is also a research issue, and the choice of a kernel function often has a bearing on the results of analysis. RBF is considered the main kernel function because of the following reasons (Chang & Lin, 2001; Keerthi & Lin, 2003):

- RBF kernel function maps samples into a higher dimensional space nonlinearly, and contrary to the linear kernel, it can manage the cases where the relation between attributes and class labels is nonlinear.
- RBF kernel has fewer hyperparameters compared to the polynomial kernel, and as a result RBF has fewer numerical difficulties.
- Sigmoid kernel is considered not valid under some parameters.

The mathematical expression of the RBF kernel is given below (Chang & Lin, 2001):

$$K(x_i x_j) = \exp\left(-g\|x_i - x_j\|^2\right), g > 0 \qquad (3.6)$$

Where g is the gamma term. Two key parameters for the kernels, gamma (g) and penalty (C) must be pre-determined to generate an optimum model. Parameter C controls the over-fitting of the model by specifying tolerance for misclassification. Meanwhile, g controls the degree of nonlinearity of the model (Chang & Lin, 2001). In this study, the RBF kernel is made up of a default penalty parameter of 100.00 and a gamma value of 0.33, which was used to generate LULC classification maps for the study period. These values have proven to produce accurate LULC mapping in previous studies (e.g., Muavhi, 2020).

3.4.3 Post-classification analysis

In simple terms, post-classification analysis refers to the analysis conducted on the classified image or post-image classification. In this study, post-classification analysis involves accuracy

assessment and change detection analysis. Post-classification analysis was conducted using ENVI Version 5.0.

3.4.3.1 Accuracy assessment

Accuracy assessment is a common assessment of any LULC map generated by the classification of satellite images. The accuracy of LULC maps is evaluated empirically by checking the number of sample points assigned to each LULC class compared to the reference data or ground truth data, which is also referred to as validation data (Richards & Jia, 2005). Based on this approach the percentage of pixels from each class in the image labelled correctly by the classification algorithm can be estimated together with the percentage of pixels from each class incorrectly labelled into every other class (Richards & Jia, 2005). The results are expressed in tabular form referred to as a confusion matrix, which is then subjected to various statistical analyses. One basic accuracy assessment measure is overall accuracy *(OA)*. This measure is estimated by summing the number of validation or testing pixels classified correctly for all classes and dividing by the total number of validation pixels for all classes. This can be mathematically expressed as follows:

$$OA = \frac{correctly\ classified\ validation\ pixels}{total\ number\ of validation\ pixels} x100 \qquad (3.\ 7)$$

Aronoff (1982) introduced the minimum overall accuracy value of 85% as the lowest expected overall accuracy of classification images. Another accuracy measure is the Kappa coefficient (K) which offers a difference measurement of observed agreement between classification and testing data and agreement occurring by chance alone (Jensen, 1986). Kappa coefficient *(Kc)* can be mathematically expressed as follows:

$$Kc = \frac{p_a - p_c}{1 - p_c} \qquad (3.\ 8)$$

Where p_a is the proportion of pixels which agree, and p_c is the proportion of pixels for expected chance agreement (Jensen, 1986). Kc may provide better accuracy of classification than would be expected by random assignment of classes. Kc ranges from 0 to 1, and Kc value can be interpreted as poor classification if Kc is less than 0.20, fair classification if Kc is in the range of 0.20 to 0.40, moderate classification if Kc ranges from 0.41 to 0.60, good classification if Kc ranges from 0.61 to 0.80, and if Kc is >0.85, it is considered an excellent classification (Altman, 1991).

Besides the *OA* and Kc, the classification of individual classes can also be computed from confusion matrix. These include user's accuracy *(UA)*, producer's accuracy *(PA)*, omission error *(OE)* and commission error *(CE)*. *PA* is the ratio of accurately classified testing pixels of a class and the total number of testing pixels of that class (Jensen, 1986). *PA* measures how well a certain LULC has been classified, which can be expressed mathematically as:

$$PA = \frac{C_c}{C_t} \times 100 \quad (3.\ 9)$$

Where *Cc* is correctly classified validation or testing pixels for a class and *Ct* is the total number of validation pixels in a class. *UA* is the ratio between correctly classified validation pixels for a class and the total number of pixels classified as belonging to that class. *UA* is a measure of the reliability or precision of the map (Jensen, 1986). For example, when it is a bare land class, how often does the classification algorithm assign pixels to the bare land class? This item is particularly important as it informs the user how well the map represents what is on the ground, and thus determines the level of confidence that can be attached to the map (Muavhi, 2020). *UA* can be computed as follows:

$$UA = \frac{C_c}{T_C} \times 100 \quad (3.\ 10)$$

Where *Cc* is correctly validation pixels for a class and *Tc* is the total number of validation pixels classified as belonging to a class. Meanwhile, *CE* represents validation pixels that belong to another class but are labelled as belonging to the class of interest, while *OE* represents validation pixels that belong to a certain class, but the algorithm has failed to classify them into the proper class (Jensen, 1986). These two parameters are computed as follows.

$$CE(\%) = 100 - UA \quad (3.\ 11)$$

$$OE(\%) = 100 - PA \quad (3.\ 12)$$

3.4.3.2 Change detection

A simple post-classification comparison method was implemented to detect LULC changes over 30 years from 1990-2020. This approach was considered because it quantifies the rate and magnitude of change. The, from-to change information is achieved by the comparison of the classified LULC maps on a pixel-by-pixel basis (Ban & Yousif, 2016; Alawamy et al., 2020). The magnitude of change *(MC)* and the percentage of change *(PC)* for each LULC class are computed based on the following equations (Alawamy et al., 2020):

$$MC(km^2) = A_i - A_f \quad (3.\ 13)$$

$$PC(\%) = \frac{A_i - A_f}{A_i} \times 100 \quad (3.\ 14)$$

Where A_i (km^2) is a class area at an initial time and A_f (km^2) is a class area at a final time.

3.4.4 LULC modelling

The term "model" has been used in different contexts and several application areas. The model can be generally defined as an abstraction or approximation of reality achieved by simplification of complex real-world relations to the point that they are understandable and analytically manageable (Goshu, 2010). LULC modelling plays a key role in understanding the change dynamics and their impacts and this is significant in implementing effective environmental management, and sustainable development resource use including development plans and the process of decision-making. To achieve simulation of LULC future trends, several modelling approaches and techniques have been introduced (Mas et al., 2014). MC model is one of the most used modelling and simulating techniques for future LULC trends (Singh et al., 2015; Khawaldah, 2016). Based on the MC's operation principle, MC is reliant on the conditions states of the cells neighbouring the cell being observed, hence MC modelling alone may sometimes not be sufficient to accurately predict LULC future trends due to the disregard of the spatial distribution of each class (Boerner et al., 1996; Ghosh et al., 2017). As a result, in recent years, CA models have proliferated in modelling and simulating LULC future patterns owing to their flexibility and simplicity including their ability to consider the temporal and spatial dimensions of the processes (Santé et al., 2010).

3.4.4.1 Cellular Automata model

CA models were first established in the late 1940s by Ulan, S and von Neumann, J (Santé et al., 2010). Wolfram (1984) first demonstrated the modelling of complex natural phenomena using CA and later laid the fundamentals for a Theory of Cellular Automata. This theory can be defined as discrete dynamic systems in which local interactions among components generate global changes in space and time (Wolfram, 2002). CA model enables clear insights into global and local patterns of LULC changes by relating the new state to its previous state (Santé et al., 2010). In other words, the CA model is a simple and dynamic modelling technique in which the condition of individual cells is enclosed inside a defined neighbourhood, following a set of transition rules. Consequently, the CA model can predict and model the spatial distribution of

the LULC pattern including its dynamics since it can add spatial properties of LULC (Santé et al., 2010). Instead of solely relying on the information based on the previous condition of LULC such as in the case of the MC model, CA also utilizes the condition of nearby cells for its transition principles (Ghosh et al., 2017). Equation 3.15 illustrates the mathematical expression of CA (Kafy et al., 2021):

$$S(t, t+1) = f(S(t), N) \quad (3.\ 15)$$

Where $S\ (t + 1)$ is the system status at the time of $(t, t + 1)$; functioned by the state probability of any time (N). In this study, the CA model was implemented to simulate the future LULC dynamics using the Modules of Land Use Change Evaluation (MOLUSCE) plugin from QGIS 2.18 software.

3.4.4.2 Modules of Land Use Change Evaluation

MOLUSCE analyses, models, and simulates LULC changes by incorporating well-known algorithms which include CA, logistic regression (LR), weights of evidence (WoE), artificial neural networks (ANN) and multi-criteria evaluation (MCE) (MOLUSCE, 2018). MOLUSCE user interface provides a simplistic interface with specific functions and modules. The CA takes input factors (LULC and spatial variables) and models (ANN, LR, WoE or MCM), meanwhile the simulator takes the probabilities of transition from the transition matrix, and then initiates a model and offers it with input factors (Jogun et al., 2019; Yatoo et al., 2020). For every class, potential transitions are estimated, and the simulator establishes a raster of the most probable transitions. In this regard, for each transition belonging to the most probable transitions, the simulator searches a fixed number of pixels with the highest certainty and then changes the class of the pixels (Yatoo et al., 2020). In general, the MOLUSCE plugin is comprised of six steps starting from the input module, evaluating correlation, area changes, transitional potential modelling, CA simulation, and validation (MOLUSCE, 2018).

3.4.4.2.1 Input module

The initial and final LULC maps as well as independent spatial variables that have been processed as per the geometry of the LULC maps are used as input parameters (MOLUSCE, 2018; Hakim et al., 2019). For this research study, the generated LULC maps for 2010 and 2015 are used as initial (first) and final (second) LULC maps and elevation, slope, landform, and distance to stream are considered independent spatial variables (Figure 3.8). Elevation and slope were estimated from a 30 m x 30 m resolution Digital Elevation Model (DEM), acquired

from the Shuttle Radar Topography Mission (SRTM) of the U.S. Geological Society, using the topographic modelling tool of ENVI software. SRTM DEM was also used to automatically extract the streams making up the drainage of the area using the hydrological tool in ArcGIS software, and then Euclidean distance was utilized to generate a distance to stream map. Conventional data on landforms (in a vector format) was acquired from the Soil and Terrain Database for South Africa database. The landform vector was resized to the dimension of the study area and converted to a raster to be used together with DEM-generated factors as independent spatial variables.

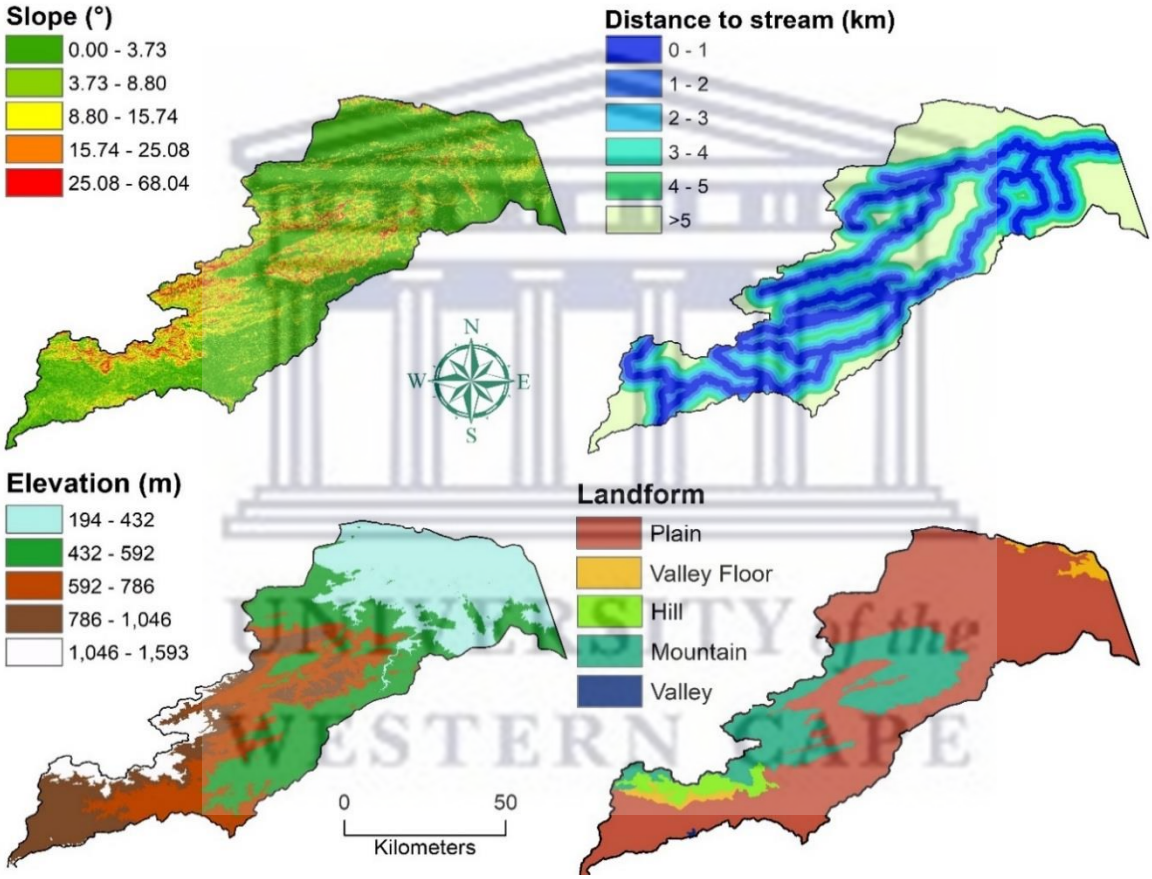

Figure 3. 8: Maps of independent spatial variable factors considered in this study.

3.4.4.2.2 Evaluation correlation

There are three techniques for evaluating the correlation among the independent spatial variables i.e., Crammer's Coefficient/Cramer's V, Pearson's Correlation and Joint Information Uncertainty (MOLUSCE, 2018). These three statistical methods report the correlation of variable pairs as values ranging from -1 to 1, where the value of -1 means negative correlation, 0 means no correlation and 1 represents a positive correlation. After careful assessment of the results given by the three methods, Pearson's Correlation, which is the most widely used

technique in evaluating the correlation of variables to be used for LULC modelling (Thanekar, 2021), was applied. Pearson's Correlation measures the degree of linear correlation between the two variables using the following equation:

$$r_{XY} = \frac{cov\,(X,Y)}{\sigma_X \sigma_Y} \quad (3.\ 16)$$

where *cov (X, Y)* is the covariance between the two variables X and Y and σ is the standard deviation.

Pearson Correlation report is shown in Figure 3.9. From the results, it can be observed that the distance to the stream variable is inversely related to other variables. Meanwhile, for the related variables, landform and elevation show the highest correlation value (>0.5). These two variables are correlated in nature since elevation variation determines landform type. Nonetheless, both negative and positive correlation values are accepted in LULC modelling (MOLUSCE, 2018; Thanekar, 2021).

3.4.4.2.3 Area changes

At this stage, LULC change statistics between the initial year and final year are computed and displayed in tabular form, together with the transition matrix table (Tables 3.4 and 3.5). The transition matrix shows the probability/proportions of pixels changing from one LULC to another (MOLUSCE, 2018). Table 3.4 shows that natural vegetation dominated the Luvuvhu catchment in both 2010 and 2015. Nonetheless, natural vegetation is the only LULC that suffered a loss in terms of area coverage while the remaining five LULCs experienced gains by 2015. Regarding the transition matrix report, all pixels classified as waterbody in 2010 remained waterbody by 2015; also, this LULC achieved the lowest change by 2015 (0.49). Meanwhile, 80% of pixels of built-up remained built-up by 2015. The remaining LULC saw a drastic change over a five years. Moreover, this implies that these have a high probability of changing into other LULCs. Meanwhile, the probability of waterbody and built-up to change to other LULC is extremely low.

Table 3. 4: Class statistics of the study area from 2010 to 2015.

LULC (sq. km)	2010	2015	Δ	2010%	2015%	Δ %
Built-up	131.23	205.62	74.39	2.21411571	3.46913154	1.25501583
Waterbody	24.81	25.30	0.49	0.41866761	0.42689762	0.00823001
Plantation	163.78	188.46	24.68	2.76330946	3.1796842	0.41637474
Agricultural Land	131.92	140.83	8.91	2.22564076	2.37604344	0.15040268
Natural Vegetation	4521.61	3114.30	-1407.31	76.2871235	52.5434832	-23.74364
Built-up	953.74	2252.58	1298.84	16.091143	38.00476	21.9136171

Table 3. 5: Transition matrix report of LULC.

LULC	Built-up	Waterbody	Plantation	Agricultural Land	Natural Vegetation	Bare Land
Built-up	0.81009	0.00350	0.00509	0.01559	0.06957	0.09616
Waterbody	0.00103	0.95991	0.02956	0.00569	0.00249	0.00132
Plantation	0.01802	0.00323	0.34831	0.11722	0.49318	0.02005
Agricultural Land	0.02516	0.00591	0.07010	0.20455	0.61668	0.07760
Natural Vegetation	0.02858	0.00269	0.02537	0.01910	0.58268	0.34158
Bare land	0.05939	0.00095	0.00513	0.00606	0.27374	0.65474

3.4.4.2.4 Transitional potential modelling

MOLUSCE renders four methods for modelling LULC change, which include ANN, WoE, MCE and LR. All these techniques use LULC change information and the spatial variables as inputs for calculating and plotting LULC changes. Researchers have applied the ANN algorithm owing to its optimal accuracy compared to the remaining three algorithms (MOLUSCE 2018; Hakim et al., 2019; Yatoo et al., 2020; Kafy et al., 2021; Thanekar, 2021).

For this reason, the ANN algorithm was selected as the transitional modelling algorithm for LULC changes in this study.

ANN is comprised of neurons which are like neurons of the human brain. These neurons are used to find relationships in data (Pijanowski et al., 2002). MOLUSCE plugin uses a Multi-Layer Perception (MLP), which is the most utilized form of ANN algorithm (Rumelhart et al., 1986), together with a back propagation algorithm. In the MLP-ANN, the initial pre-processing of the provided data into a set of independent spatial variables is conducted using dummy coding of various categories into variables like 0 and 1 (Yatoo et al., 2020). MLP-ANN further performs normalization of factor variables, sampling as well as training of the model (Jogun et al., 2019; Yatoo et al., 2020). In general, the normalization of factor variables enables the achievement of more efficient and effective training including more accurate modelling and prediction results. MOLUSCE utilizes the following linear normalization equation (Yatoo et al., 2020):

$$X_n = \frac{X - m_x}{\sigma_x} \quad (3.\ 17)$$

Where X is a variable, X_n is a normalized variable, m_x is the mean of X and σ_x is the standard deviation of X.

In the back propagation algorithm, momentum is used for the learning process and weight corrections are calculated as follows (Yatoo et al., 2020):

$$W(n+1) = r * dw(n) + m * dw(n-1) \quad (3.\ 18)$$

Where w is a vector of neuron weights, dw is a vector of weights changes, n is an iteration number, r is learning rate and m is momentum.

The following inputs are used to customize the ANN modelling in MOLUSCE (MOLUSCE, 2018):

- The neighbourhood: this defines the count of neighbour pixels around the current pixel. Size=1 means 9 pixels (3x3 region), size=2 means 25 pixels (5x5), etc.
- Learning rate, momentum, and maximum iteration number: these are the parameters of learning. Big learning rates and momentum allow fast learning, but the learning process can be unstable (spikes on the graph). Small learning rate and momentum mean stable but slow learning.

- Hidden layers input takes input string of numbers; N^1 N^2 … N^k, where N^1 is the number of neurons in 1st hidden layer, N^2 is the number of neurons in 2nd hidden layer and so on, N^k is the number of neurons of the last hidden layer (k^{th} layer).

The following outputs are created (MOLUSCE, 2018):

- The graph area: this graph contains errors in training and validation sets. It is the main information about the learning process.
- The minimum validation and overall error: contain information about the least attained error on a validation set of samples.
- The delta overall accuracy contains the difference between the least reached error and the current error.
- The current validation Kappa: this shows the Kappa value.

In this study a neighbourhood was set to 1, which means 9 (3 × 3) cells, to define the neighbourhood pixel for the model. Both the learning rate and momentum have been set to 0.001 to stabilise the learning graph (MOLUSCE, 2018). Furthermore, the maximum iteration was set to 100 to eliminate the problem of over-fitting the model (Yatoo et al., 2020) (Figure 3.9).

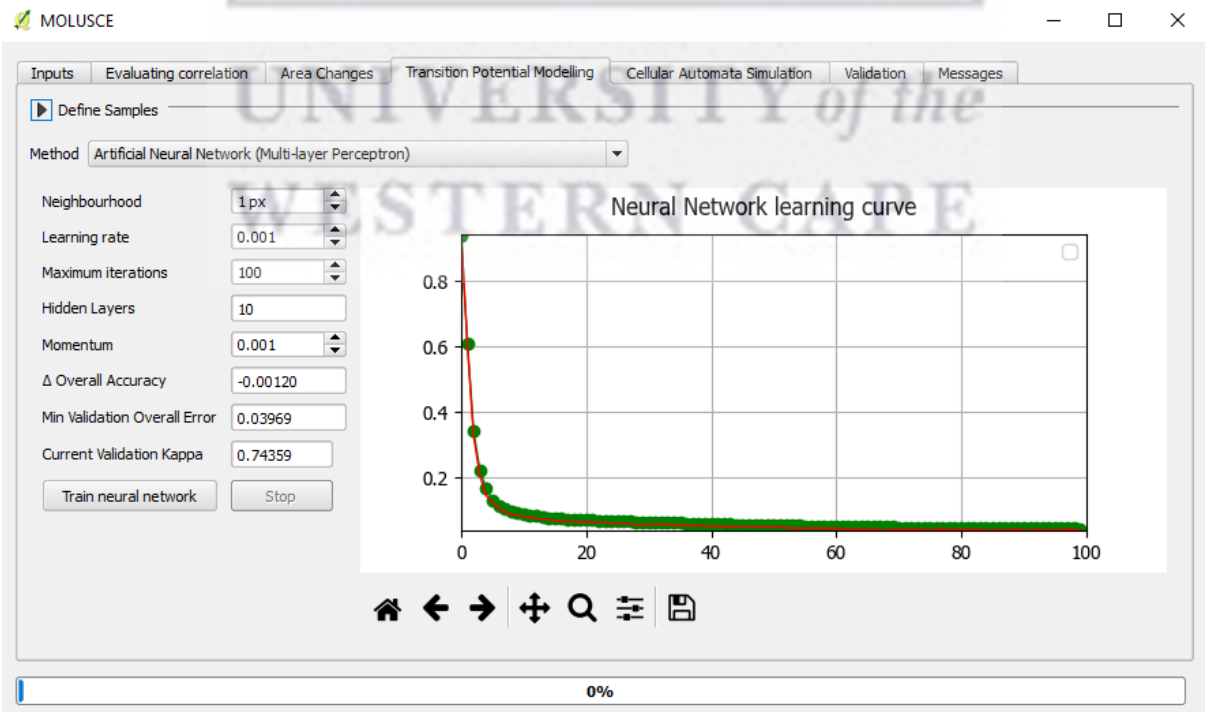

Figure 3. 9: ANN input values for LULC modelling of Luvuvhu catchment.

3.4.4.2.5 Cellular Automata Simulation

After the Kappa value from the previous step is in accordance with the assessment standard, then the third-year LULC change prediction process is conducted using the Cellular Automata (CA) simulation method (Hakim et al., 2018). The third year LULC in this study is 2020. The number of iteration simulations should be filled with the value of 1 (for the validation process first) (MOLUSCE, 2018; Hakim et al., 2019).

3.4.4.2.6 Validation

Validation is a vital part of the LULC prediction approach. At this stage, the functionality, reliability, and acceptance of the model are examined (MOLUSCE 2018; Yatoo et al., 2020; Kafy et al., 2021). In the MOLUSCE plugin, validation is conducted between the reference map (actual third-year LULC) and simulated map (third-year LULC prediction) by calculating the overall accuracy (% of correctness) and Kappa statistics (i.e., overall Kappa, histogram Kappa and location Kappa). When the overall accuracy and Kappa statistics are according to the assessment standard, the CA simulation stage is then used to predict or model future LULC trends. The year of prediction depends on the number of iterations multiplied by the second year minus the first year (Hakim et al., 2019). In this study, the iteration values of 2 and 3 were used for the projection of 2025 and 2030, respectively.

3.5 SWAT model description and application

The SWAT model is a physically based, distributed, daily model developed to simulate water management environments (Arnold et al. 1998). The SWAT model is a hybrid model that operates on the physical processes within the catchment but employs conceptual and empirical algorithms to compute hydrological characteristics (Arnold et al., 2012; Sidle, 2021). Researchers have used the SWAT model to evaluate the impacts of LULC change on catchment hydrology (Mengistu et al., 2019). During simulation, the SWAT model separates the catchment hydrology into two major components i.e., the land phase and the routing phase (Arnold et al., 2012). The land phase regulates the amount of water, nutrients, sediments, and pesticide loadings to the main channel of each sub-basin (Kiros et al., 2015). The routing phase defines the movement of water, sediments, and nutrients to the catchment outlet (Arnold et al., 2012). The SWAT model divides catchments into sub-basins, which are further subdivided into hydrological response units (HRUs) based on LULC, soil type, and slope (Affessa et al., 2022). The hydrological components of the water cycle (i.e., precipitation, surface runoff,

interception, evapotranspiration, percolation, and lateral flow) for each HRU are simulated based on the water balance approach (Lin et al., 2015). The following water balance equation is used:

$$SW_t = SW_O + \sum_{i=1}^{t}\left(R_{day} - Q_{surf} - E_a - W_{seep} - Q_{gw}\right) \quad (3.\ 19)$$

Where, SW_t is the final soil water content (mm), SW_O Is the initial soil water content (mm), t is the time (days), R_{day} is the amount of daily precipitation (mm), Q_{surf} is the amount of surface runoff (mm), E_a is the amount of evapotranspiration (mm), W_{seep} is the amount of water entering the vadose zone from the soil profile (mm), Q_{gw} is the amount of subsurface return flow (mm).

There are two methods provided by the SWAT model that can be used to predict surface runoff, namely: the Soil Conservation Service (SCS) curve number and the Green & Ampt infiltration method (Lin et al., 2015). The SCS curve number equation can be expressed as:

$$Q_{surf} = \frac{\left(R_{day} - 0.2S\right)^2}{\left(R_{day} + 0.8S\right)}, \text{ if } R_{day} > 0.2S;\ Q_{surf} = 0 \quad (3.\ 20)$$

Where, Q_{surf} is the accumulated runoff or rainfall excess (mm), R_{day} is the rainfall depth for the day (mm), S is the retention parameter (mm).

The retention parameter is defined by the following equation:

$$S = 25.4\left(\frac{100}{CN} - 10\right) \quad (3.\ 21)$$

Where, CN is the curve number for the day.

In this study, the SWAT model was run as an extension (QSWAT) on QGIS 3.16.8 where two input datasets (i.e., spatial and weather data) were used to set up the model. The spatial data used during surface runoff simulation include a digital elevation model, LULC maps, and soil data, while the weather data used include daily rainfall, temperature, and relative humidity. The SWAT model was selected due to its accessibility and high computational efficiency. However, the model may also pose difficulties and errors during simulation, therefore educational tutorial videos and user manual guides were used for setting and running the SWAT model.

3.6 SWAT model input data

3.6.1 Digital elevation model (DEM)

A DEM is one of the important input parameters that represent the elevation data of the catchment in the SWAT model. A DEM was clipped and processed in QGIS 3.16.8 software to extract flow direction, flow accumulation and generation of streams. Although a DEM may be obtained at different resolutions, higher resolution provides better topographic details compared to low resolution (Buakhao & Kangrang, 2016). However, for large catchments such as the Luvuvhu catchment using a less detailed DEM helps in data management. Therefore, this study made use of the SRTM at 90 m resolution acquired from the USGS website (https://earthexplorer.usgs.gov/) (Figure 3.10).

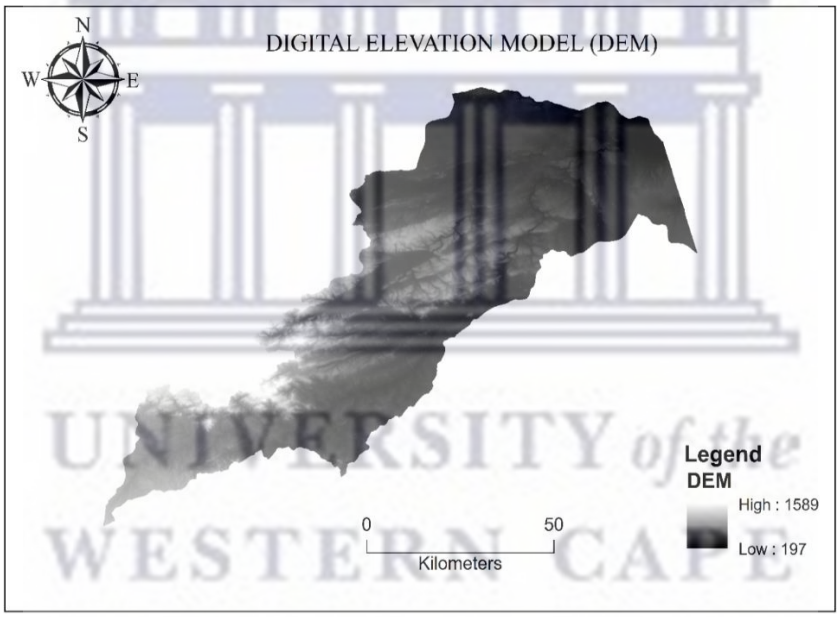

Figure 3. 10: DEM of Luvuvhu catchment.

3.6.2 LULC maps

LULC classes are important in determining the hydrologic response of a catchment. The methodology applied to generate LULC maps was described in Section 3.4.2. LULC maps of two intervals (1990 and 2020) were used to run the SWAT model for surface runoff comparison. The LULC maps comprised six (6) LULC classes namely, waterbody, bare land, built-up, plantation, agricultural land, and natural vegetation. Before modelling, SWAT codes were allocated to each LULC class to establish the relationship between LULC maps and the SWAT model (Table 3.6).

Table 3. 6: LULC types in Luvuvhu catchment.

LULC	SWAT code
Built-up	URBN
Waterbody	WATR
Plantation	FRSE
Agricultural Land	AGRL
Natural Vegetation	MIGS
Bare Land	BARR

3.6.3 Soil map and soil properties

A soil map is also a prerequisite input for running the SWAT model and is important for accurate vegetation cover, nutrient cycling and water yield during simulation. The soil map used for the SWAT model set-up in this study was obtained from the Food and Agriculture Organisation (FAO) of the United Nations with a spatial scale of 1: 5 000 000 (Figure 3.11). The soil map shows five soil units within the Luvuvhu catchment. The identified soil units on the soil map provided the SWAT model with soil properties required for simulation.

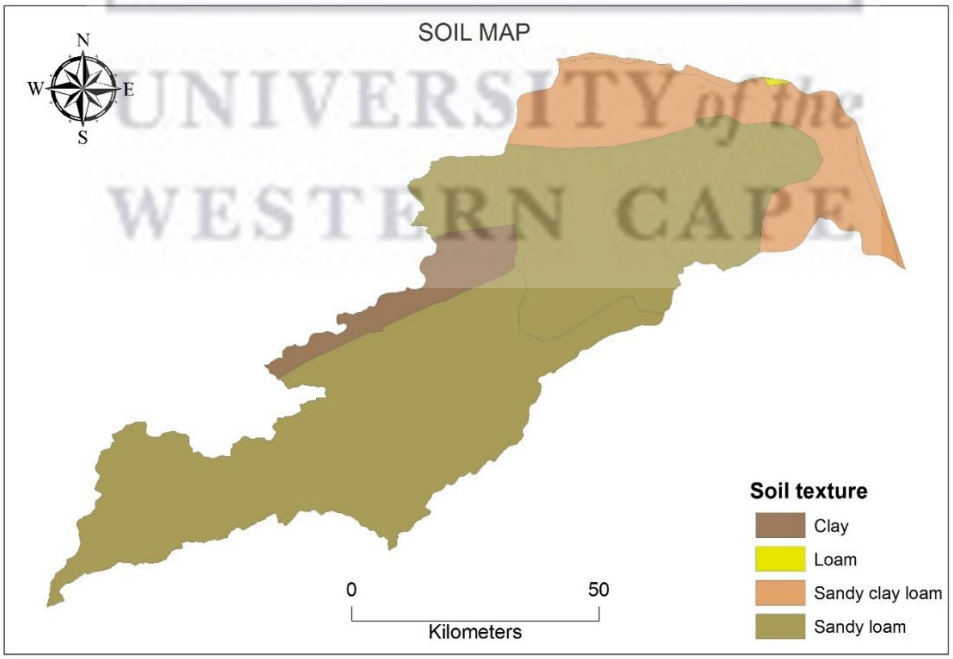

Figure 3. 11: Luvuvhu catchment soil map (Source: FAO).

3.6.4 Weather data

Hydrological modelling requires long-term daily observed weather data for simulation purposes (Sidle, 2021). The meteorological data used during the simulation were obtained from the Agricultural Research Council (ARC) for 6 stations located in the Luvuvhu catchment. The climate data includes precipitation relative humidity, wind speed, and minimum and maximum temperatures from 1990 to 2020. The weather stations used in this study were selected based on data availability and their distribution within the Luvuvhu catchment. Figure 3.12 shows the location of the different weather stations.

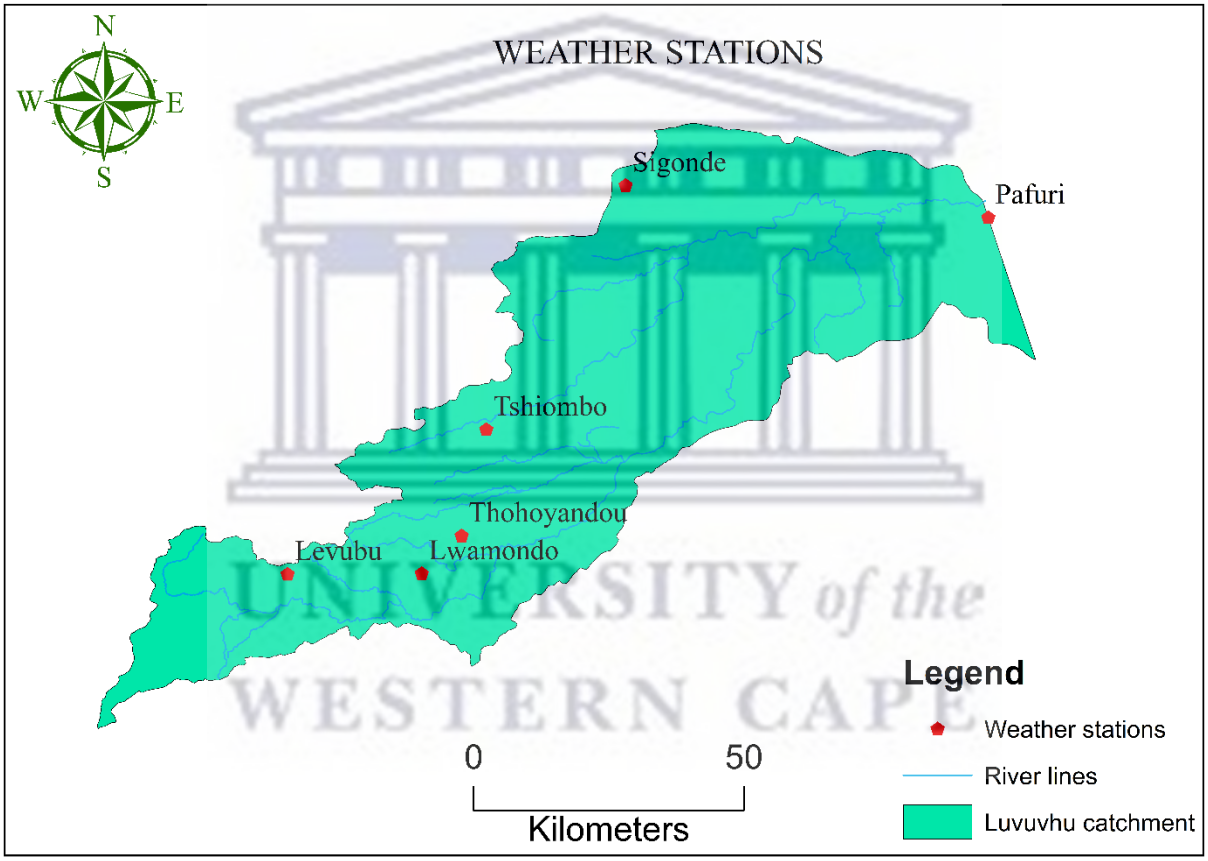

Figure 3. 12: Location of meteorological station used in the study.

3.7 SWAT model setup

The spatial datasets used in the study were referenced in the Universal Transverse Mercator (UTM) zone 36S with WGS 1984 projection to avoid a lack of compatibility between datasets. The model was set to run from 1990 to 2020 including a warm-up period of 2 years to provide stable model conditions. Hence, 31 years was simulated to evaluate the hydrological response to LULC changes in the Luvuvhu catchment. The four main steps implemented to develop the

model for the modelling process on QSWAT include (1) catchment delineation, (2) create HRUs, (3) edit inputs and run QSWAT, and (4) visualise. Figure 3.13 outlines all the procedures followed during the model set-up.

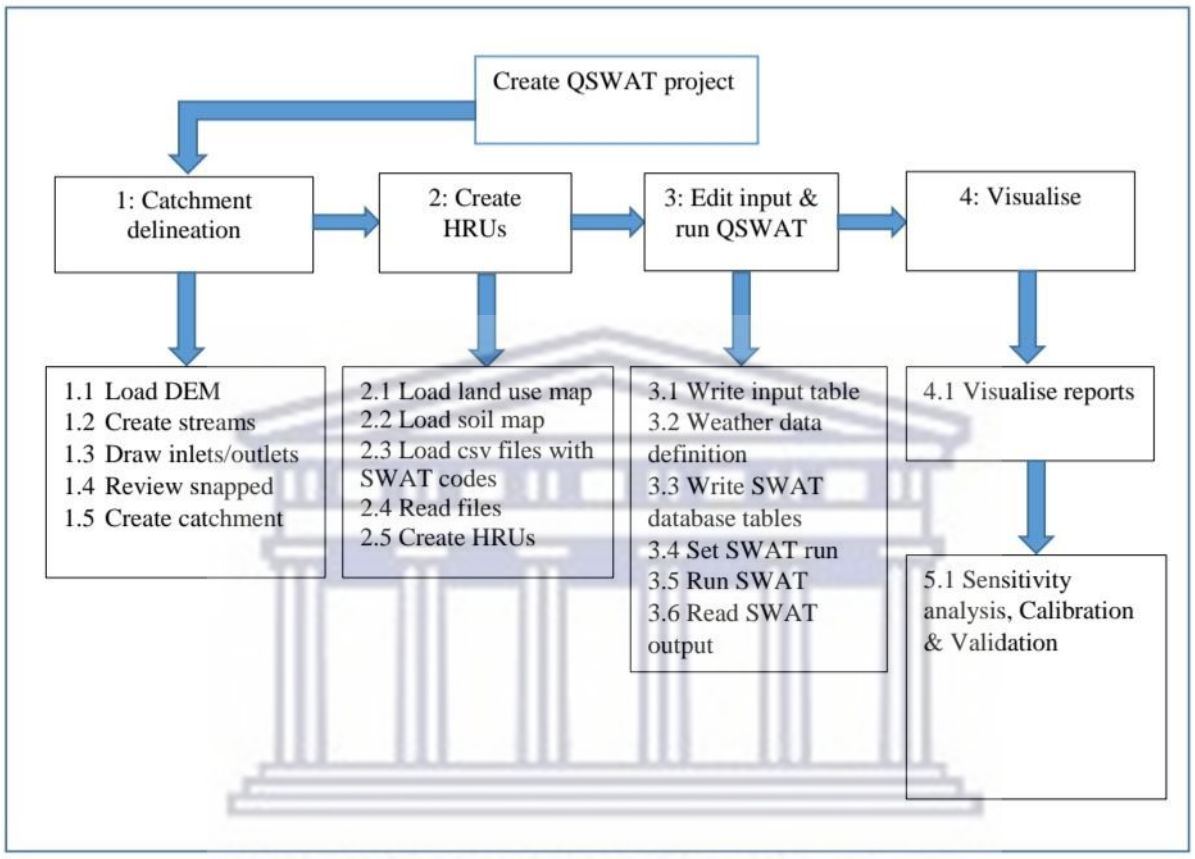

Figure 3. 13: The SWAT model process flow diagram for setup and running QSWAT.

3.7.1 Catchment delineation

The SWAT model consists of two catchment delineation methods, the DEM-based method, and the manual pre-defined method of reaches and sub-basins (Luo et al., 2011). The delineation of the catchment, sub-catchments and stream networks for this study was automatically generated based on the input of the SRTM DEM **(**Figure 3. 10**)**. The SWAT watershed delineation module makes use of the topographic information contained in the DEM. After the DEM was loaded into the SWAT model the streams were created based on the flow direction and flow accumulation observed from the DEM and one outlet was drawn manually. The total area of the delineated Luvuvhu catchment was 184.7 km², which resulted in a total of 17 sub-basins.

3.7.2 Hydrological response units (HRU)

HRUs are land units that have the same topography, soil characteristics and LULC, which are assumed to share similar hydrologic properties (Mengistu et al., 2019). The SWAT Hydraulic Response Unit Analysis Tool conducts the delineation of the HRUs after the catchment is divided into sub-basins. This tool characterises the sub-basins based on slope, land use and soil texture. A user-defined threshold percentage was employed to discretize each sub-basin to delineate the HRUs. The threshold percentage is the amount of LULC, soil or slope that covers a certain area of the sub-basin that is defined in each HRU. This study adopted a threshold percentage of 10 % for LULC, soil type, and slope from the study by Thavhana et al. (2018), which was conducted in the same study area. The HRU delineation process resulted in the generation of 147 HRUs within the 17 delineated sub-basins.

3.7.3 Edit input and run QSWAT

The SWAT Input Editor allows users to identify important input data that is required for the model to run successfully. For all the input data to reflect in the SWAT project, the SWAT input editor was connected to the SWAT project and reference database. During the simulation, each weather station was assigned to a sub-basin based on weather station proximity to import meteorological data. However, in cases where there is no observed weather station located close to the sub-basin, QSWAT simulates weather data automatically from the weather generator (Thavhana et al., 2018). Rainfall, temperature, wind speed, humidity, and solar radiation were used as input data to run the model. The SWAT input tables containing all the data required to run the SWAT model were created. Finally, the SWAT model was set up and run successfully.

3.8 Sensitivity analysis

Sensitivity analysis is the process of examining the influence, significance, and sensitivity of a set of parameters within a catchment (Chilagane et al., 2021). The parameter sensitivity process helps in determining the model simulation accuracy of the hydrological processes within a catchment. Furthermore, sensitivity analysis determines the degree of change in model output given the changes in model input (Arnold et al., 2012). Parameter sensitivity analysis plays a crucial part in identifying the most significant parameters of the model within a given catchment. A considerable number of parameters influence different processes in different catchments; these parameters subject hydrological models to uncertainties (Thavhana et al.,

2018). For this study, sensitivity analysis was achieved using the Sequential Uncertainty Fitting (SUFI-2) in the SWAT calibration uncertainty procedure (SWAT-CUP). The SWAT-CUP provides users with the ability to use a variety of parameters that are responsible for water quality, surface runoff, soil properties, and weather management. The SWAT-CUP also provides the option of two methods for sensitivity analysis namely, local (one-at-a-time) and global sensitivity analysis. This study made use of the global sensitivity analysis, where all parameter values change after each iteration. The parameters used in this study were adapted from the study of Thavhana et al. (2018), which was conducted in the same study area.

3.9 Model calibration, validation, and model performance evaluation

Calibration is the reduction of model uncertainty through better parameterisation under the same given set of catchment conditions (Moriasi et al., 2007; Arnold et al., 2012; Chilagane et al., 2021). Validation is the process of determining the ability of the model to simulate real-world features considering the intended use of the model after calibration. Singh et al. (2010) described validation as evaluating the calibrated model using independent observed data. The calibration and validation of the model were both conducted using the SUFI-2 algorithm in SWAT-CUP. This study made use of the split-sampling method, dividing the observed data into calibration and validation data to ensure data independence. The initial parameter ranges used during calibration are outlined in Table 3.7. Three iterations were conducted for calibration; therefore, all parameter ranges were adjusted after each iteration to eliminate parameter values that ranged outside the absolute SWAT values. Monthly flow data from the periods 1992-1999 and 2006-2012 were used to conduct calibration and validation, respectively, using the observed data from the streamflow gauge A9H013 at the lower part of the Luvuvhu catchment where the outlet is located.

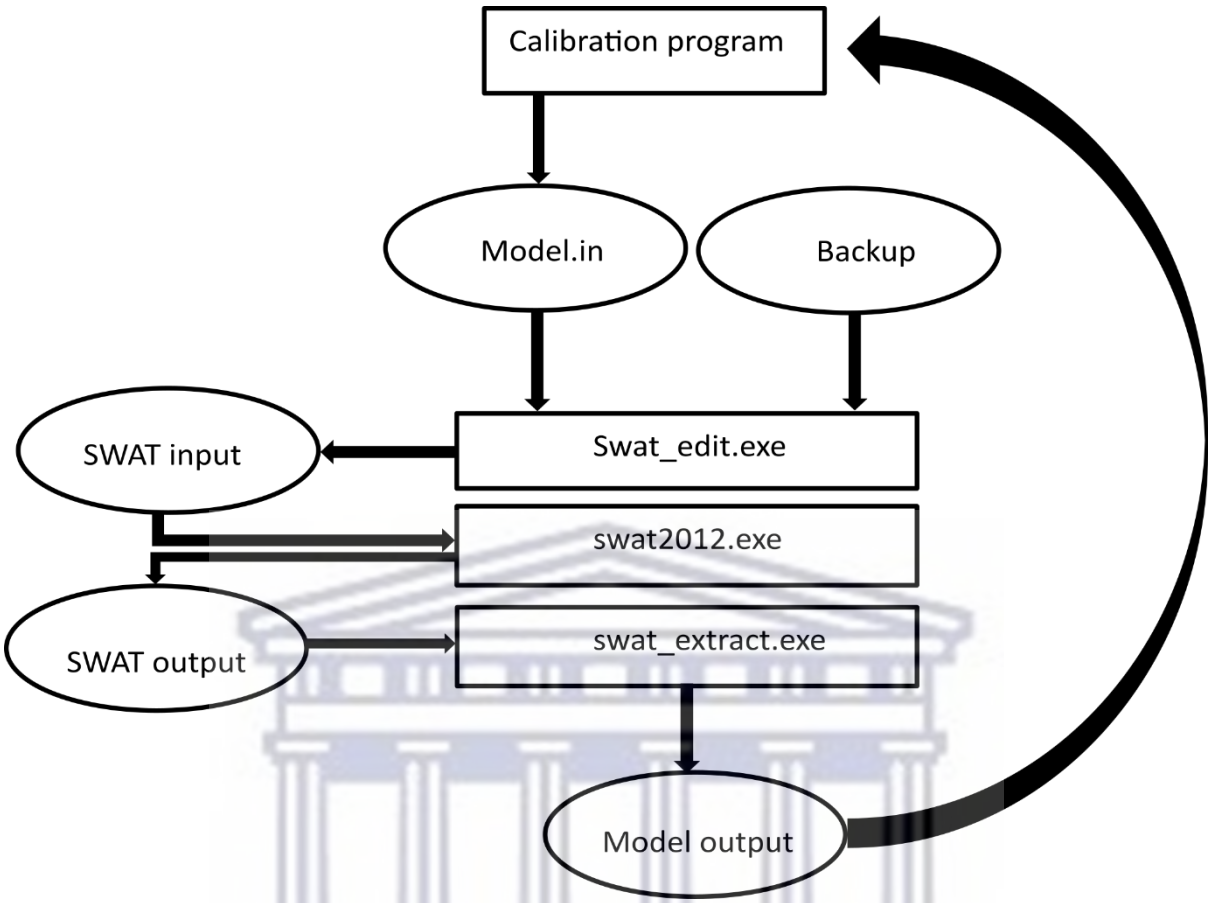

Figure 3. 14: Process of calibration using SWAT-CUP (Afonso De Oliveira Serrão et al., 2022)

Three criteria were used to evaluate SWAT model performance. The model evaluation was based on statistical criteria, which include the Nash-Sutcliffe efficiency (NSE), the coefficient of determination (R^2), and per cent bias (PBIAS). Each performance parameter pertains to a specific purpose during the comparison of observed and simulated flows. The NSE determines the proportional amount of the residual variance in relation to the variance of the measured data, to evaluate how best the plot between observed and simulated data fits the 1:1 line. NSE ranges from -∞ to 1, the closer the NSE value is to 1, the higher the accuracy of the model. R^2 represents the strength of the linear correlation that exists between the observed and simulated data and ranges from 0 to 1. R^2 values greater than 0.5 show less error variance and are therefore acceptable measures. PBAIS measures the tendency of the resulting simulated data to be higher or lower than the observed data (Abbas et al., 2016). A positive PBIAS value indicates model underestimation, while a negative PBIAS value shows model overestimation (Moriasi et al., 2007; Abbas et al., 2016). Table 3.7 below shows the model performance assessment criteria based on Moriasi et al. (2007).

Table 3. 7: Hydrological evaluation indices (Moriasi et al., 2007).

Name	Definition	Performance measure
Nash Sutcliffe Efficiency (NSE)	$NSE = 1 - \frac{\sum_{i=1}^{n}(S_i - \bar{s})^2}{\sum_{i-1}^{n}(O_i - \bar{O})^2}$	< 0 Unacceptable > 0.5 Acceptable 1 optimal value
Coefficient of determination (R^2)	$R^2 = \frac{\left[\sum_{i=1}^{n}(O_i - \bar{O})(S_i - \bar{S})\right]^2}{\sum_{i=1}^{n}(O_i - \bar{O})^2 \sum_{i=1}^{n}(S_i - \bar{S})^2}$	> 0.5 Acceptable
Percent bias (PBIAS)	$PBIAS = \frac{\sum_{i-1}^{n}(O_i - S_i) \times 100}{\sum_{i=1}^{n} O_i}$	± 25% Acceptable

CHAPTER 4: RESULTS AND DISCUSSION

4.1 Accuracy assessment of image classification

PA is the ratio of correctly classified testing or validation pixels of a class and the total number of validation pixels of that class (Jensen, 1986). Meanwhile, UA is the ratio of correctly classified validation pixels for a class and the total number of validation pixels classified as fitting to that class (Jensen, 1986). Seven LULC classification images generated for the study period from 1990-2020 (Figure 4.1) attained an estimated overall accuracy in the range of 93% to 98% and Kappa coefficients beyond 0.9, which represents good classification (Aronoff, 1982; Altman, 1991; Muavhi, 2020). The year 2020 attained the highest Kappa coefficient and overall accuracy, in contrast these main accuracy measures were the lowest for the 1995 classification image (Table 4.1). LULC classes attained an estimated producer's accuracy (PA) and user's accuracy (UA) of ≥70%, and commission error (CE) and omission error (OE) of <30% for all classified images. PA is associated with OE, while UA is related to CE (Equations 3.11 and 3.12). As a result, the lower the PA and UA, the higher the misclassification errors i.e., OE and CE, respectively. For instance, in 1990 built-up acquired a PA of 70.03% and an OE of 29.97%, while natural vegetation achieved a UA of 77.73% and a CE of 22.27%.

The confusion matrix reported a PA of <80% for built-up areas in 1990, 1995, 2000 and 2010. These were the years in which built-up areas achieved the lowest PA. Objects such as buildings and roads can be difficult to identify in low and medium-spatial resolution satellite images (i.e., 30 m of Landsat) (Bouzekri et al., 2015; Janiola & Puno, 2018). In addition, although the separability measures of >1.85 are acceptable (Latty and Hoffer, 1980), built-up achieved low separability measures with most LULC classes, particularly in the earlier years of the study period (Figure. 3.2). However, in the later years of the study period i.e., 2015 and 2020, built-up reached a PA of 90% (Table 4.1). As settlements and other infrastructures associated with built-up become dense over time, sensors with medium spatial resolution such as Landsat can allow excellent classification. Waterbody, natural vegetation, and bare land attained PA beyond 90% for the entire study period. Conversely, built-up acquired a UA ranging from 80-100% for all years.

In the case of built-up in 1990, since 70.03% of validation pixels are classified correctly as demonstrated by the PA, the UA parameter is the ratio of correctly classified pixels of built-up (70.03%) and the total number of validation pixels from all LULC classes classified as built-up. In addition, the UA parameter also assesses if the remaining 29.97% representing the OE

of validation pixels of built-up is incorrectly classified as fitting to the remaining five LULC classes. Jensen (1986) describes UA as the precision or reliability of an algorithm in classifying LULC type in the ground. Therefore, the higher UA implies that few to no pixels are misclassified as other LULC classes in the ground. Meanwhile, Muavhi (2020) considers UA as a parameter for estimating the level of confidence that can be attributed to pixels classified as belonging to a land cover type in an image. In general, all LULC classes attained a UA in the range of 80-100% for all years, except for natural vegetation in 1990, which attained a UA of 77.73%. Therefore, a confidence level beyond 80% can be attributed to all classified pixels in the LULC classification images. Consequently, the estimated main accuracy measures (overall accuracy and Kappa coefficient) and accuracies per class (PA, UA, CE, and OE) provide a major platform for the subsequent analysis of LULC spatial distribution and changes.

Table 4. 1: Accuracy assessment of LULC classification in the study area.

1990				
Overall accuracy	94.2731			
Kappa coefficient	0.9274			
Individual accuracy	**Producer's accuracy**	**User's accuracy**	**Commission error**	**Omission error**
Waterbody	99.16	99.72	0.28	0.84
Plantation	99.86	99.59	0.41	0.14
Agricultural Land	97.93	98.71	1.29	2.07
Natural Vegetation	99.85	77.73	22.27	0.15
Bare Land	93.22	98.40	1.60	6.78
Built-up	70.03	100.00	0.00	29.97
1995				
Overall accuracy	93.4750			
Kappa coefficient	0.9077			
Waterbody	97.25	100.00	0.00	2.75
Plantation	96.32	86.50	13.50	3.68
Agricultural Land	70.53	100.00	0.00	29.47
Natural Vegetation	99.66	92.49	7.51	0.34
Bare Land	100.00	94.84	5.16	0.00
Built-up	70.26	100.00	0.00	29.74

2000				
Overall accuracy	95.7162			
Kappa coefficient	0.9460			
Waterbody	100.00	100.00	0.00	0.00
Plantation	97.48	100.00	0.00	2.52
Agricultural Land	98.33	93.41	6.59	1.67
Natural Vegetation	100.00	94.98	5.02	0.00
Bare Land	98.53	92.13	7.87	1.47
Built-up	70.01	100.00	0.00	29.99
2005				
Overall accuracy	96.6128			
Kappa coefficient	0.9570			
Waterbody	99.19	94.25	5.75	0.81
Plantation	92.59	99.81	0.19	7.41
Agricultural Land	99.81	91.20	8.80	0.19
Natural Vegetation	93.51	96.16	3.84	6.49
Bare Land	99.54	98.79	1.21	0.46
Built-up	86.52	97.07	2.93	13.48
2010				
Overall accuracy	94.0982			
Kappa coefficient	0.9261			
Waterbody	100.00	100.00	0.00	0.00
Plantation	78.01	100.00	0.00	21.99
Agricultural Land	98.82	100.00	0.00	1.18
Natural Vegetation	100.00	83.89	16.11	0.00
Bare Land	98.99	97.04	2.96	1.01
Built-up	75.31	98.92	1.08	24.69
2015				
Overall accuracy	95.7533			
Kappa coefficient	0.9453			
Waterbody	100.00	99.55	0.45	0.00
Plantation	99.16	100.00	0.00	0.84

Agricultural Land	96.20	98.33	1.67	3.80
Natural Vegetation	98.33	87.65	12.35	3.62
Bare Land	91.83	97.95	2.05	8.17
Built-up	95.34	80.83	19.17	4.66
2020				
Overall accuracy	98.5845			
Kappa coefficient	0.9453			
Waterbody	100.00	100.00	0.00	0.00
Plantation	97.59	99.42	0.58	2.41
Agricultural Land	99.06	100.00	0.00	0.94
Natural Vegetation	99.34	97.51	2.49	0.66
Bare Land	98.52	98.13	1.87	1.48
Built-up	90.94	92.49	7.51	9.06

4.2 LULC distribution and change over the study period

The patterns of LULC variations in the catchment were estimated from Landsat images using the SVM algorithm. The spatial distribution of LULC in the Luvuvhu catchment from 1990 to 2020 is shown in Figure 4.1. Over the past three decades, plantation and agricultural land were mostly found in the western part of the Upper Luvuvhu catchment. The plantation category is dominated by Eucalyptus plantations which are the most preferred commercial timber plantations in the region since they can generate up to 10 times as much timber per hectare than native species (Bate et al., 1999; Kundu et al., 2015). Plantation was noted to reveal two change patterns during the study period. In 1990, plantation covered an area of 227.9 km² then declined by 96.080 km^2 in 1995, which can be attributed to timber harvesting and forest removal for commercial agriculture and built-up areas. An increasing trend of plantation can be noted from 2005 to 2020, with the catchment having second-highest plantation coverage in 2020. Plantation such as Eucalyptus is a major contributor to the country's economy, thus the increasing trend from 152.9 km² in 2005 to 208.8 km² in 2020. Although the coverage of plantations flactuates due to production over the years, this LULC class shows an overall decrease from 227.9 km² in 1990 to 208.8 km² in 2020. Regardless of vast economic benefits, Eucalyptus plantations may pose many ecological problems (Liu and Li, 2010) such as reducing stream flow and dam levels (Hoogar et al., 2019). In this catchment, the Vondo dam

is one of the most important dams for the supply of water to irrigation schemes and communities in the western parts of the Upper Luvuvhu catchment (Kundu et al., 2015).

Although it is evident in the classification maps that a significant part of the agricultural (cultivated) land spatially falls closer to the plantation region, agricultural land has expanded towards the low-lying areas of the catchment (Figure 4.1). Large-scale commercial agricultural activities are mostly found near the Albasin Dam in the Levubu area, while the northern highlands and the riverbanks mostly consist of small-scale and subsistence farming (Mukwada et al., 2021). The Luvuvhu catchment area is an underdevoloped and economically poor community. Therefore, subsistence farming has increased food security and has played a major role in reducing unemployment in the Luvuvhu catchment. From 1995 to 2020, over a twofold increase in area coverage of agricultural land occurred. Despite numerous benefits from this land cover, agricultural land which depends on surface water bodies for irrigation during dry seasons, can further reduce available water. It has been reported that significant irrigation developments in the Upper Luvuvhu Catchment have resulted in a decrease in water for domestic and industrial supply (Muavhi and Mutoti, 2022).

With regards to a waterbody, this land cover occupied about 5 km^2 of the total area of the catchment in 1990, which dropped to 3 km^2 in 1995. The catchment experienced about threefold increase of waterbody area coverage up to 9 km^2 by 2000. The year 2000 marked one of the heavy rainfall periods in the catchment and severe socio-economic impacts triggered by this heavy rainfall (CRIDF, 2018). The overland flow of rainwater contributed to the increase in the overall area coverage of surface water bodies. Post 2000, the region suffered several episodes of drought from 2002 to 2004 (Mazibuko et al., 2021). Therefore, in 2005 the area coverage of the waterbody decreased to 7 km^2. The year 2005 also marked the completion of the Nandoni Dam, which makes up the Nandoni Dam sub-system, the largest and most recent development in the Luvuvhu Catchment. The main purpose of this dam is to provide regional water supply to Malamulele, Thohoyandou, Louis Trichardt, and surrounding areas as well as the revitalization of 11 km^2 subsistence irrigation schemes (DWA, 2012). From 2010 to 2020 the area coverage of waterbody gradually increased from 24 km^2 in 2010, 25 km^2 in 2015 to 29 km^2 in 2020. The 11 km^2 of Nandoni Dam contributed to the six-fold increase of waterbody in the catchment from 1990 (5 km^2) to 2020 (29 km^2). In general, bare land and natural vegetation were the most dominant land cover types for the study period (Figures 4.2 and 4.3).

From 1990 to 2020, natural vegetation occupied 50% to 80% of the catchment, while bare land occupied up to 45% of the catchment. On the other hand, waterbodies occupied <1% of the area, thus making it the smallest LULC in terms of area coverage. In general, waterbodies, plantations, and agricultural land, occupied less than 6% of the catchment for the entire study period. Natural vegetation suffered extensive losses of up to 1121.730 km^2 from 1990 to 2020. Part of the natural vegetation was lost to built-up and agricultural land particularly in the Upper Luvuvhu catchment where agricultural activities are extensive. Furthermore, due to the population growth that has occurred over the study period, the catchment experienced urban expansion, hence the substantial increase in built-up. The built-up area revealed a continuous increase over the study period. The total area under this LULC class has been 29.9 km^2, 120.4 km^2, and 314 km^2 in 1990, 2005 and 2020, respectively. The tremendous increase in this category can be attributed to the expansion of residential and commercial establishments.

Bare land is the second most dominant LULC class in the Luvuvhu catchment. This class experienced an increase of up to 899.8 km^2 from 1990 to 2020. Bare land dominates the north-west part of the Lower Luvuvhu catchment and is rarely exploited by other LULC classes. The occurrence of bare land in the lower part of the catchment can be attributed to the unfavourable climatic conditions of the area. The lower area of the catchment is characterized by high annual temperature and receives low annual rainfall (Kundu et al., 2015). However, flash floods, which are common in the catchment may result in, sheet, rill, and gully erosion (CRIDF, 2018). Furthermore, the increase in bare land may be due to the removal of vegetation cover due to overgrazing, wood consumption and clay mining (State of Rivers Report, 2001). As stated previously, soil erosion reduces land productivity and can cause sedimentation of catchments downstream, which has negative impacts on water quality and aquatic life (Kundu et al., 2015).

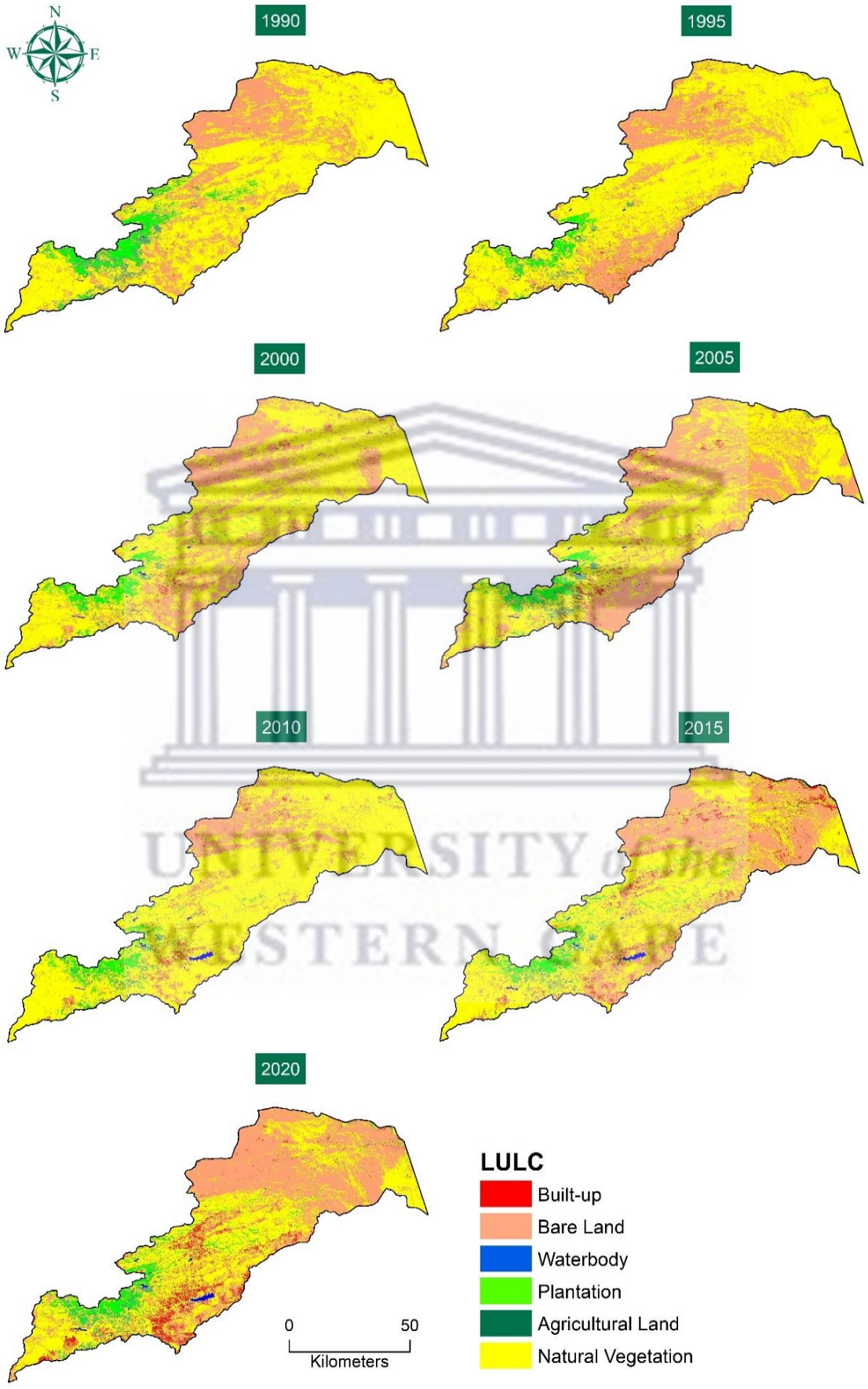

Figure 4. 1: LULC classification maps for the study period.

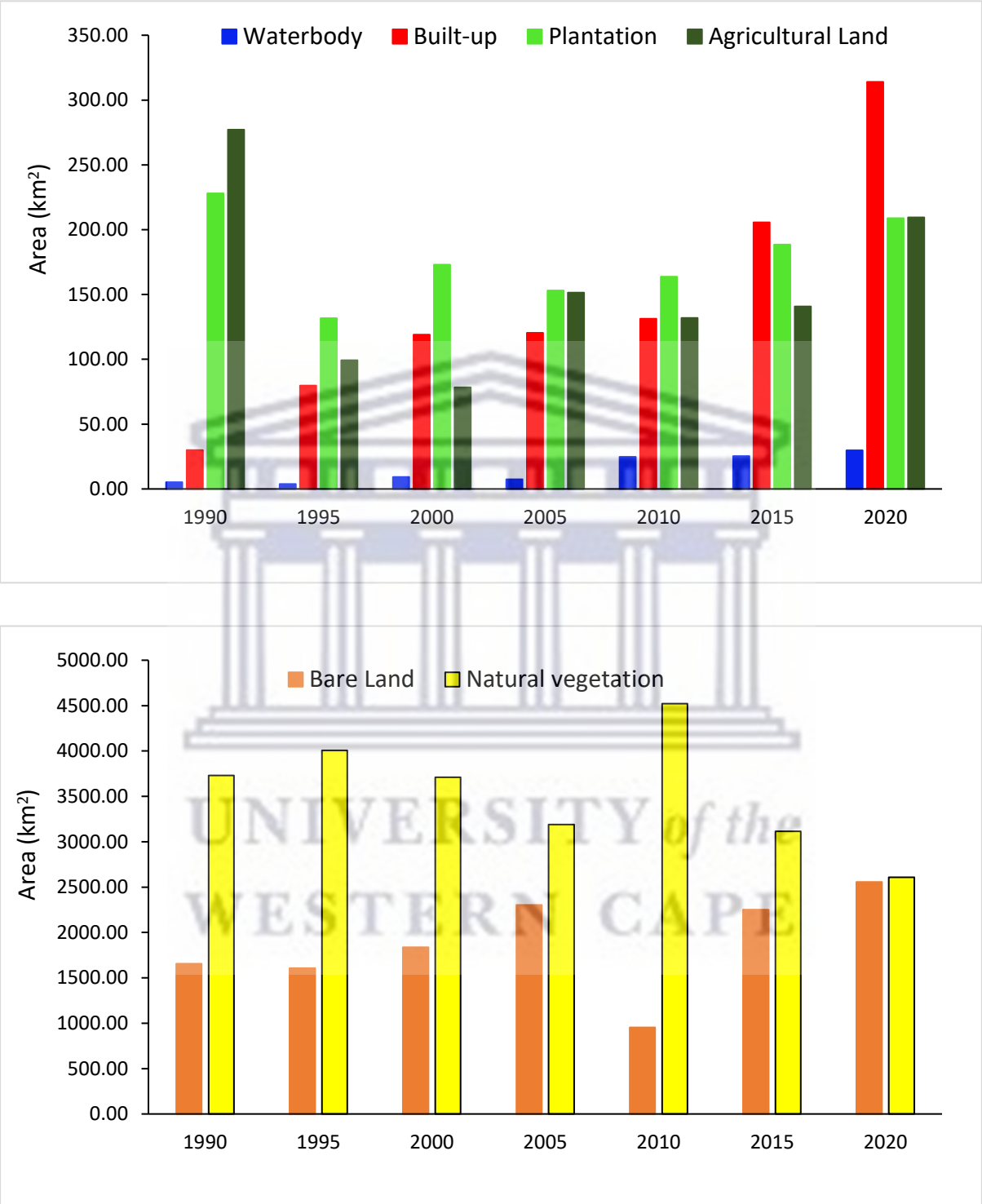

Figure 4. 2: Changes in areas covered by various LULC types during the 1990-2020 period.

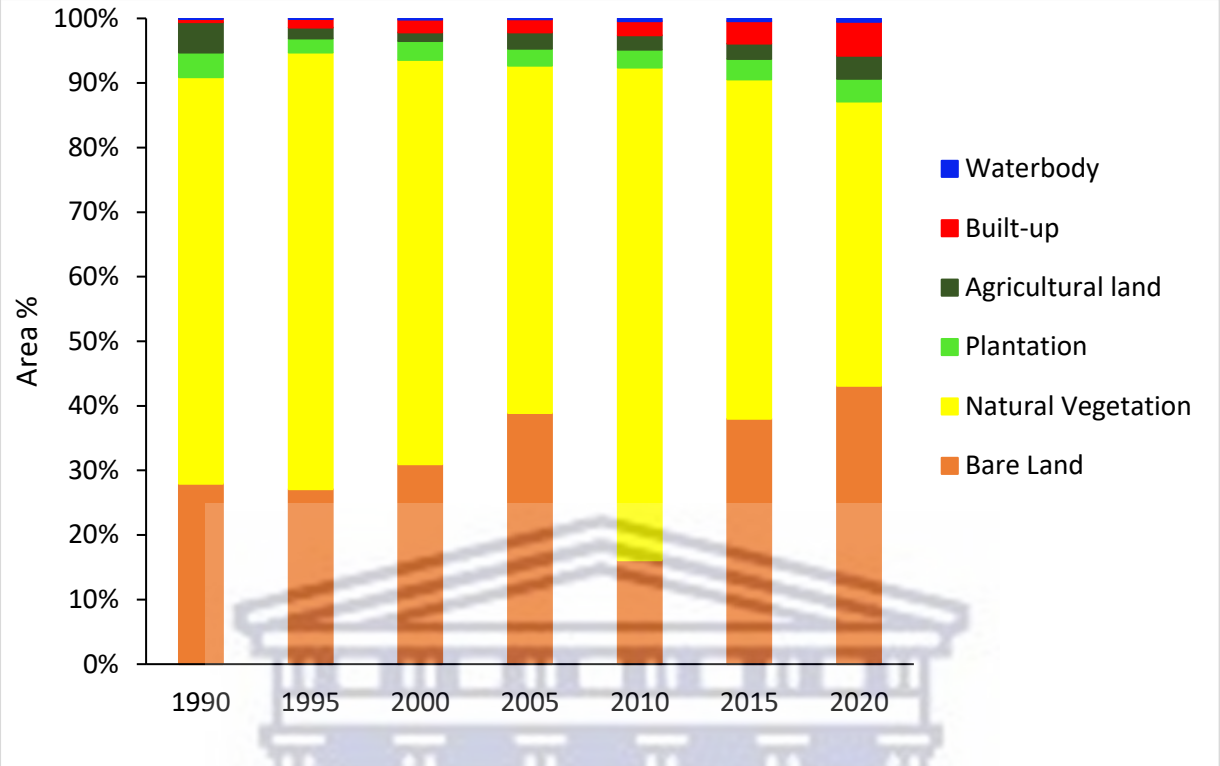

Figure 4. 3: Changes in the proportions of areas under different LULC types.

4.3 LULC modelling

The LULC future prediction was conducted for the years 2025 and 2030. In this study, the ANN-CA-based based simulation model was implemented to predict the future LULC for the Luvuvhu catchment. The projected LULC trends in 2025 and 2030 are shown in Figure 4.5, while the changes in predicted area coverage for the years 2025 and 2030 are shown in Table 4.2 and 4.4, respectively. The expected rate and percentage of future LULC changes were analysed by the transition probability matrix, as shown in Table 4.3 and 4.5 for the years 2025 and 2030, respectively. The transition probability matrix shows the probability/proportions of pixels changing from one LULC to another (MOLUSCE, 2018). The modelled LULC simulation from 2020 to 2025 shows that built-up will increase by about 120 km^2, plantation by 17 km^2, agricultural land by 51 km^2 and bare land by 168 km^2. However, natural vegetation will lose up to 356 km^2 in 2025. Most of the natural vegetation will be converted to bare land (0.185) as shown in the transition probability matrix. The Lower Luvuvhu catchment which is characterized by drought conditions (Kundu et al., 2015) will be covered mostly by bare land. The lower area of the catchment is rarely subjected to agricultural activities, settlement and other expansions that play a role in the removal of natural vegetation. Therefore, the conversion of natural vegetation to bare land may be triggered by harsh climatic conditions that cause

natural desertification. Regardless of having the lowest probability of changing to other LULC classes, waterbody may lose close to 2 km^2 of area coverage from 2020 to 2025. As population growth persists, the volume of water in current waterbodies within the Luvuvhu catchment may decrease due to high water consumption. This corresponds with the study of Oberholster et al., (2008), which predicted that, by the year 2025, the quantity of water sources in Luvuvhu catchment will be reduced and this could lead to the water supply not meeting the demand. The transition probability matrix shows that waterbody is more likely to change to natural vegetation than other LULC classes. Furthermore, water level reduction in waterbodies creates open inland space that could potentially turn into cropland or natural vegetation. It is reported that aquatic invasive plants, particularly algae and reeds which are characterized as natural vegetation in this study, have become a major problem in the Luvuvhu catchment (Makhera et al., 2010), in terms of water quantity and quality. The predicted LULC trends are expected to continue from 2025 to 2030, with natural vegetation being the LULC most susceptible to conversion to other LULC classes. Waterbody will continue to decrease provided there are no dam constructions in the Luvuvhu catchment for the predicted years. While natural vegetation decreases by almost 316 km^2. Agricultural land is expected to continue to increase by 35 km^2, bare land by 176 km^2, built-up area by 104 km^2 and plantation by 1 km^2. The model validation results showed that overall accuracy and Kappa were 84.12 and 0.75, respectively, which is an acceptable accuracy level for LULC modelling (MOLUSCE, 2018; Ullah et al., 2019).

Simulation of future LULC trends is essential, because if transformation continues especially in the case of natural vegetation, the biodiversity and micro-climate of the catchment may be altered (Ullah et al., 2019). The projected LULC trends can be summed up as follows: as population density increases so is the built-up areas and the demand for water and food, which leads to extensive agricultural practices and significant abstraction of water for domestic and agricultural purposes. This results in an increase in agricultural land and built-up to support the growing population. Expansion of agricultural land and urbanization is projected to be mostly at the expense of natural vegetation and bare land which is common in the catchment. Finally, the CA model provides an efficient package for future LULC prediction with more accurate results. It is important to note that the results of the simulation and projection might be affected by factors such as the spatial resolution of the remotely sensed image used, due to the similarity in spectral properties between LULC classes. Furthermore, factors such as climate change, advancement in technology and techniques, and political and economic developments may

influence the resulting future LULC trends. Therefore, further research may consider these variables while predicting LULC trends for better accuracy.

Table 4. 2: LULC trends from 2020 to 2025 in the catchment.

Area	**km^2**			**%**		
LULC	**2020**	**2025**	**Δ**	**2020**	**2025**	**Δ**
Built-up	314.050	435.020	120.970	5.299	7.339	2.041
Waterbody	29.860	28.040	-1.820	0.504	0.473	-0.031
Plantation	208.800	226.260	17.460	3.523	3.817	0.295
Agricultural Land	209.530	261.010	51.480	3.535	4.404	0.869
Natural Vegetation	2608.400	2252.070	-356.330	44.008	37.996	-6.012
Bare Land	2556.440	2724.680	168.240	43.132	45.970	2.838

Table 4. 3: Transition probability matrix results from 2020 to 2025.

LULC	Built-up	Waterbody	Plantation	Agricultural Land	Natural Vegetation	Bare Land
Built-up	0.916	0.000	0.002	0.004	0.076	0.003
Waterbody	0.008	0.939	0.005	0.008	0.039	0.001
Plantation	0.003	0.000	0.976	0.008	0.014	0.000
Agricultural Land	0.030	0.000	0.011	0.749	0.209	0.000
Natural Vegetation	0.004	0.000	0.003	0.035	0.773	0.185
Bare Land	0.051	0.000	0.004	0.003	0.064	0.877

Table 4. 4: LULC change statistics from 2025 to 2030 in the catchment.

Area	**km^2**			**%**		
LULC	**2025**	**2030**	**Δ**	**2025**	**2030**	**Δ**
Built-up	435.020	538.650	103.630	7.339	9.088	1.748
Waterbody	28.040	27.250	-0.790	0.473	0.460	-0.013
Plantation	226.260	227.330	1.070	3.817	3.835	0.018
Agricultural Land	261.010	296.190	35.180	4.404	4.997	0.594
Natural Vegetation	2252.070	1936.480	-315.590	37.996	32.672	-5.325
Bare Land	2724.680	2901.190	176.510	45.970	48.948	2.978

Table 4. 5: Transition matrix results from 2025 to 2030.

LULC	Built-up	Water body	Plantation	Agricultural Land	Natural Vegetation	Bare Land
Built-up	0.915	0.000	0.000	0.002	0.049	0.033
Waterbody	0.004	0.967	0.001	0.003	0.024	0.001
Plantation	0.001	0.000	0.984	0.003	0.011	0.000
Agricultural Land	0.020	0.000	0.001	0.824	0.129	0.025
Natural Vegetation	0.005	0.000	0.002	0.032	0.739	0.222
Bare Land	0.046	0.000	0.000	0.003	0.078	0.873

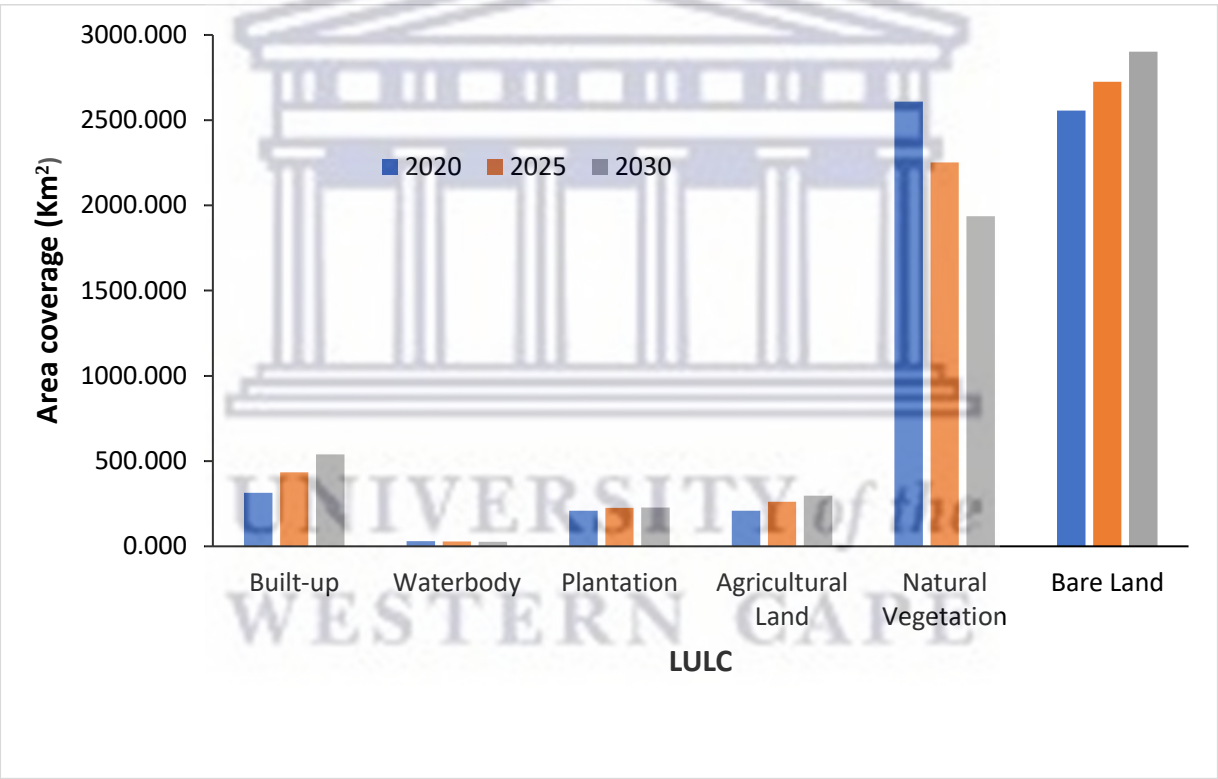

Figure 4. 4: Changes of areas covered by various LULC types projected for the 2020-2030 period.

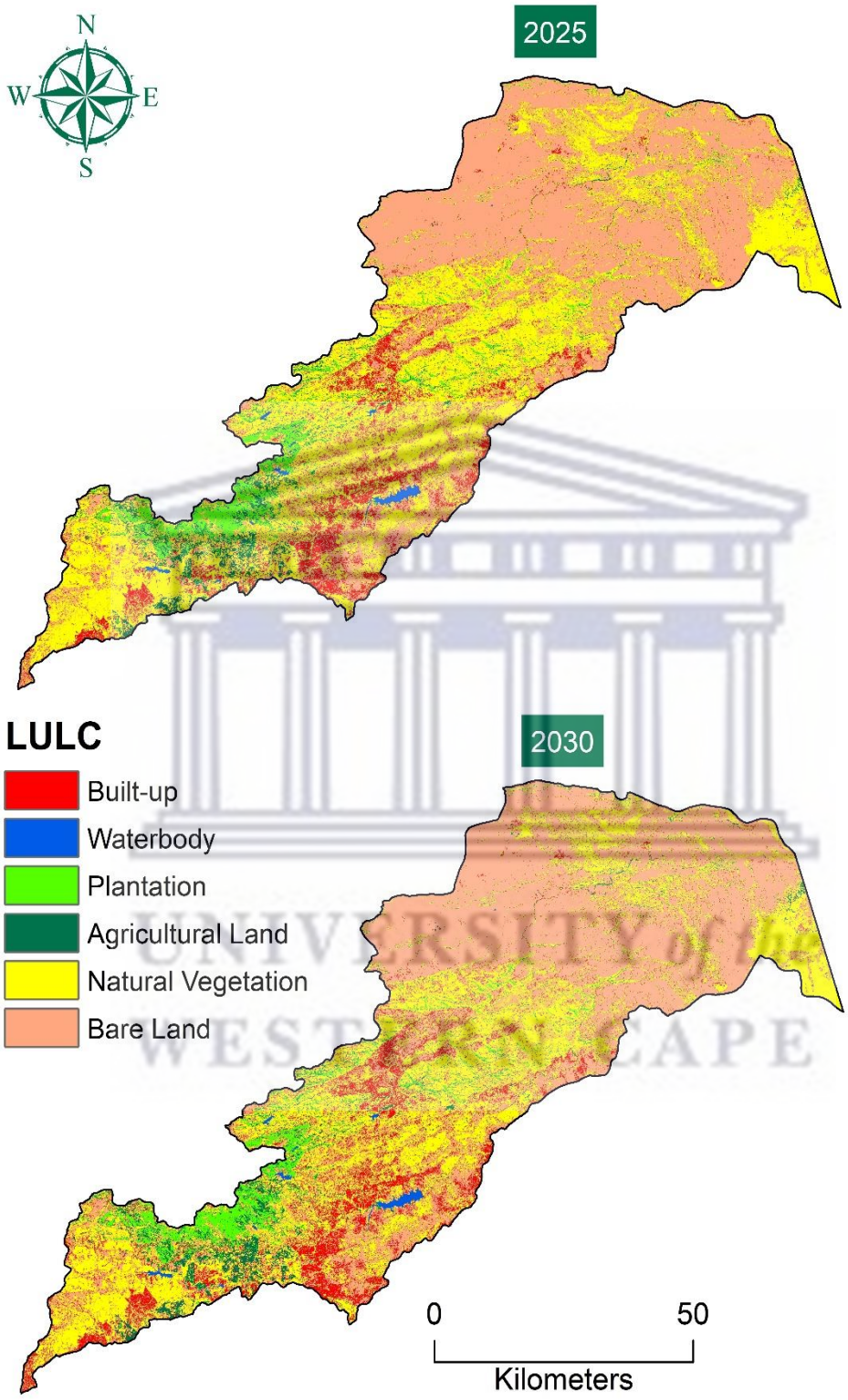

Figure 4. 5: Projected LULC trends for 2025 and 2030 in the Luvuvhu catchment.

4.4 Hydrological response

Hydrological simulation analysis was conducted using the SWAT model, for the assessment of surface runoff response to LULC changes. Surface runoff was determined by the SCS Curve Number approach built within the SWAT model. The model was run for 31years from 1990 to 2020. The simulation of the surface runoff was conducted for two land use periods, 1990 and 2020. Stream flow gauge A9H013 was used for calibration and validation of the model. The location of stream flow gauge A9H013 within the Luvuvhu catchment is shown in Figure 4.6. The calibration and validation results were measured using the model performance criteria R^2, NSE and PBIAS. According to Moriasi et al. (2007), the model performance criteria of R^2 values < 0.5 and NSE values of ≤ 0.5 are unsatisfactory or unacceptable.

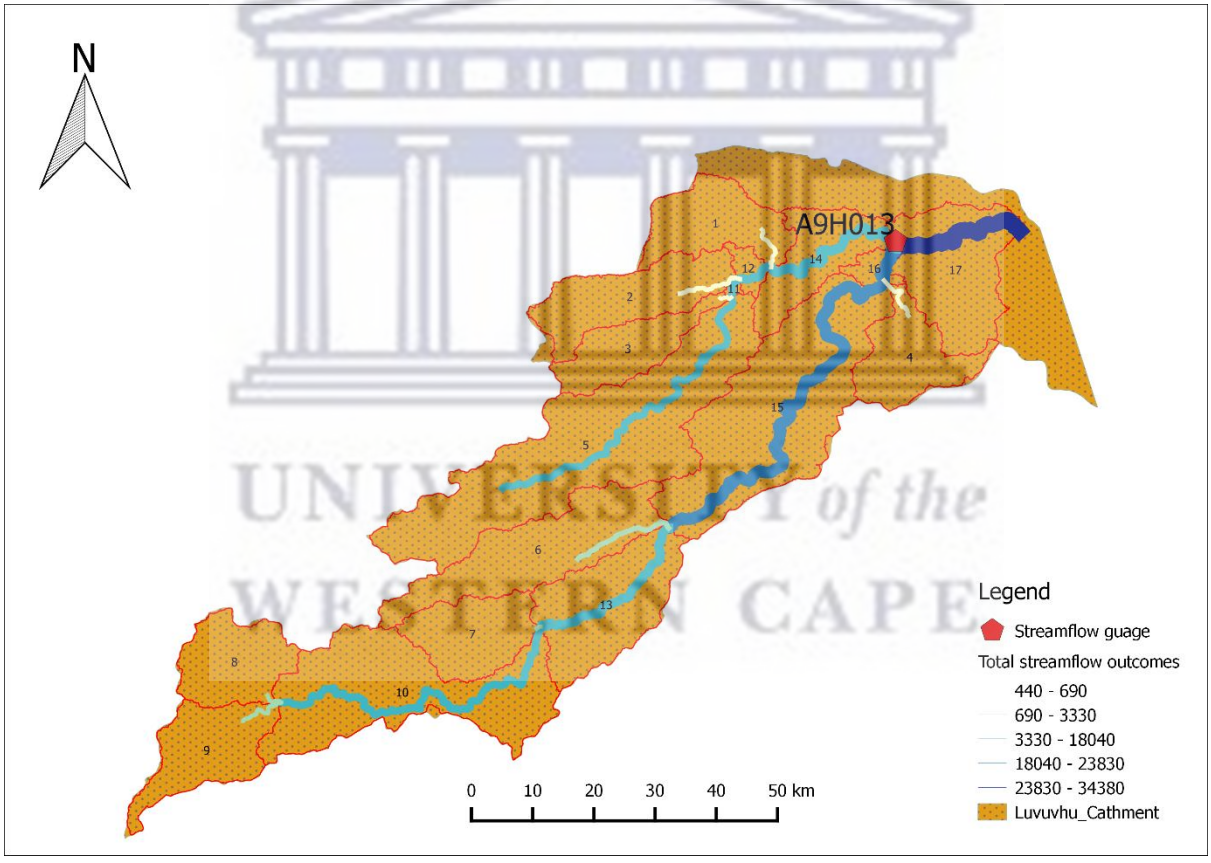

Figure 4. 6: The location of the stream gauge used for observed data.

4.4.1 Sensitivity analysis

A total of 12 parameters were considered and used collectively to assess runoff in the Luvuvhu catchment. The relative (r) and replace (v) methods were used during parameterization for sensitivity analysis, calibration, and validation. With r representing parameters where the existing parameter value is multiplied by (1+ a given value), while v means the existing

parameter value is replaced by the given value. In this study the relative (r) was selected to describe spatially sensitive soil parameters i.e., r__SOL_AWC.sol, r__SOL_K.sol and r__CN2.mgt. Sensitivity analysis results show the three most sensitive parameters for the Luvuvhu catchment. These include v__ALPHA_BNK.rte: Baseflow alpha factor for bank storage, which represents channel water routing processes. The baseflow alpha factor is typically low for steep catchments, and higher (close to 1) for flat catchments (Pandi et al., 2023). Another sensitive parameter was v__ALPHA_BF.gw: Baseflow alpha factor (days), which represents groundwater processes. The value of ALPHA_BF.gw ranges from 0.1 to 0.3 for watersheds that respond slowly to recharge, and from 0.9 to 1.0 for watersheds that respond rapidly to recharge (Qi et al., 2017). The third sensitive parameter identified in the study area was r__CN2.mgt: Initial SCS (Soil Conservation Service) runoff curve number for moisture condition II, which directly controls surface runoff processes. The SCS number is a function of factors such as permeability, soil water properties and land use (Can et al., 2015). The r__CN2.mgt parameter was closely monitored to evaluate how it predicts runoff and infiltration from access rainfall. A decrease of r__CN2.mgt parameter value directly leads to a decrease in surface runoff (Abbas et al., 2016).

Table 4. 6: Sensitive SWAT parameters and final fitted values.

No.	Input Parameter	Description of Parameter	Min range	Max range	Fitted values
1	r__CN2.mgt	Initial SCS (Soil Conservation Service) runoff curve no. for moisture condition II	35	98	0.1949
2	v__ALPHA_BF.gw	Baseflow alpha factor (days)	0	1	0.9487
3	v__GW_DELAY.gw	Groundwater delay time (days)	0	50	0.7283
4	v__GWQMN.gw	Threshold depth of water in the shallow aquifer required for return flow to occur (mm)	0	2000	1574.2635
5	v__GW_REVAP.gw	Groundwater "revap" coefficient	0	0.2	0.04181
6	v__ESCO.hru	Soil evaporation compensation factor	0	1	0.8114
7	v__CH_K2.rte	Effective hydraulic conductivity in main channel alluvium (mm/hr)	50	500	282.7345
8	v__ALPHA_BNK.rte	Baseflow alpha factor for bank storage	0.1	1	0.1008
9	r__SOL_K.sol	Saturated hydraulic conductivity (mm/hr)	0	100	6.5484
10	r__SOL_AWC.sol	Available water capacity of the soil layer (mm/mm)	0	1	0.5925
11	v__SURLAG.bsn	Surface runoff lag coefficient (days)	0	24	5.7019
12	v__REVAPMN.gw	Threshold depth of water in the shallow aquifer for "revap" to occur (mm)	0	500	101.0591

4.4.2 Model calibration, validation, and performance criteria evaluation

The relationship between the average monthly rainfall, the observed monthly runoff, and the simulated monthly runoff in the Luvuvhu catchment was evaluated. Figure 4.7 shows the hydrograph and linear regression graph for the calibration period from 1992 to 1999. Figure 4.8 shows the hydrograph and linear regression graph for the validation period from 2006 to 2012. The hydrographs show the correlation between the observed and simulated runoff data, while the linear regression graphs show the relationship between the observed and simulated data. Although the model can simulate high peak flows, it is apparent from the hydrograph that the model underestimated and overestimated some of the peak flows. The resulting analysis shows that the SWAT model was unable to simulate high flows during calibration and validation. This may be because the SWAT model uses the SCS-CN approach, which defines rainfall events as the sum of rainfall that occurs during a single day and neglects the intensity and duration of the rainfall (Abbas et al., 2016). Therefore, in cases where several storms occur during a single day, the SWAT model is unable to accurately model the specific time of day the rainfall event occurred. According to Abbas et al. (2016), the model tends to overestimate high flows and underestimate low flows. However, in this study, the extent to which peak flows are underestimated is more pronounced than those of the overestimated low flows. During the calibration period, the model slightly underestimated the February 1996 and February 1999 peak flows and further overestimated the low flow in August 1995. During the validation period the model underestimated the peak flow in March 2010. Furthermore, the model overestimated the peak flow in February 2012 and underestimated the low flows in July 2006 and September 2011. The Luvuvhu catchment experiences a wet season between October and April, while a dry season is experienced during winter and spring between May and November (Mathivha et al., 2021). Therefore, the results show that simulated surface runoff is low in the dry season and high during the wet season. The highest simulated peak flow during the calibration period was in February 1996 equalling 568.2 m^3/s for the 1990 LULC period and 567.5 m^3/s for the 2020 LULC period, with an observed runoff of 823.19 m^3/s. This high runoff can be attributed to the 1995-1996 flooding period that occurred in the Luvuvhu catchment (Mukwanda et al., 2021). The lowest simulated peak flow during calibration was in February 1998 equalling 194.9 m^3/s for the 1990 LULC and 198.1 m^3/s for the 2020 LULC, this is even though the rainfall season in the Luvuvhu catchment is between October and April. Mazibuko et al. (2021) linked the years 1997 to 1998 to a prolonged drought season which resulted in the lower peak flows during the local wet season of the catchment. The highest simulated low flows are observed

following the high flow period that occurred in 1996 and 1999. These years are considered to have had a high impact on the runoff in the Luvuvhu catchment area due to the flooding events (Mazibuko et al. (2021). The lowest low flow simulated during the calibration period was 12.59 m³/s for 1990 LULC and 12.21 m³/s for the 2020 LULC observed in August 1994.

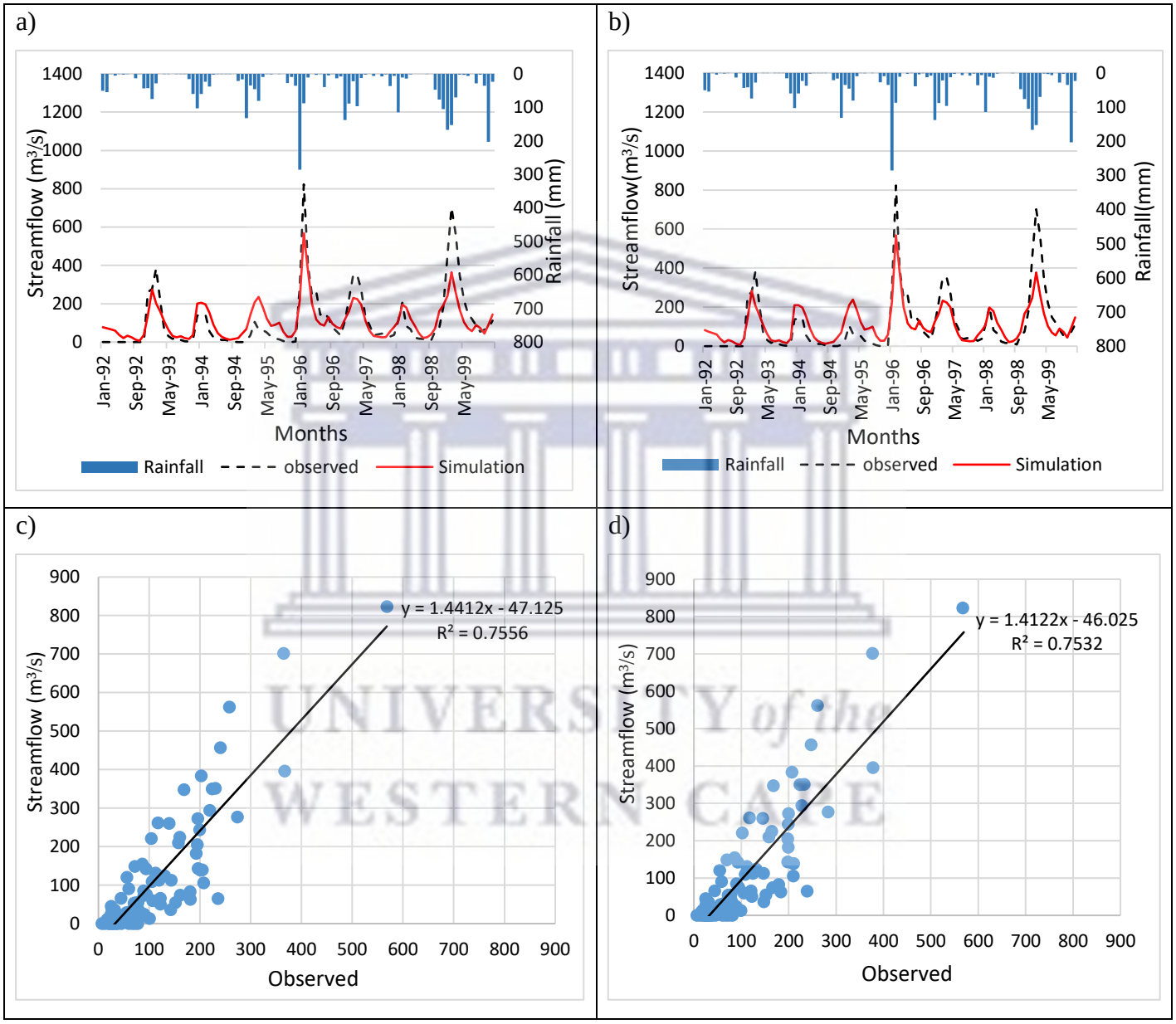

Figure 4. 7: (a) Hydrograph for 1990 LULC, (b) Hydrograph for 2020 LULC, (c) Linear regression graph for 1990 LULC, and (d) Linear regression graph for 2020 LULC for the calibration period (1992-1999).

During the validation period from 2006-2012 Figure 4.8, the highest simulated peak flows were observed in January 2011, equalling 311.9 m³/s for the 1990 LULC period and 320.8 m³/s for the 2020 LULC, while observed was recorded at 291.4 m³/s. The years 2006 and 2011 are associated with high rainfall that resulted in floods in the Luvuvhu catchment (Mukwada et al.,

2021). Lower peak flow during validation was in January 2007 with a simulated runoff of 195.8 m^3/s for the 1990 LULC and 200.8 m^3/s for the 2020 LULC, with an observed runoff of 113.4 m^3/s. Similar to the calibration period, the lower peak flows during the validation period were experienced during confirmed drought seasons in the Luvuvhu catchment. Runoff simulation between wet and dry seasons showed that the wet season obtained better performance. This is supported by Rahbeh et al. (2011) stating that the SWAT model tends to have better simulation performance in wet periods than that in dry periods. Dry seasons experienced low flows as expected in runoff simulation, however, the prediction of low flows can be challenging due to the complex groundwater processes that are linked to the hydrology of low flow (Yuan and Forshay, 2021). Furthermore, low flows are seasonal occurrences that form an essential part of flow regimes (Smakhtin, 2001). The results showed a good correlation between simulated, observed average monthly discharge and average monthly rainfall, these correlations were consistent for both validation and calibration periods.

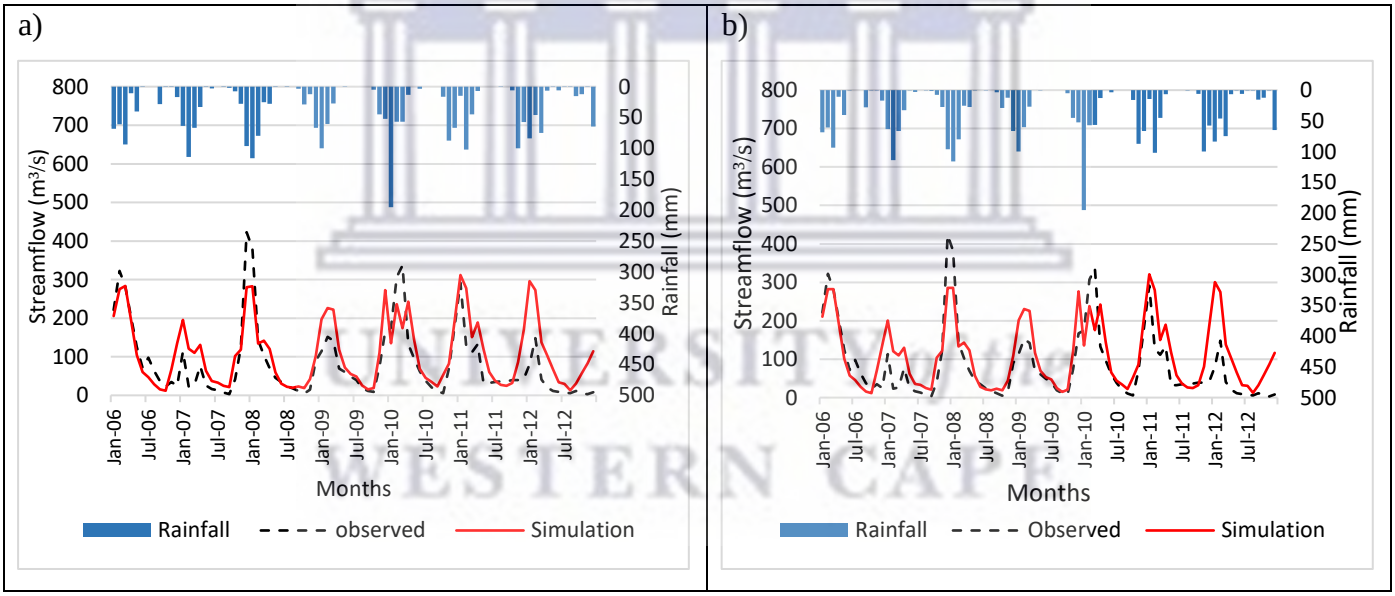

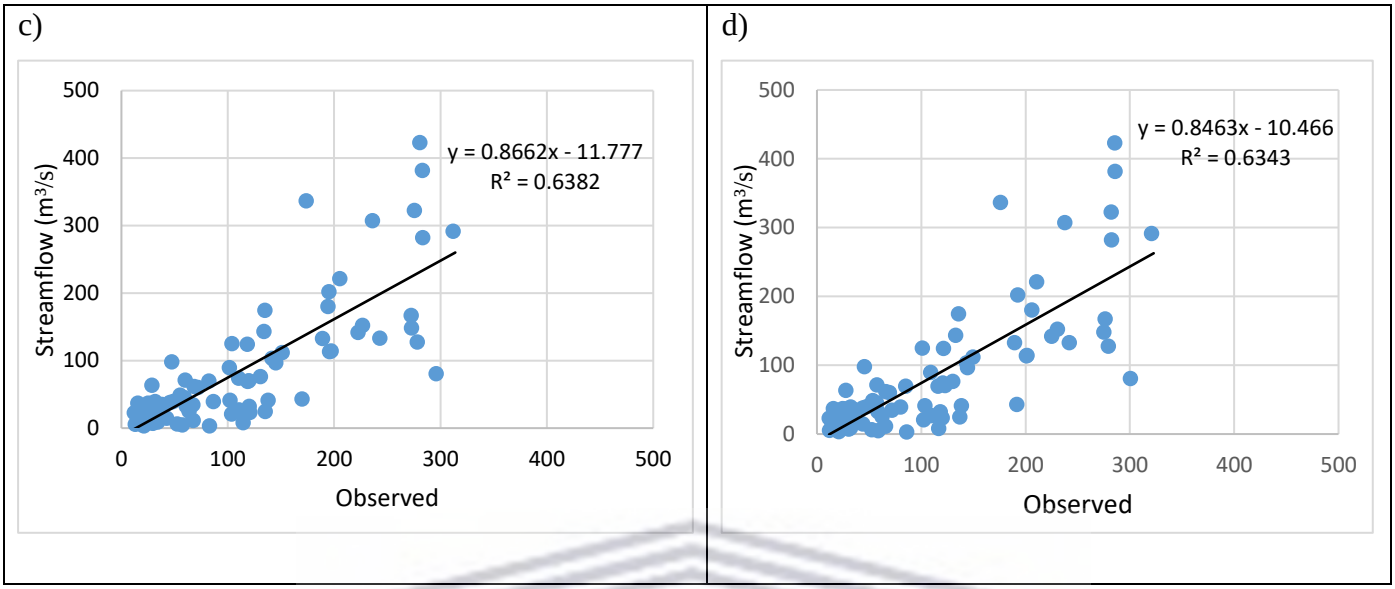

Figure 4. 8: (a) Hydrograph for 1990 LULC, (b) Hydrograph for 2020 LULC, (c) Linear regression graph for 1990 LULC, and (d) Linear regression graph for 2020 LULC for the validation period (2006-2012).

The performance of the simulation during the calibration and validation periods showed good or acceptable model performance criteria. The NSE was used as the major objective function during calibration and validation. The calibration and validation statistics for LULC maps 1990 and 2020 are given in Table 4.7. Model performance for the calibrated period using 1990 LULC map shows satisfactory results with an R^2 value of 0.76, NSE of 0.68 and PBIAS of 0.9. On the other hand, the validation model performance was recorded with an R^2 value of 0.64, NSE of 0.54 and PBIAS of -31.8. The model performance results for the 2020 LULC map in the calibration period show an R^2 value of 0.75, NSE of 0.69 and PBIAS of -4.3 while validation results show an R^2 value of 0.63, NSE of 0.53 and PBIAS of -33.0. These results show a general overestimation of the model due to negative PBIAS. However, the NSE, R^2 and PBIAS results for the calibration periods appear to be better than those recorded for validation periods. According to the performance criteria outlined by Moriasi et al. (2007), the obtained model performance values are satisfactory. This indicates that the calibrated model can be used for various applications such as the impact of LULC change and climate change on surface runoff, water resource planning and water resource management. Therefore, the calibrated model in this study is good enough for the assessment of the impacts of LULC changes on runoff in the Luvuvhu catchment area.

Table 4. 7: Model performance results for calibration and validation.

Model performance criteria		1990 LULC	2020 LULC
NSE	Calibration	0.68	0.69
	Validation	0.54	0.53
R^2	Calibration	0.76	0.75
	Validation	0.64	0.63
PBIAS	Calibration	0.9	-0.4
	Validation	-31.8	-33.0

4.5 The impacts LULC changes on surface runoff

Hydrological modelling was originally developed to evaluate the hydrological response of a particular catchment given its climate, topography, soil and LULC (Sidle, 2021). In this study the SWAT model was used to assess the hydrologic response of the Luvuvhu catchment, which is influenced by both natural and human activities that alter the land cover. Over the years, the SWAT model and GIS based spatial modelling have become essential in the assessment of LULC change impacts on runoff (Kiros et al., 2015). LULC properties aid in regulating water flows above and below the earth's surface, thus the hydrology of a catchment is influenced by the LULC changes that occur in that catchment. In this study, the surface runoff was modelled based on the LULC changes observed from the year 1990 to 2020 for comparison.

Literature suggests that the amount of change in catchment water yield is indirectly proportional to the percentage of forest cover of a catchment. Thus, an increase in vegetation cover results in a decrease in surface flow, while the removal of vegetation cover leads to an increase in surface flow (Affessa et al., 2022). A comparison of LULC maps for the years 1990, 1995, 2000, 2005, 2010 and 2020 indicates that the LULC classes in the Luvuvhu catchment were altered. The built-up area showed a significant increase of 4.8% in the period from 1990 to 2020, as expected. The greatest built-up increase occurred in the later years of the study period (2015-2020); this shows that development in the Luvuvhu catchment is new and highly active. However, the change in built-up is not significant enough to cause great runoff change. Agricultural land showed a fluctuation in the period from 1990 to 2020, however overall results show a decrease from 4.7% to 3.5%. Plantation and natural vegetation show a decrease of 0.3% and 18.9% from 1990 to 2020, respectively. Lastly, bare land in the Luvuvhu catchment increased by 15.2%. Therefore, given the high percentage proportion of change in bare land

and natural vegetation, these two LULC classes may have influenced the change in surface runoff in the Luvuvhu catchment.

The SWAT model was calibrated using the LULC map of 1990 and 2020 to assess the effects of LULC change on surface runoff. The climatic data, soil map and topography used during the simulation of the two land use scenarios were kept constant, while the LULC period map was changed. Components of the water balance such as surface runoff, evapotranspiration and water yield were considered in the assessment of hydrological response to LULC changes after calibration of the model. The simulation results from the two LULC periods showed changes in all hydrological components. The mean annual surface runoff increased from 169.14 mm to 181.49 mm between 1990 and 2020. On average, overall surface runoff increased by 7.3%. In contrast, evapotranspiration decreased from 279.7 mm to 275.08 mm, the reduction of evapotranspiration influences the increase of runoff (Mishra et al., 2014). Evapotranspiration is higher in natural forests than on land cover with sparse vegetation (Owuor et al., 2016). Therefore, the removal of vegetation cover reduces evapotranspiration and increases the rate of surface runoff. Water yield showed little to no change from 557.2 mm to 557.06 mm. Astuti et al. (2019) state that the change in water yield is mostly due to an increase in surface runoff, however, in this study, only a 7% increase was observed, thus the negligible change in water yield. An increase in surface runoff also leads to reduced infiltration and a decrease in groundwater recharge (Mishra et al., 2014). However, the impact of LULC change on groundwater is not discussed in this study. The variation of the hydrological components over the study period supports the impact of LULC changes. The resulting increase in catchment discharge observed in this study was influenced by the LULC changes that occurred in the catchment. The subsequent 18.9% decrease in natural vegetation and the 15.2% increase in bare land caused the change in hydrological components. Serpa et al. (2015) and Wang et al. (2017) stated that deforested lands have high surface runoff and low groundwater recharge than forest areas. Furthermore, agricultural land and bare land require less soil moisture than forest cover or plantation, and rainfall satisfies the soil moisture deficit in these land cover classes more rapidly than in plantations, thus leading to high runoff generation (Deng et al., 2015). Therefore, the LULC changes observed in this study align with the literature, that the reduction of natural vegetation and plantation decreases infiltration thus leading to increased surface runoff (Chilagane et al., 2021).

Table 4. 8: Effect of LULC change on surface runoff

LULC Class description in SWAT	Description of LULC	LULC Change from 1990 to 2020 (%)	Change in runoff (%)
URBN	Built-up	4.793	7.3%
WATR	Water body	0.416	
FRSE	Plantation	-0.322	
AGRL	Agricultural Land	1. 2	
MIGS	Natural Vegetation	-18.933	
BARR	Bare Land	15.188	

CHAPTER 5: CONCLUSIONS AND RECOMMENDATIONS

5.1. Conclusion

The study aimed to assess the impacts of LULC change on surface runoff in the Luvuvhu catchment from 1990 to 2020. To achieve the main objective of the study, a multi-temporal analysis of satellite images and field observations was used for analysing the change in LULC. A process-based hydrological modelling approach was used to evaluate the impacts of LULC change on surface runoff. Mathematical models, Cellular Automata, Markov Chain Projection Model, and the semi-distributed Soil Water Assessment Tool (SWAT) model were used to analyse the collected data sets. Landsat imagery (Landsat 5 TM and Landsat 8 OLI) was used to determine the spatiotemporal patterns of LULC in the study area from 1990 to 2020. LULC classification over the study period revealed that the major changes in the Luvuvhu catchment were the increment of bare land and the reduction of natural vegetation. Bare land increased by 15.2% at the expense of natural vegetation which decreased by 18.9%. The LULC classification results showed overall accuracies ranging from 93% to 98% and Kappa coefficients beyond 0.9 which indicate a good classification. The LULC predictions from 2020 to 2025 show that, built-up, plantation, agricultural land and bare land will continue to increase, while natural vegetation and waterbody decreases. Overall LULC classification and future projection results outline the LULC changes that have and continue to occur within the Luvuvhu catchment. Future LULC predictions for 2025 and 2030 show that the observed LULC trends will persist until the year 2030. Natural vegetation in the Lower part of the catchment will mostly be converted to bare land, and agricultural activities will continue to expand due to the persisting population growth. The results from the SWAT model simulation show that LULC changes have a significant impact on surface runoff and other hydrological components. The simulated results showed an increase in the mean annual surface runoff of 7.3% between the two LULC maps from 169.14 mm in 1990 to 181.49 mm in 2020. SWAT simulation also shows a slight overestimation of daily peak flows and better simulations in low flows. This may be attributed to the daily runoff variation during wet and dry seasons. Furthermore, the distinct shift from the rainy season to the dry season is clearly simulated. However, simulation results show satisfactory model performance for both calibration and validation. The study concludes the increase in surface runoff in the Luvuvhu catchment was due to the 18.9% decrease in natural vegetation, as well as the 15.2% increase in bare land. Thus, the results show that the surface runoff in the Luvuvhu catchment was altered due to the

significant LULC changes detected in the two classes during LULC modelling. Due to the predicted continuation of LULC changes, surface runoff has the potential to continue increasing which may cause catchment management problems such as flooding, and erosion of riverbanks or stream channels due to high peak flow rate. Therefore, developing catchment management strategies is of great importance and will play a key role in reducing the effects of LULC changes.

5.2. Recommendations

The results acquired in this study were dependent on LULC changes and provided some insight into the implications of LULC changes on runoff. There is a need for future studies to isolate the effect of variations in climatic data for different years or different LULC scenarios. This may provide a holistic view of how additional factors affect runoff in the Luvuvhu catchment. The assessment of LULC change impacts on future runoff and groundwater is also of significance and has not been discussed in detail in this study. There are limited studies that have investigated the impact of LULC change on groundwater recharge. Future research may focus on the impacts of LULC change on groundwater availability and the rate at which groundwater is changing in the Luvuvhu catchment. In addition, future research may predict the availability of groundwater based on the prediction of LULC changes. This study emphasizes that land use problems such as the impacts of LULC changes on runoff are influenced by unregulated LULC changes. Land use planners and policymakers should focus on developing sustainable land use methods that will have minimum effects on surface runoff for better management of water resources.

REFERENCES

Abbas T, Nabi G, Boota MW, Hussain F, Azam MI, Jin H, and Faisal M. (2016). Uncertainty analysis of runoff and sedimentation in a forested watershed using sequential uncertainty fitting method. *Sciences in Cold and Arid Regions*, 8(4), 0297–0310.

Affessa, G. M., Belew, A. Z., Tenagashaw, D. Y., and Tamirat, D. M. (2022). Land use/cover change impacts on hydrology using SWAT model on Borkena watershed, Ethiopia. *Water Conservation Science and Engineering*, *7*(1), 55–63.

Afonso De Oliveira Serrão, E., Silva, M. T., Ferreira, T. R., Paiva De Ataide, L. C., Assis Dos Santos, C., Meiguins De Lima, A. M., De Paulo Rodrigues Da Silva, V., De Assis Salviano De Sousa, F., and Cardoso Gomes, D. J. (2022). Impacts of land use and land cover changes on hydrological processes and sediment yield determined using the SWAT model. *International Journal of Sediment Research*, *37*(1), 54–69.

Alawamy, J. S., Balasundram, S. K., Mohd. Hanif, A. H., and Boon Sung, C. T. (2020b). Detecting and Analyzing Land Use and Land Cover Changes in the Region of Al-Jabal Al-Akhdar, Libya Using Time-Series Landsat Data from 1985 to 2017. *Sustainability*, 12(11), 4490.

Altman, D.G. (1991). Practical statistics for medical research: London, Chapman and Hall.

Anand, J., Gosain, A. and Khosa, R. (2018). Prediction of land use changes based on Land Change Modeler and attribution of changes in the water balance of Ganga basin to land use change using the SWAT model. *Science of the Total Environment*, *644*, 503-519.

Angelaki, A., Nain, S. S., Singh, V., and Sihag, P. (2018). Estimation of models for cumulative infiltration of soil using machine learning methods. ISH *Journal of Hydraulic Engineering*, 1-8.

Aplin, P., (2004). Remote sensing: land cover. Progress in Physical Geography, 28, 283-293.

Arnold J. G, Moriasi D. N, Gassman P. W, Abbaspour K. C, White M. J, Srinivasan R, Santhi C, Harmel R. D, van Griensven A, Van Liew M. W, Kannan N, Jha M. K. (2012). SWAT: Model use, calibration and validation. *American Society of Agricultural and Biological Engineers* 55: 1491-1508.

Arnold J. G., Srinivasan R., Muttiah R. S. and Williams J. R. (1998). Large area hydrologic modelling and assessment part I: model development. *Journal of the American Water Resources Association 34*, 73–89.

Aronoff, S. (1982). The map accuracy report-A user's view: Photogrammetric Engineering and Remote Sensing, v. 48(8), 1309-1312.

Aspinall, R. (2004). Modelling land use change with generalized linear models—a multi-model analysis of change between 1860 and 2000 in Gallatin Valley, Montana. *Journal of Environmental Management*, *72*(1-2), 91-103.

Astuti, I. S., Sahoo, K., Milewski, A., and Mishra, D. R. (2019). Impact of land use land cover (LULC) change on surface runoff in an increasingly urbanized tropical watershed. *Water Resources Management*, *33*, 4087-4103.

Babykalpana, Y. and ThanushKodi, K. (2010). Supervised/ Unsupervised Classification of LULC using remotely Sensed Data for Coimbatore city, India. International Journal of Computer Applications, vol. 2(7), 26-30.

Ban Y., Yousif O. (2016). Change Detection Techniques: A Review. In: Ban Y. (ed.) Multitemporal Remote Sensing. Remote Sensing and Digital Image Processing, vol 20. Springer, Cham.

Bate, R.R., Tren, R. and Mooney, L. (1999). An econometric and institutional economic analysis of water use in the Crocodile River Catchment, Mpumalanga province, South Africa, WRC report No. 885/1/99, Pretoria, South Africa.

Bell, E.J. and Hinojosa, R.C. (1977). Markov analysis of land use change: continuous time and stationary processes. Socio-Economic Planning Sciences, vol. 11(1), 13-17.

Beven, K. J., Lamb, R., Kirkby, M. J., & Freer, J. E. (2020). A history of TOPMODEL. *Hydrology and Earth System Sciences Discussions*, *2020*, 1-44.Boerner, R.E., DeMers, M.N., Simpson, J.W., Artigas, F.J., Silva, A. and Berns, L.A. (1996). Markov models of inertia and dynamism on two contiguous Ohio landscapes. Geographical. Analysis, vol. 28(1), 56-66.

Bouzekri, S., Lasbet, A. A., and Lachehab, A. (2015). A new spectral index for extraction of built-up area using Landsat-8 data. *Journal of the Indian Society of Remote Sensing*, *43*, 867-873.

Bovolo, F.B. and Bruzzone, L. (2007). A theoretical framework for unsupervised change detection based on change vector analysis in the polar domain. IEEE Transactions on Geoscience and Remote Sensing, vol. 45, 218-236.

Briassoulis, H. (2020). Analysis of Land Use Change: Theoretical and Modelling Approaches. Regional Research Institute, West Virginia University.

Bristow, J.W. and Venter, F.J.1986. Notes on the Permian to recent geology of the Kruger National Park,-Koedoe 29:85-104 Pretoria.ISSN 0075-6458.

Buakhao, W., and Kangrang, A. (2016). DEM resolution impact on the estimation of the physical characteristics of watersheds by using SWAT. *Advances in Civil Engineering*, *2016*.

Can, T., Xiaoling, C., Jianzhong, L., Gassman, P. W., Sabine, S., and José-Miguel, S. P. (2015). Assessing impacts of different land use scenarios on water budget of Fuhe River, China using SWAT model. *International Journal of Agricultural and Biological Engineering*, *8*(3), 95-109.

Chang, C. C., and Lin, C. J. (2001). Training v-support vector classifiers: theory and algorithms. *Neural Computation* , *13*(9), 2119-2147.

Chang, C.I. (ed.). (2003). Hyperspectral Imaging: Techniques for Spectral Detection and Classification. Kluwer Academic, New York.

Chemura, A., Rwasoka, D., Mutanga, O., Dube, T. and Mushore, T., (2020). The impact of land-use/land cover changes on water balance of the heterogeneous Buzi sub-catchment, Zimbabwe. *Remote Sensing Applications: Society and Environment*, 18, 100292.

Chilagane, N. A., Kashaigili, J. J., Mutayoba, E., Lyimo, P., Munishi, P., Tam, C., and Burgess, N. (2021). Impact of land use and land cover changes on surface runoff and sediment yield in the Little Ruaha River Catchment. *Open Journal of Modern Hydrology*, *11*(3), 54-74.

Claassen, M. (1996). Assessment of selected metal and biocide bioaccumulation in fish from the Berg, Luvuvhu, Olifants and Sabie Rivers, South Africa (Master's degree). University of Johannesburg.

CRIDF (Climate Resilient Infrastructure Development Facility). (2018). Investing £24,000 in flood forecasting systems in the Limpopo River Basin saves £140,000 per annum in flood damage.

Cunjak, R., Linnansaari, T. and Caissie, D., (2013). The complex interaction of ecology and hydrology in a small catchment: a salmon's perspective. *Hydrological Processes*, 27(5), 741-749.

Dabboor, M., Howell, S., Shokr, M. and Yackel, J. (2014). The Jeffries–Matusita distance for the case of complex Wishart distribution as a separability criterion for fully polarimetric SAR data. *International Journal of Remote Sensing*, vol. 35 (19), 6859-6873.

Dang, A. N., and Kawasaki, A. (2017). Integrating biophysical and socio-economic factors for land-use and land-cover change projection in agricultural economic regions. *Ecological Modelling*, *344*, 29–37.

Deng, X., Shi, Q., Zhang, Q., Shi, C., and Yin, F. (2015). Impacts of land use and land cover changes on surface energy and water balance in the Heihe River Basin of China, 2000–2010. *Physics and Chemistry of the Earth, Parts* A/B/C, 79-82, 2-10.

Department of Statistics South Africa. (2022). *Mid-year population estimates*. Pretoria: Statistics South Africa, 1-5.

Devia, G., Ganasri, B. and Dwarakish, G. (2015). A Review on Hydrological Models. *Aquatic Procedia*, 4, 1001-1007.

Dewan, A. and Yamaguchi, Y. (2008). Using remote sensing and GIS to detect and monitor land use and land cover change in Dhaka Metropolitan of Bangladesh during 1960–2005. *Environmental Monitoring and Assessment*, 150(1-4), 237-249.

Dixon, B., and Earls, J. (2012). Effects of urbanization on streamflow using SWAT with real and simulated meteorological data. Applied *Geography*, 35(1-2), 174-190.

DWA – Department of Water Affairs, 2012. Minister Establishes Nine (9) Catchment Management Agencies, March 30th, 2012. DWA, Pretoria.

Dwarakish, G. and Ganasri, B. (2015). Impact of land use change on hydrological systems: A review of current modeling approaches. *Cogent Geoscience*, 1(1), 1115691.

Falcucci, A., Maiorano, L. and Boitani, L., (2006). Changes in land-use/land-cover patterns in Italy and their implications for biodiversity conservation. *Landscape Ecology*, 22(4), 617-631.

Geist, H. and Lambin, E. (2002). Proximate Causes and Underlying Driving Forces of Tropical Deforestation. *BioScience*, 52(2), 143.

Gessesse, B., Bewket, W. and Bräuning, A. (2014). Model-Based Characterization and Monitoring of Runoff and Soil Erosion in Response to Land Use/land Cover Changes in the Modjo Watershed, Ethiopia. *Land Degradation & Development*, *26*(7), 711-724.

Getahun, Yitea and HAJ, Van. (2015). Assessing the Impacts of Land Use-Cover Change on Hydrology of Melka Kuntrie Subbasin in Ethiopia, Using a Conceptual Hydrological Model. *Journal of Wastewater Treatment & Analysis.* 06. 10.4172/2157-7587.1000210.

Ghosh, P., Mukhopadhyay, A., Chanda, A., Mondal, P., Akhand, A., Mukherjee, S., Nayak, S.K., Ghosh, S., Mitra, D., Ghosh, T. and Hazra, S. (2017). Application of Cellular automata and Markov-chain model in geospatial environmental modeling- A review, Remote Sensing Applications: Society and Environment, vol. 5, 64-77.

Gibson, L., Münch, Z., Palmer, A. and Mantel, S. (2018). Future land cover change scenarios in South African grasslands – implications of altered biophysical drivers on land management. *Heliyon*, 4(7), e00693.

Goshu, E. L. (2010). *Faculty of Science Department of Earth Sciences Remote sensing and GIS Stream* (Doctoral dissertation, Addis Ababa University).

Götze, A., Cilliers, S., Bezuidenhout, H. and Kellner, K. (2003). Analysis of the riparian vegetation (Ia land type) of the proposed Vhembe-Dongola National Park, Limpopo Province, South Africa. *Koedoe*, 46(2).

Griscom, H. R., Miller, S. N., Gyedu-Ababio, T., and Sivanpillai, R. (2009). Mapping land cover change of the Luvuvhu catchment, South Africa for environmental modelling. *GeoJournal*, *75*(2), 163–173.

Guo, Y., Fang, G., Xu, Y.-P., Tian, X., and Xie, J. (2020). Identifying how future climate and land use/cover changes impact streamflow in Xinanjiang Basin, East China. *Science of the Total Environment, 710,* 136275.

Guzha, A., Rufino, M., Okoth, S., Jacobs, S., and Nóbrega, R. (2018). Impacts of land use and land cover change on surface runoff, discharge and low flows: Evidence from East Africa. *Journal of Hydrology: Regional Studies*, 15, 49-67.

Hakim, A.M.Y., Baja, S., Rampisela, D.A. and Arif, S. (2019). Spatial dynamic prediction of land use land cover change (case study: Tamalanrea sub-district, Makassar city), in: IOP Conference Series: Earth and Environmental Science. *Institute of Physics Publishing*, vol. 280, 012023.

Hassaballah, K., Mohamed, Y., Uhlenbrook, S. and Biro, K. (2017). Analysis of streamflow response to land use and land cover changes using satellite data and hydrological modelling: case study of Dinder and Rahad tributaries of the Blue Nile (Ethiopia–Sudan). *Hydrology and Earth System Sciences*, 21(10), 5217-5242.

Herold, M., Scepan, J. and Clarke, K. (2002). The Use of Remote Sensing and Landscape Metrics to Describe Structures and Changes in Urban Land Uses. *Environment and Planning A: Economy and Space*, 34(8), 1443-1458.

Hoogar, R., Malakannavar, S. and Sujatha, H.T. (2019). Impact of eucalyptus plantations on ground water and soil ecosystem in dry regions. *Journal of Pharmacognosy and Phytochemistry*, vol. 8(4), 2929-2933.

Hope, R., Jewitt, G. and Gowing, J. (2004). Linking the hydrological cycle and rural livelihoods: a case study in the Luvuvhu catchment, South Africa. *Physics and Chemistry of the Earth*, Parts A/B/C, 29(15-18), 1209-1217.

Hosseini, M. and Ashraf, M. (2015). Application of Hydrological Models Related to Land Use Land Cover Change. *Application of the SWAT Model for Water Components Separation in Iran*, 1-32.

Hu, Q., Willson, G. D., Chen, X., and Akyuz, A. (2005). Effects of climate and landcover change on stream discharge in the Ozark Highlands, USA. *Environmental Modeling & Assessment*, 10(1), 9-19.

Huang, Y., Yang, B., Wang, M., Liu, B. and Yang, X. (2020). Analysis of the future land cover change in Beijing using CA–Markov chain model. *Environmental Earth Sciences*, vol. 79(2).

Islam, K., Jashimuddin, M., Nath, B. and Nath, T.K. (2018). Land use classification and change detection by using multi-temporal remotely sensed imagery: The case of Chunati wildlife sanctuary, Bangladesh. *The Egyptian Journal of Remote Sensing and Space Science*, vol 20 (1), p. 37-47.

Janiola, M.D.C. and Puno, G.R. (2018). Land use and land cover (LULC) change detection using multi-temporal Landsat imagery: A case study in Allah Valley Landscape in Southern, Philippines. *Journal of Biodiversity and Environmental Sciences*, vol. 12(2), 98-108.

Jensen, J.R. (1986). Introductory digital image processing: New Jersey, Englewood Cliffs, Prentice-Hall.

Jewitt, G. P. W., Garratt, J. A., Calder, I. R., and Fuller, L. (2004). Water resources planning and modelling tools for the assessment of land use change in the Luvuvhu Catchment, South Africa. *Physics and Chemistry of the Earth, Parts A/B/C*, *29*(15–18), 1233–1241.

Jingan, S., Jiupai, N., Chaofu, W., and Deti, X. (2005). Land use change and its corresponding ecological responses: A review. *Journal of Geographical Sciences*, *15*(3), 305–328.

Jogun, T., Lukic´, A. and Gasˇparovic´, M. (2019). Simulation model of land cover changes in a post-socialist peripheral rural area: Pozˇega-Slavonia County, Croatia. Hrvatski Geografski Glasnik, vol. 81(1), 31-59.

Kafi, K.M., Shafri, H.Z.M. and Shariff, A.B.M. (2014). An analysis of LULC change detection using remotely sensed data, A Case study of Bauchi City. *IOP Conference Series: Earth and Environmental Science*, vol. 20(2014), 012056.

Kafy, A.-A., Naim, M.N.H., Subramanyam, G., Faisal, A.-A.-, Ahmed, N.U., Rakib, A. A. and Sattar, G.S. (2021). Cellular Automata approach in dynamic modelling of land cover changes using RapidEye images in Dhaka, Bangladesh. Environmental Challenges, 4, 100084.

Keerthi, S.S. and Lin. C.J. (2003). Asymptotic behaviours of support vector machines with Gaussian kernel. Neural Computation, vol. 15(7), 1667-89.

Khawaldah, H.A. (2016). A Prediction of Future Land Use/Land Cover in Amman Area Using GIS-Based Markov Model and Remote Sensing. *Journal of Geographic Information System*, vol. 8, p. 412-427.

Kindu, M., Schneider, T., Teketay, D. and Knoke, T. (2015). Drivers of land use/land cover changes in Munessa-Shashemene landscape of the south-central highlands of Ethiopia. *Environmental Monitoring and Assessment*, 187(7).

Kiros, G., Shetty, A. and Nandagiri, L. (2015). Performance Evaluation of SWAT Model for Land Use and Land Cover Changes under different Climatic Conditions: A Review. *Journal of Wastewater Treatment & Analysis*, 06(03).

Kundu, P., Mathivha, T. and Nkuna, T. (2015). The Use of GIS and Remote Sensing Techniques to Evaluate the Impact of Land use and Land Cover Change on the Hydrology of Luvuvhu River Catchment in Limpopo Province. WRC Report No. 2246/1/15, Pretoria, South Africa.

Kundu, P., Singo, R., Odiyo, J., Mathivha, F., and Nkuna, R. (2013). Extraction and analysis of morphologic and hydrologic properties for Luvuvhu River Catchment in Limpopo province, South Africa. *Water and Society*.

Lambin, E. F., Rounsevell, M. D., and Geist, H. J. (2000). Are agricultural land-use models able to predict changes in land-use intensity? *Agriculture, Ecosystems & Environment*, *82*(1-3), 321-331.

Lambin, E., Geist, H. and Lepers, E. (2003). Dynamics of Land-Use and Land-Cover Change in Tropical Regions. *Annual Review of Environment and Resources*, 28(1), 205-241.

Lambin, E., Turner, B., Geist, H., Agbola, S., Angelsen, A., Bruce, J., Coomes, O., Dirzo, R., Fischer, G., Folke, C., George, P., Homewood, K., Imbernon, J., Leemans, R., Li, X., Moran, E., Mortimore, M., Ramakrishnan, P., Richards, J., Skånes, H., Steffen, W., Stone, G., Svedin, U., Veldkamp, T., Vogel, C. and Xu, J. (2001). The causes of land-use and land-cover change moving beyond the myths. *Global Environmental Change*, 11(4), 261-269.

Lambin, E.F. (2004). Modelling land-use change. *Environmental Modelling: Finding Simplicity in Complexity, London*, 245-254.

Latty, R.S. and Hoffer, R.M. (1980). Waveband evaluation of proposed Thematic Mapper in forest cover classification. Proc. of the Fall Technical Meeting, ACSM-ASP, Niagara Falls, New York, 1-12.

Li, G., Zhang, F., Jing, Y., Liu, Y., and Sun, G. (2017). Response of evapotranspiration to changes in land use and land cover and climate in China during 2001–2013. *Science of The Total Environment*, 596–597, 256–265. doi.org/10.1016/j.scitotenv.2017.04.080.

Li, P., Li, H., Yang, G., Zhang, Q. and Diao, Y. (2018). Assessing the Hydrologic Impacts of Land Use Change in the Taihu Lake Basin of China from 1985 to 2010. *Water*, 10(11), 1512.

Lin, B., Chen, X., Yao, H., Chen, Y., Liu, M., Gao, L., and James, A. (2015). Analyses of landuse change impacts on catchment runoff using different time indicators based on SWAT model. Ecological Indicators, 58, 55–63.

Liping, C., Yujun, S. and Saeed, S. (2018). Monitoring and predicting land use and land cover changes using remote sensing and GIS techniques—A case study of a hilly area, Jiangle, China. *PLOS ONE*, 13(7), e0200493.

Liu, H. and Li, J. (2010). The Study of the Ecological Problems of Eucalyptus Plantation and Sustainable Development in Maoming Xiaoliang. *Journal of Sustainable Development*, vol. 3(1), 197-201.

Liu, M., and Hu, D. (2019). Response of Wetland Evapotranspiration to Land Use/Cover Change and Climate Change in Liaohe River Delta, China. *Water*, 11(5), 955.

Liu, Y., Zhuang, Q., Chen, M., Pan, Z., Tchebakova, N., Sokolov, A., Parfenova, E. (2013). Response of evapotranspiration and water availability to changing climate and land cover on the Mongolian Plateau during the 21st century. *Global and Planetary Change*, 108, 85-99.

Livesley, S. J., Baudinette, B., and Glover, D. (2014). Rainfall interception and stem flow by eucalypt street trees – The impacts of canopy density and bark type. *Urban Forestry & Urban Greening, 13(1)*, 192–197.

Lo, C.P. and Yang, X. (2002). Drivers of land-use/land-cover changes and dynamic modeling for the Atlanta, Georgia metropolitan area. *Photogrammetric Engineering and Remote Sensing*, *68*(10), 1073-1082.

Lørup, J. K., Refsgaard, J. C., and Mazvimavi, D. (1998). Assessing the effect of land use change on catchment runoff by combined use of statistical tests and hydrological modelling: Case studies from Zimbabwe. *Journal of Hydrology, 205*(3–4), 147–163.

Lothar, H., Dieter, F., Puzicha, J. and Buhmann, J.M. (1999). Support vector machines for land usage classification in LANDSAT TM imagery. Proc. of IGARSS, vol. 1, 348-350.

Luo, Y., Su, B., Yuan, J., Li, H., and Zhang, Q. (2011). GIS techniques for watershed delineation of SWAT model in plain polders. *Procedia Environmental Sciences*, *10*, 2050-2057.

Makhera, M., Gumbo, J. R. and Chigayo, K. (2010). Monitoring of microcystin-LR in Luvuvhu River catchment: Implications for human health. *African Journal of Biotechnology*, vol. 10(3), 405-412.

Mallupattu, P. and Sreenivasula Reddy, J. (2013). Analysis of Land Use/Land Cover Changes Using Remote Sensing Data and GIS at an Urban Area, Tirupati, India. *The Scientific World Journal*, 2013, 1-6.

Manoj, J., Subramonia, R.S., Srinivasan, K.S., Pathak, S. and Sharma, J.R. (2013). Class Separability Analysis and Classifier Comparison using Quad-polarization Radar Imagery. *Journal of Indian Society of Remote Sensing*, vol. 41(1), p. 177-182.

Mas, J. F., Kolb, M., Paegelow, M., Olmedo, M. T. C., & Houet, T. (2014). Inductive pattern-based land use/cover change models: A comparison of four software packages. *Environmental Modelling & Software*, *51*, 94-111.Matheussen, B., Kirschbaum, R.L., Goodman, I.A., O'Donnell, G.M., Lettenmaier, D.P. (2000). Effects of land cover change on streamflow in the interior Columbia River Basin (USA and Canada). *Hydrological Processes 14*, 867–885.

Mathivha, F., Kundu, P., and Singo, L. (2016). The impacts of land cover change on stream discharges in Luvuvhu River Catchment, Vhembe District, Limpopo Province, South Africa. *Urban Water III*.

Mathivha, F., Nkosi, M. and Mutoti, M. (2021). Evaluating the relationship between hydrological extremes and groundwater in Luvuvhu River Catchment, South Africa. *Journal of Hydrology: Regional Studies*, 37, 100897.

Maviza, A., and Ahmed, F. (2020). Analysis of past and future multi-temporal land use and land cover changes in the semi-arid Upper-Mzingwane sub-catchment in the Matabeleland south province of Zimbabwe. *International Journal of Remote Sensing*, 41(14), 5206–5227.

Mazhar, F. and Fadia, F. (2019). A Time Series Analysis of Satellite Imageries for Land Use & Land Cover (LULC) Change Detection of Gujranwala City, Pakistan from 1999-2019. *Indian Journal of Science and Technology*, vol. 12(46), 1-9.

Mazibuko S.M., Mukwada G. and Moeletsi M.E. (2021). Assessing the frequency of drought/flood severity in the Luvuvhu River catchment, Limpopo Province, South Africa. *Water SA*, 47(2 April).

Mazvimavi, D., Madamombe, E. and Makurira, H. (2007). Assessment of environmental flow requirements for river basin planning in Zimbabwe. *Physics and Chemistry of the Earth, Parts A/B/C*, 32(15-18), 995-1006.

Mengistu, A. G., van Rensburg, L. D., and Woyessa, Y. E. (2019). Techniques for calibration and validation of SWAT model in data scarce arid and semi-arid catchments in South Africa. *Journal of Hydrology: Regional Studies*, *25*, *100621*.

Mengistu, T., Chung, I., Kim, M., Chang, S. and Lee, J. (2022). Impacts and Implications of Land Use Land Cover Dynamics on Groundwater Recharge and Surface Runoff in East African Watershed. *Water*, 14(13), 2068.

Mishra, N., Khare, D., Gupta, K. K., and Shukla, R. (2014). Impact of land use change on groundwater—a review. *Advances in Water Resource and Protection*, *2*(28), 28-41.

MOLUSCE. (2018). MOLUSCE modules for land use change evaluation-Quick help. https://github.com/nextgis/molusce/blob/master/doc/en/QuickHelp.pdf. Accessed 28 September 2021.

Moriasi D. N., Arnold J. G., Van Liew M. W., Bingner R. L., Harmel R. D., and Veith T. L. (2007). Model Evaluation Guidelines for Systematic Quantification of Accuracy in Watershed Simulations. Transactions of the ASABE, 50(3), 885-900.

Muavhi, N. (2020). Evaluation of effectiveness of supervised classification algorithms in land cover classification using ASTER images-A case study from the Mankweng (Turfloop) Area and its environs, Limpopo Province, South Africa. *South African Journal of Geomatics*, *9*(1), 61-74.

Muavhi, N. (2021). A simple approach for monitoring vegetation change using time series remote sensing analysis: A case study from the Thathe Vondo Area in Limpopo Province, South Africa. *South African Journal of Science*, *117*(7-8), 1-9.

Muavhi, N. and Mutoti, M.I. (2022) "Using geospatial techniques and analytic hierarchy process to map groundwater potential zones," *Groundwater* [Preprint].

Mukwada, G., Mazibuko, S. M., Moeletsi, M., and Robinson, G. M. (2021). Can famine be averted? A spatiotemporal assessment of the impact of climate change on food security in the Luvuvhu River Catchment of South Africa. *Land*, *10*(5), 527.

Munthali, M., Davis, N., Adeola, A., Botai, J., Kamwi, J., Chisale, H. and Orimoogunje, O., (2019). Local Perception of Drivers of Land-Use and Land-Cover Change Dynamics across Dedza District, Central Malawi Region. *Sustainability*, 11(3), 832.

Nagendra, H., Munroe, D. K., and Southworth, J. (2004). From pattern to process: Landscape fragmentation and the analysis of land use/ land cover change. *Agriculture, Ecosystems & Environment*, 101(2-3), 111-115.

Ngondo, J., Mango, J., Ruiqing, L., Nobert, J., Dubi, A. and Heqin, C. (2021). Land-Use and Land-Cover (LULC) Change Detection and the Implications for Coastal Water Resource Management in the Wami–Ruvu Basin, Tanzania. Sustainability, vol. 13, 4092.

Nkuna, T. and Odiyo, J. (2011). Filling of missing rainfall data in Luvuvhu River Catchment using artificial neural networks. *Physics and Chemistry of the Earth*, Parts A/B/C, 36(14-15), 830-835.

Nourani, V., Roughani, A. and Gebremichael, M. (2011). Topmodel capability for rainfall-runoff modeling of the Ammameh watershed at different time scales using different terrain algorithms. *Journal of Urban and Environmental Engineering*, 5(1), 1-14.

Ntanganedzeni, B. and Nobert, J. (2020). Flood risk assessment in Luvuvhu River, Limpopo province, South Africa. *Physics and Chemistry of the Earth*, Parts A/B/C, 102959.

Oberholster, P.J., Botha, A.M., and Cloete, T.E. (2008). Biological and chemical evaluation of sewage water pollution in the Rietvlei nature reserve wetland area, South Africa. *Environmental Pollution*, vol. 156, 184-192.

Odiyo, J., Makungo, R. and Nkuna, T. (2015). Long-term changes and variability in rainfall and streamflow in Luvuvhu River Catchment, South Africa. *South African Journal of Science*, 111(7/8).

Odiyo, J., Phangisa, J. and Makungo, R. (2012). Rainfall–runoff modelling for estimating Latonyanda River flow contributions to Luvuvhu River downstream of Albasini Dam. Physics and Chemistry of the Earth, Parts A/B/C, 50-52, 5-13.

Odongo, V., van Oel, P., van der Tol, C. and Su, Z. (2019). Impact of land use and land cover transitions and climate on evapotranspiration in the Lake Naivasha Basin, Kenya. *Science of The Total Environment*, 682, 19-30.

Owuor, S., Butterbach-Bahl, K., Guzha, A., Rufino, M., Pelster, D., Díaz-Pinés, E. and Breuer, L. (2016). Groundwater recharge rates and surface runoff response to land use and land cover changes in semi-arid environments. *Ecological Processes*, 5(1).

Ozdemir, H. and Elbaşı, E. (2015). Benchmarking land use change impacts on direct runoff in ungauged urban watersheds. *Physics and Chemistry of the Earth, Parts A/B/C*, 79-82, 100-107.

Ozturk, D. (2015). Urban growth simulation of Atakum (Samsun, Turkey) using cellular automata-Markov chain and multi-layer perceptron-Markov chain models. Remote Sensing, vol. 7, 5918-5950.

Padma, S. and Sanjeevi, S. (2014). Jeffries Matusita based mixed measure for improved spectral matching in hyperspectral image analysis. *International Journal of Applied Earth Observation and Geoinformation*, vol. 32, 138-151.

Pandi, D., Kothandaraman, S., and Kuppusamy, M. (2023). Simulation of Water Balance Components Using SWAT Model at Sub Catchment Level. *Sustainability*, *15*(2), 1438.

Peng, T., and Wang, S.-. (2012). Effects of land use, land cover and rainfall regimes on the surface runoff and soil loss on karst slopes in southwest China. *CATENA*, *90*, 53–62.

Petchprayoon, P., Blanken, P., Ekkawatpanit, C. and Hussein, K., (2010). Hydrological impacts of land use/land cover change in a large river basin in central-northern Thailand. *International Journal of Climatology*, 30(13), 1917-1930.

Pijanowski, B.C., Brown, D.G., Shellito, B.A., and Manik, G.A. (2002). Using neural networks and GIS to forecast land use changes: a Land transformation model. Computers, Environment and Urban System, vol. 26(6), 553-575.

Powell, R. L., Matzke, N., Souza, C.D., Clark, M., Numata, I., Hess, L.L. and Roberts, D.A. (2004). Sources of Error in Accuracy Assessment of Thematic Land-Cover Maps in the Brazilian Amazon. Remote Sensing of Environment, vol. 90 (2), 221-234.

Qi, Z., Kang, G., Chu, C., Qiu, Y., Xu, Z., and Wang, Y. (2017). Comparison of SWAT and GWLF model simulation performance in humid south and semi-arid north of China. *Water*, *9*(8), 567.

Rahbeh, M., Chanasyk, D., and Miller, J. (2011). Two-way calibration-validation of SWAT model for a small prairie watershed with short observed record. *Canadian Water Resources Journal/Revue Canadienne des Ressources Hydriques*, *36*(3), 247-270.

Ramankutty, N., and Foley, J. A. (1999). Estimating historical changes in global land cover: Croplands from 1700 to 1992. *Global Biogeochemical Cycles*, *13*(4), 997–1027.

Rendana, M., Rahim, S.A., Idris, W.M.R., Lihan, T., and Rahman, Z.A. (2015). CA-Markov for predicting land use changes in tropical catchment area: a case study in Cameron Highland, Malaysia. *Journal of Applied Sciences*, vol. 15(4), 689-695.

Research Systems Inc. (2008). ENVI Tutorials: Research Systems Inc, Boulder CO.

Richards, J.A. and Jia, X. (2005). Remote sensing digital image analysis, 4th edition: Berlin, Springer-Verlag.

Robinson, M., Cognard-Plancq, A., Cosandey, C., David, J., Durand, P., Führer, H., Hall, R., Hendriques, M., Marc, V., McCarthy, R., McDonnell, M., Martin, C., Nisbet, T., O'Dea, P., Rodgers, M. and Zollner, A. (2003). Studies of the impact of forests on peak flows and baseflows: a European perspective. *Forest Ecology and Management*, 186(1-3), 85-97.

Rumelhart, D., Hinton, G., and Williams, R. (1986). Learning internal representations by error propagation. In D.E. Rumelhart and J.L. McClelland (eds.), Parallel distributed processing: Explorations in the microstructures of cognition, vol. 1, 318 p. *Cambridge*: MIT Press.

Sajikumar, N. and Remya, R. (2015). Impact of land cover and land use change on runoff characteristics. *Journal of Environmental Management*, *161*, 460-468.

Santé, I., García, A.M., Miranda, D. and Crecente, R. (2010). Cellular automata models for the simulation of real-world urban processes: A review and analysis. Landscape and Urban Planning, vol. 96(2), 108-122.

Schaldach, R., and Priess, J. A. (2008). Integrated Models of the Land System: A Review of Modelling Approaches on the Regional to Global Scale. *Living Reviews in Landscape Research*, 2.

Serpa, D., Nunes, J., Santos, J., Sampaio, E., Jacinto, R., Veiga, S., Lima, J., Moreira, M., Corte-Real, J., Keizer, J. and Abrantes, N. (2015). Impacts of climate and land use changes on the hydrological and erosion processes of two contrasting Mediterranean catchments. *Science of The Total Environment*, *538*, 64-77.

Shrestha, B., Ahmad, S., and Stephen, H. (2020). Impact of Land Cover Change on Surface Runoff in the Walnut Gulch Experimental Watershed. In *Watershed Management Conference 2020* (pp. 205-218). Reston, VA: American Society of Civil Engineers.

Sidle, R., 2021. Strategies for smarter catchment hydrology models: incorporating scaling and better process representation. *Geoscience Letters*, 8(1).

Singh, A. (1989). Review Article Digital change detection techniques using remotely sensed data. *International Journal of Remote Sensing*, 10:6, 989-1003.

Singh, H. V. (2010). *Modeling impact of land use/cover changes on water quality and quantity of Fish River watershed* (Doctoral dissertation).

Singh, R. and Gupta, S. (2015). Change Detection and Hydrologic Responses Simulation for LULC Changes using Remote Sensing and GIS. In: *20th International Conference on Hydraulics, Water Resources and River Engineering*. India: India.

Smakhtin, V., (2001). Low flow hydrology: a review. *Journal of Hydrology*, 240(3-4), 147-186.

Sohl, T., & Sleeter, B. (2012). Role of remote sensing for land-use and land-cover change modeling. In *Remote Sensing of Land Use and Land Cover*, 225–239.

Sousa-Neto, E. R., Gomes, L., Nascimento, N., Pacheco, F., and Ometto, J. P. (2018). Land Use and Land Cover Transition in Brazil and Their Effects on Greenhouse Gas Emissions. *Soil Management and Climate Change*, 309-321.

State of Rivers Report (2001) Letaba and Luvuvhu river systems. WRC report no: TT 165/01 *Water Research Commission Pretoria* ISBN No: 1 86845 82s.

Sterling, S., Ducharne, A. and Polcher, J., (2012). The impact of global land-cover changes on the terrestrial water cycle. *Nature Climate Change*, *3*(4), 385-390.

Strayer, D., Beighley, R., Thompson, L., Brooks, S., Nilsson, C., Pinay, G. and Naiman, R., (2003). Effects of Land Cover on Stream Ecosystems: Roles of Empirical Models and Scaling Issues. *Ecosystems*, 6(5), 407-423.

Sun, D., Yang, H., Guan, D., Yang, M., Wu, J., Yuan, F., Jin, C., Wang, A. and Zhang, Y. (2018). The effects of land use change on soil infiltration capacity in China: A meta-analysis. *Science of The Total Environment*, 626, 1394-1401.

Swain, P. H. and Davis, S. M. (1978). Remote Sensing: The Quantitative Approach. New York: McGraw-Hill Publishers.

Swain, P.H. Robertson, T.V. and Wacker, A.G. (1971). Comparison of the Divergence and B-Distance in Feature Selection. LARS Report. Purdue University.

Tadele K. & Förch G. (2007). Impact of land use/land cover change on streamflow: a case study of Hare watershed, Ethiopia, 80–84. FWU (Research Institute for Water Resources and Environment). *FWU Water Resources Publications no.06*/2007. ISSN 1613–1045.

Takamatsu, M., Kawasaki, A., Rogers, P. P., and Malakie, J. L. (2013). Development of a land-use forecast tool for future water resources assessment: Case study for the Mekong River 3S Sub-basins. Sustainability Science, 9(2), 157-172.

Tang, Z., Engel, B. A., Pijanowski, B. C., and Lim, K. J. (2005). Forecasting land use change and its environmental impact at a watershed scale. *Journal of Environmental Management, 76(1),* 35–45.

Tena, Mwaanga and Nguvulu. (2019). Impact of Land Use/Land Cover Change on Hydrological Components in Chongwe River Catchment. *Sustainability*, 11(22), 6415.

Thanekar, G. S., and Krishna, R. V. (2021). Land Use Land Cover Prediction Analysis.

Thavhana, M., Savage, M. and Moeletsi, M., 2018. SWAT model uncertainty analysis, calibration and validation for runoff simulation in the Luvuvhu River catchment, South Africa. *Physics and Chemistry of the Earth*, Parts A/B/C, 105, 115-124.

Théau J. (2017). Change Detection. In: Shekhar S., Xiong H., Zhou X. (eds.) *Encyclopedia of GIS. Springer, Cham.*

Tizora, P., Le Roux, A., Mans, G. and Cooper, A. (2018). Adapting the Dyna-CLUE model for simulating land use and land cover change in the Western Cape Province. *South African Journal of Geomatics*, 7(2), 190.

Tomer, M. D., and Schilling, K. E. (2009). A simple approach to distinguish land-use and climate-change effects on watershed hydrology. *Journal of Hydrology*, 376(1-2), 24-33.

Townshend, J.R and Justice, C.O. (1988). Selecting the Spatial Resolution of satellite Sensors Required for Global Monitoring of Land Transformations. *International Journal of Remote Sensing*, 187-236.

Turner MG, Pearson SM, Bolstad P, Wear DN. (2003). Effects of land-cover change on spatial pattern of forest communities in the southern Appalachian Mountains (USA). *Landscape Ecol. 18*:449–64.

Ullah, S., Ahmad, K., Sajjad, R.U., Abbasi, A.M., Nazeer, A. and Tahir, A.A. (2019). Analysis and simulation of land cover changes and their impacts on land surface temperature in a lower Himalayan region. *Journal of Environmental Management*, vol. 245, 348-357.

Van Delden, H., van Vliet, J., Rutledge, D. T., and Kirkby, M. J. (2011). Comparison of scale and scaling issues in integrated land-use models for policy support. *Agriculture, Ecosystems & Environment, 142*(1-2), 18-28.

Vapnik, V.N. (1998). Statistical learning theory. Wiley, New York.

Veldkamp, A. and Lambin, E., (2001). Predicting land-use change. *Agriculture, Ecosystems & Environment*, 85(1-3), 1-6.

Verburg, P. H., Schot, P. P., Dijst, M. J., and Veldkamp, A. (2004). Land use change modelling: current practice and research priorities. *GeoJournal, 61*(4), 309-324.

Verburg, P. H., Steeg, J. V., Veldkamp, A., and Willemen, L. (2009). From land cover change to land function dynamics: A major challenge to improve land characterization. *Journal of Environmental Management*, 90(3), 1327-1335.

Vivekananda, G.N. Swathi, R. and Sujith, A. (2020): Multi-temporal image analysis for LULC classification and change detection, *European Journal of Remote Sensing*, vol. 8(2), 189-199.

Wang, F., Ge, Q., Yu, Q., Wang, H. and Xu, X., (2017). Impacts of land-use and land-cover changes on river runoff in Yellow River basin for period of 1956–2012. *Chinese Geographical Science*, 27(1), 13-24.

Wang, R., and Kalin, L. (2018). Combined and synergistic effects of climate change and urbanization on water quality in the Wolf Bay watershed, southern Alabama. *Journal of Environmental Sciences, 64*, 107–121.

Wang, Y., Li, X. and Li, J., (2014). Study on the Response of Ecological Capacity to Land-Use/Cover Change in Wuhan City: A Remote Sensing and GIS Based Approach. *The Scientific World Journal*, 2014, 1-11.

Warburton, M. L., Schulze, R. E., and Jewitt, G. P. W. (2012). Hydrological impacts of land use change in three diverse South African catchments. *Journal of Hydrology*, 414–415, 118–135.

Woldesenbet, T. A., Elagib, N. A., Ribbe, L., and Heinrich, J. (2017). Hydrological responses to land use/cover changes in the source region of the Upper Blue Nile Basin, Ethiopia. *Science of The Total Environment*, 575, 724–741.

Wolfram, S. (1984). Cellular automata: a model of complexity. *Nature*, vol. 31, 419-424.

Wolfram, S. (2002). A New Kind of Science. Wolfram Media, Canada.

Xu, C. (1999). From GCMs to river flow: a review of downscaling methods and hydrologic modelling approaches. *Progress in Physical Geography: Earth and Environment*, 23(2), 229-249.

Xu, Q., Wang, T., Cai, C., LI, Z., Shi, Z., and Fang, R. (2013). Responses of runoff and soil erosion to vegetation removal and tillage on steep lands. *Pedosphere, 23*(4), 532-541.

Xu, X., Yang, D., Yang, H. and Lei, H. (2014). Attribution analysis based on the Budyko hypothesis for detecting the dominant cause of runoff decline in Haihe basin. *Journal of Hydrology*, 510, 530-540.

Yadav, Y. (2019). Dynamics of Land use Land Cover Change and Mapping of Tree outside Forest (TOF) in Terai, Nepal. *International Journal of Environmental Sciences & Natural Resources*, *19*(1).

Yatoo, S.A., Sahu, P., Kalubarme, M.H. and Kansara, B.B. (2020). Monitoring land use changes and its future prospects using cellular automata simulation and artificial neural network for Ahmedabad city, India. GeoJournal, 23.

Yu, W., Liu, T., Valdez, R., Gwinn, M. and Khoury, M. (2010). Application of support vector machine modeling for prediction of common diseases: the case of diabetes and pre-diabetes. *BMC Medical Informatics and Decision Making*, vol. 10**(**16), 1-7.

Yuan, L., and Forshay, K. J. (2021). Enhanced streamflow prediction with SWAT using support vector regression for spatial calibration: A case study in the Illinois River watershed, US. *Plos one*, *16*(4), e0248489.

Yuan, T., Yiping, X., Lei, Z. and Danqing, L. (2015). Land use and cover change simulation and prediction in Hangzhou city based on CA-Markov model. International Proceedings of Chemical, Biological and Environmental Engineering, vol. 90(2015), 108-113.

Zhang, P., Liu, R., Bao, Y., Wang, J., Yu, W. and Shen, Z. (2014). Uncertainty of SWAT model at different DEM resolutions in a large mountainous watershed. *Water Research*, 53, pp.132-144.

Zhang, Y., and Schilling, K. (2006). Increasing streamflow and baseflow in Mississippi River since the 1940s: Effect of land use change. *Journal of Hydrology*, 324(1-4), 412-422.

Zhang, Z., Wang, S., Sun, G., McNulty, S., Zhang, H., Li, J., Zhang, M., Klaghofer, E., Stauss, P.,. (2008). Evaluation of the MIKE SHE Model for Application in the Loess Plateau, China. *Journal of the American Water Resources Association* (JAWRA) 44(5):1108-1120.

Appendix: LULC class separability

Input File: FLAASH_1990
ROI Name: (Jeffries-Matusita, Transformed Divergence)

Waterbody [Blue] 726 points:
Agricultural Land [Sea Green] 1239 points: (1.99999677 2.00000000)
Plantation [Green] 719 points: (1.99981564 2.00000000)
Natural Vegetation [Yellow] 3091 points: (2.00000000 2.00000000)
Bare Land [Coral] 841 points: (2.00000000 2.00000000)
Built-up [Magenta] 412 points: (1.99999229 2.00000000)

Agricultural Land [Sea Green] 1239 points:
Waterbody [Blue] 726 points: (1.99999677 2.00000000)
Plantation [Green] 719 points: (1.99472199 1.99999999)
Natural Vegetation [Yellow] 3091 points: (1.95166990 2.00000000)
Bare Land [Coral] 841 points: (1.99932560 2.00000000)
Built-up [Magenta] 412 points: (1.90591557 1.99791777)

Plantation [Green] 719 points:
Waterbody [Blue] 726 points: (1.99981564 2.00000000)
Agricultural Land [Sea Green] 1239 points: (1.99472199 1.99999999)
Natural Vegetation [Yellow] 3091 points: (2.00000000 2.00000000)
Bare Land [Coral] 841 points: (1.99999999 2.00000000)
Built-up [Magenta] 412 points: (1.99998784 2.00000000)

Natural Vegetation [Yellow] 3091 points:
Waterbody [Blue] 726 points: (2.00000000 2.00000000)
Agricultural Land [Sea Green] 1239 points: (1.95166990 2.00000000)
Plantation [Green] 719 points: (2.00000000 2.00000000)
Bare Land [Coral] 841 points: (1.99915669 1.99994651)
Built-up [Magenta] 412 points: (1.86161022 1.95638599)

Bare Land [Coral] 841 points:
Waterbody [Blue] 726 points: (2.00000000 2.00000000)
Agricultural Land [Sea Green] 1239 points: (1.99932560 2.00000000)
Plantation [Green] 719 points: (1.99999999 2.00000000)
Natural Vegetation [Yellow] 3091 points: (1.99915669 1.99994651)
Built-up [Magenta] 412 points: (1.99630844 1.99976135)

Built-up [Magenta] 412 points:
Waterbody [Blue] 726 points: (1.99999229 2.00000000)
Agricultural Land [Sea Green] 1239 points: (1.90591557 1.99791777)
Plantation [Green] 719 points: (1.99998784 2.00000000)
Natural Vegetation [Yellow] 3091 points: (1.86161022 1.95638599)
Bare Land [Coral] 841 points: (1.99630844 1.99976135)

Pair Separation (least to most);

Natural Vegetation [Yellow] 3091 points and Built-up [Magenta] 412 points - 1.86161022
Agricultural Land [Sea Green] 1239 points and Built-up [Magenta] 412 points - 1.90591557
Agricultural Land [Sea Green] 1239 points and Natural Vegetation [Yellow] 3091 points - 1.95166990
Agricultural Land [Sea Green] 1239 points and Plantation [Green] 719 points - 1.99472199
Bare Land [Coral] 841 points and Built-up [Magenta] 412 points - 1.99630844
Natural Vegetation [Yellow] 3091 points and Bare Land [Coral] 841 points - 1.99915669
Agricultural Land [Sea Green] 1239 points and Bare Land [Coral] 841 points - 1.99932560

Waterbody [Blue] 726 points and Plantation [Green] 719 points - 1.99981564
Plantation [Green] 719 points and Built-up [Magenta] 412 points - 1.99998784
Waterbody [Blue] 726 points and Built-up [Magenta] 412 points - 1.99999229
Waterbody [Blue] 726 points and Agricultural Land [Sea Green] 1239 points - 1.99999677
Plantation [Green] 719 points and Bare Land [Coral] 841 points - 1.99999999
Plantation [Green] 719 points and Natural Vegetation [Yellow] 3091 points - 2.00000000
Waterbody [Blue] 726 points and Bare Land [Coral] 841 points - 2.00000000
Waterbody [Blue] 726 points and Natural Vegetation [Yellow] 3091 points - 2.00000000

Input File: FLAASH_1995
ROI Name: (Jeffries-Matusita, Transformed Divergence)

Agricultural Land [Sea Green] 638 points:
Plantation [Green] 620 points: (1.99984773 1.99997727)
Natural Vegetation [Yellow] 1866 points: (1.91772168 1.99999925)
Bare Land [Coral] 1573 points: (1.99809054 2.00000000)
Waterbody [Blue] 381 points: (2.00000000 2.00000000)
Built-up [Red] 347 points: (1.99818208 1.99997658)

Plantation [Green] 620 points:
Agricultural Land [Sea Green] 638 points: (1.99984773 1.99997727)
Natural Vegetation [Yellow] 1866 points: (1.98759825 1.99989028)
Bare Land [Coral] 1573 points: (1.99999751 2.00000000)
Waterbody [Blue] 381 points: (1.99999983 2.00000000)
Built-up [Red] 347 points: (2.00000000 2.00000000)

Natural Vegetation [Yellow] 1866 points:
Agricultural Land [Sea Green] 638 points: (1.91772168 1.99999925)
Plantation [Green] 620 points: (1.98759825 1.99989028)
Bare Land [Coral] 1573 points: (1.98887585 2.00000000)
Waterbody [Blue] 381 points: (2.00000000 2.00000000)
Built-up [Red] 347 points: (1.99932366 1.99998190)

Bare Land [Coral] 1573 points:
Agricultural Land [Sea Green] 638 points: (1.99809054 2.00000000)
Plantation [Green] 620 points: (1.99999751 2.00000000)
Natural Vegetation [Yellow] 1866 points: (1.98887585 2.00000000)
Waterbody [Blue] 381 points: (2.00000000 2.00000000)
Built-up [Red] 347 points: (1.97276469 1.99999448)

Waterbody [Blue] 381 points:
Agricultural Land [Sea Green] 638 points: (2.00000000 2.00000000)
Plantation [Green] 620 points: (1.99999983 2.00000000)
Natural Vegetation [Yellow] 1866 points: (2.00000000 2.00000000)
Bare Land [Coral] 1573 points: (2.00000000 2.00000000)
Built-up [Red] 347 points: (2.00000000 2.00000000)

Built-up [Red] 347 points:
Agricultural Land [Sea Green] 638 points: (1.99818208 1.99997658)
Plantation [Green] 620 points: (2.00000000 2.00000000)
Natural Vegetation [Yellow] 1866 points: (1.99932366 1.99998190)
Bare Land [Coral] 1573 points: (1.97276469 1.99999448)
Waterbody [Blue] 381 points: (2.00000000 2.00000000)

Pair Separation (least to most);

Agricultural Land [Sea Green] 638 points and Natural Vegetation [Yellow] 1866 points - 1.91772168
Bare Land [Coral] 1573 points and Built-up [Red] 347 points - 1.97276469

Plantation [Green] 620 points and Natural Vegetation [Yellow] 1866 points - 1.98759825
Natural Vegetation [Yellow] 1866 points and Bare Land [Coral] 1573 points - 1.98887585
Agricultural Land [Sea Green] 638 points and Bare Land [Coral] 1573 points - 1.99809054
Agricultural Land [Sea Green] 638 points and Built-up [Red] 347 points - 1.99818208
Natural Vegetation [Yellow] 1866 points and Built-up [Red] 347 points - 1.99932366
Agricultural Land [Sea Green] 638 points and Plantation [Green] 620 points - 1.99984773
Plantation [Green] 620 points and Bare Land [Coral] 1573 points - 1.99999751
Plantation [Green] 620 points and Waterbody [Blue] 381 points - 1.99999983
Agricultural Land [Sea Green] 638 points and Waterbody [Blue] 381 points - 2.00000000
Bare Land [Coral] 573 points and Waterbody [Blue] 381 points - 2.00000000
Plantation [Green] 620 points and Built-up [Red] 347 points - 2.00000000
Natural Vegetation [Yellow] 1866 points and Waterbody [Blue] 381 points - 2.00000000
Waterbody [Blue] 381 points and Built-up [Red] 347 points - 2.00000000

Input File: Atmos-Corrected_2000
ROI Name: (Jeffries-Matusita, Transformed Divergence)

Waterbody [Blue] 715 points:
Bare land [Coral] 1036 points: (2.00000000 2.00000000)
Agricultural Land [Sea Green] 449 points: (2.00000000 2.00000000)
Natural Vegetation [Yellow] 2006 points: (1.99999905 2.00000000)
Built-up [Magenta] 251 points: (2.00000000 2.00000000)
Plantation [Green] 463 points: (1.99529297 2.00000000)

Bare land [Coral] 1036 points:
Waterbody [Blue] 715 points: (2.00000000 2.00000000)
Agricultural Land [Sea Green] 449 points: (1.99992879 2.00000000)
Natural Vegetation [Yellow] 2006 points: (1.96359660 1.99997266)
Built-up [Magenta] 251 points: (1.86090815 1.98883878)
Plantation [Green] 463 points: (1.99999972 2.00000000)

Agricultural Land [Sea Green] 449 points:
Waterbody [Blue] 715 points: (2.00000000 2.00000000)
Bare land [Coral] 1036 points: (1.99992879 2.00000000)
Natural Vegetation [Yellow] 2006 points: (1.97181050 1.99696238)
Plantation [Green] 463 points: (1.99999883 1.99999998)

Natural Vegetation [Yellow] 2006 points:
Waterbody [Blue] 715 points: (1.99999905 2.00000000)
Bare land [Coral] 1036 points: (1.96359660 1.99997266)
Agricultural Land [Sea Green] 449 points: (1.97181050 1.99696238)
Built-up [Magenta] 251 points: (1.94414859 1.99858326)
Natural Forest [Green] 463 points: (1.99023457 1.99999988)

Built-up [Magenta] 51 points:
Waterbody [Blue] 715 points: (2.00000000 2.00000000)
Bare land [Coral] 1036 points: (1.86090815 1.98883878)
Agricultural Land [Sea Green] 449 points: (1.98803346 1.99928732)
Natural Vegetation [Yellow] 2006 points: (1.94414859 1.99858326)
Natural Forest [Green] 463 points: (1.99977711 2.00000000)

Natural Forest [Green] 463 points:
Waterbody [Blue] 715 points: (1.99529297 2.00000000)
Bare land [Coral] 1036 points: (1.99999972 2.00000000)
Agricultural Land [Sea Green] 449 points: (1.99999883 1.99999998)
Natural Vegetation [Yellow] 2006 points: (1.99023457 1.99999988)
Built-up [Magenta] 251 points: (1.99977711 2.00000000)

Pair Separation (least to most);

Bare land [Coral] 1036 points and Built-up [Magenta] 251 points - 1.86090815
Natural Vegetation [Yellow] 2006 points and Built-up [Magenta] 251 points - 1.94414859
Bare land [Coral] 1036 points and Natural Vegetation [Yellow] 2006 points - 1.96359660
Agricultural Land [Sea Green] 449 points and Natural Vegetation [Yellow] 2006 points - 1.97181050
Agricultural Land [Sea Green] 449 points and Built-up [Magenta] 251 points - 1.98803346
Other Vegetation [Yellow] 2006 points and Plantation [Green] 463 points - 1.99023457
Waterbody [Blue] 715 points and Plantation [Green] 463 points - 1.99529297
Built-up [Magenta] 251 points and Plantation [Green] 463 points - 1.99977711
Bare land [Coral] 1036 points and Agricultural Land [Sea Green] 449 points - 1.99992879
Agricultural Land [Sea Green] 449 points and Plantation [Green] 463 points - 1.99999883
Waterbody [Blue] 715 points and Natural Vegetation [Yellow] 2006 points - 1.99999905
Bare land [Coral] 1036 points and Plantation [Green] 463 points - 1.99999972
Waterbody [Blue] 715 points and Bare land [Coral] 1036 points - 2.00000000
Waterbody [Blue] 715 points and Built-up [Magenta] 251 points - 2.00000000
Waterbody [Blue] 715 points and Agricultural Land [Sea Green] 449 points - 2.00000000

Input File: FLAASH_2005
ROI Name: (Jeffries-Matusita, Transformed Divergence)

Waterbody [Blue] 546 points:
Plantation [Green] 458 points: (1.99999732 2.00000000)
Bare Land [Coral] 3534 points: (2.00000000 2.00000000)
Built-up [Magenta] 222 points: (2.00000000 2.00000000)
Agricultural Land [Sea Green] 478 points: (2.00000000 2.00000000)
Natural Vegetation [Yellow] 1424 points: (1.99686103 2.00000000)

Plantation [Green] 458 points:
Waterbody [Blue] 546 points: (1.99999732 2.00000000)
Bare Land [Coral] 3534 points: (1.99999938 2.00000000)
Built-up [Magenta] 222 points: (2.00000000 2.00000000)
Agricultural Land [Sea Green] 478 points: (1.99998661 1.99999993)
Natural Vegetation [Yellow] 1424 points: (1.99671093 1.99999997)

Bare Land [Coral] 3534 points:
Waterbody [Blue] 546 points: (2.00000000 2.00000000)
Plantation [Green] 458 points: (1.99999938 2.00000000)
Built-up [Magenta] 222 points: (1.99603492 1.99943271)
Agricultural Land [Sea Green] 478 points: (1.99999726 2.00000000)
Natural Vegetation [Yellow] 1424 points: (1.97355967 1.99999239)

Built-up [Magenta] 222 points:
Waterbody [Blue] 546 points: (2.00000000 2.00000000)
Plantation [Green] 458 points: (2.00000000 2.00000000)
Bare Land [Coral] 3534 points: (1.99603492 1.99943271)
Agricultural Land [Sea Green] 478 points: (1.99999033 2.00000000)
Natural Vegetation [Yellow] 1424 points: (1.99866711 1.99970181)

Agricultural Land [Sea Green] 478 points:
Waterbody [Blue] 546 points: (2.00000000 2.00000000)
Plantation [Green] 458 points: (1.99998661 1.99999993)
Bare Land [Coral] 3534 points: (1.99999726 2.00000000)
Built-up [Magenta] 222 points: (1.99999033 2.00000000)
Natural Vegetation [Yellow] 1424 points: (1.98105321 1.99615849)

Natural vegetation [Yellow] 1424 points:
Waterbody [Blue] 546 points: (1.99686103 2.00000000)

Plantation [Green] 458 points: (1.99671093 1.99999997)
Bare Land [Coral] 3534 points: (1.97355967 1.99999239)
Built-up [Magenta] 222 points: (1.99866711 1.99970181)
Agricultural Land [Sea Green] 478 points: (1.98105321 1.99615849)

Pair Separation (least to most);

Bare Land [Coral] 3534 points and Natural vegetation [Yellow] 1424 points - 1.97355967
Agricultural Land [Sea Green] 478 points and Natural vegetation [Yellow] 1424 points - 1.98105321
Bare Land [Coral] 3534 points and Built-up [Magenta] 222 points - 1.99603492
Plantation [Green] 458 points and Natural Vegetation [Yellow] 1424 points - 1.99671093
Waterbody [Blue] 546 points and Natural vegetation [Yellow] 1424 points - 1.99686103
Built-up [Magenta] 222 points and Natural vegetation [Yellow] 1424 points - 1.99866711
Plantation [Green] 458 points and Agricultural Land [Sea Green] 478 points - 1.99998661
Built-up [Magenta] 122 points and Agricultural Land [Sea Green] 478 points - 1.99999033
Bare Land [Coral] 3534 points and Agricultural Land [Sea Green] 478 points - 1.99999726
Waterbody [Blue] 546 points and Plantation [Green] 458 points - 1.99999732
Plantation [Green] 458 points and Bare Land [Coral] 3534 points - 1.99999938
Waterbody [Blue] 546 points and Agricultural Land [Sea Green] 478 points - 2.00000000
Waterbody [Blue] 546 points and Bare Land [Coral] 3534 points - 2.00000000
Plantation [Green] 458 points and Built-up [Magenta] 122 points - 2.00000000
Waterbody [Blue] 546 points and Built-up [Magenta] 122 points - 2.00000000
Input File: FLAASH-2010
ROI Name: (Jeffries-Matusita, Transformed Divergence)

Waterbody [Blue] 997 points:
Plantation [Green] 825 points: (1.99997951 2.00000000)
Agricultural Land [Sea Green] 601 points: (2.00000000 2.00000000)
Natural Vegetation [Yellow] 2398 points: (1.99997281 2.00000000)
Bare Land [Coral] 819 points: (2.00000000 2.00000000)
Built-up [Magenta] 252 points: (2.00000000 2.00000000)

Plantation [Green] 825 points:
Waterbody [Blue] 997 points: (1.99997951 2.00000000)
Agricultural Land [Sea Green] 601 points: (1.99999972 1.99999992)
Natural Vegetation [Yellow] 2398 points: (1.91171602 1.99996078)
Bare Land [Coral] 819 points: (1.99999997 2.00000000)
Built-up [Magenta] 252 points: (1.99999733 2.00000000)

Agricultural Land [Sea Green] 601 points:
Waterbody [Blue] 997 points: (2.00000000 2.00000000)
Plantation [Green] 825 points: (1.99999972 1.99999992)
Natural Vegetation [Yellow] 2398 points: (1.97217550 1.98362168)
Bare Land [Coral] 819 points: (1.99999962 2.00000000)
Built-up [Magenta] 252 points: (1.98457443 1.99999158)

Other Vegetation [Yellow] 2398 points:
Waterbody [Blue] 997 points: (1.99997281 2.00000000)
Plantation [Green] 825 points: (1.91171602 1.99996078)
Agricultural Land [Sea Green] 601 points: (1.97217550 1.98362168)
Bare Land [Coral] 819 points: (1.99815076 1.99971676)
Built-up [Magenta] 252 points: (1.83344401 1.95225900)

Bare Land [Coral] 819 points:
Waterbody [Blue] 997 points: (2.00000000 2.00000000)
Plantation [Green] 825 points: (1.99999997 2.00000000)
Agricultural Land [Sea Green] 601 points: (1.99999962 2.00000000)
Natural Vegetation [Yellow] 2398 points: (1.99815076 1.99971676)

Built-up [Magenta] 252 points: (1.97204206 1.99663558)

Built-up [Magenta] 252 points:
Waterbody [Blue] 997 points: (2.00000000 2.00000000)
Plantation [Green] 825 points: (1.99999733 2.00000000)
Agricultural Land [Sea Green] 601 points: (1.98457443 1.99999158)
Natural vegetation [Yellow] 2398 points: (1.83344401 1.95225900)
Bare Land [Coral] 819 points: (1.97204206 1.99663558)

Pair Separation (least to most);

Natural Vegetation [Yellow] 2398 points and Built-up [Magenta] 252 points - 1.83344401
Plantation [Green] 825 points and Natural Vegetation [Yellow] 2398 points - 1.91171602
Bare Land [Coral] 819 points and Built-up [Magenta] 52 points - 1.97204206
Agricultural Land [Sea Green] 601 points and Natural vegetation [Yellow] 2398 points - 1.97217550
Agricultural Land [Sea Green] 601 points and Built-up [Magenta] 252 points - 1.98457443
Natural vegetation [Yellow] 2398 points and Bare Land [Coral] 819 points - 1.99815076
Waterbody [Blue] 997 points and Natural Vegetation [Yellow] 2398 points - 1.99997281
Waterbody [Blue] 997 points and Plantation [Green] 825 points - 1.99997951
Natural Forest [Green] 825 points and Built-up [Magenta] 252 points - 1.99999733
Agricultural Land [Sea Green] 601 points and Bare Land [Coral] 819 points - 1.99999962
Plantation [Green] 825 points and Agricultural Land [Sea Green] 601 points - 1.99999972
Plantation [Green] 825 points and Bare Land [Coral] 819 points - 1.99999997
Waterbody [Blue] 997 points and Agricultural Land [Sea Green] 601 points - 2.00000000
Waterbody [Blue] 997 points and Built-up [Magenta] 252 points - 2.00000000
Waterbody [Blue] 997 points and Bare Land [Coral] 819 points - 2.00000000

Input File: FLAASH_2015
ROI Name: (Jeffries-Matusita, Transformed Divergence)

Waterbody [Blue] 1629 points:
Plantation [Green] 934 points: (2.00000000 2.00000000)
Bare Land [Coral] 5200 points: (2.00000000 2.00000000)
Agricultural Land [Sea Green] 564 points: (2.00000000 2.00000000)
Natural Vegetation [Yellow] 4047 points: (2.00000000 2.00000000)
Built-up [Magenta] 338 points: (2.00000000 2.00000000)

Plantation [Green] 934 points:
Waterbody [Blue] 1629 points: (2.00000000 2.00000000)
Bare Land [Coral] 5200 points: (2.00000000 2.00000000)
Agricultural Land [Sea Green] 564 points: (1.99999851 2.00000000)
Natural Vegetation [Yellow] 4047 points: (1.99999866 2.00000000)
Built-up [Magenta] 338 points: (2.00000000 2.00000000)

Bare Land [Coral] 5200 points:
Waterbody [Blue] 1629 points: (2.00000000 2.00000000)
Plantation [Green] 934 points: (2.00000000 2.00000000)
Agricultural Land [Sea Green] 564 points: (1.99999776 2.00000000)
Natural Vegetation [Yellow] 4047 points: (1.87747338 1.99999090)
Built-up [Magenta] 338 points: (1.93139228 1.99924529)

Agricultural Land [Sea Green] 564 points:
Waterbody [Blue] 1629 points: (2.00000000 2.00000000)
Plantation [Green] 934 points: (1.99999851 2.00000000)
Bare Land [Coral] 5200 points: (1.99999776 2.00000000)
Natural Vegetation [Yellow] 4047 points: (1.97679768 1.99990465)
Built-up [Magenta] 338 points: (1.99991942 2.00000000)

Natural Vegetation [Yellow] 4047 points:
Waterbody [Blue] 1629 points: (2.00000000 2.00000000)
Plantation [Green] 934 points: (1.99999866 2.00000000)
Bare Land [Coral] 5200 points: (1.87747338 1.99999090)
Agricultural Land [Sea Green] 564 points: (1.97679768 1.99990465)
Built-up [Magenta] 338 points: (1.97752560 1.99999622)

Built-up [Magenta] 338 points:
Waterbody [Blue] 1629 points: (2.00000000 2.00000000)
Plantation [Green] 934 points: (2.00000000 2.00000000)
Bare Land [Coral] 5200 points: (1.93139228 1.99924529)
Agricultural Land [Sea Green] 564 points: (1.99991942 2.00000000)
Natural Vegetation [Yellow] 4047 points: (1.97752560 1.99999622)

Pair Separation (least to most);

Bare Land [Coral] 5200 points and Natural Vegetation [Yellow] 4047 points - 1.87747338
Bare Land [Coral] 5200 points and Built-up [Magenta] 338 points - 1.93139228
Agricultural Land [Sea Green] 564 points and Natural vegetation [Yellow] 4047 points - 1.97679768
Natural Vegetation [Yellow] 4047 points and Built-up [Magenta] 338 points - 1.97752560
Agricultural Land [Sea Green] 564 points and Built-up [Magenta] 338 points - 1.99991942
Bare Land [Coral] 5200 points and Agricultural Land [Sea Green] 564 points - 1.99999776
Plantation [Green] 934 points and Agricultural Land [Sea Green] 564 points - 1.99999851
Plantation [Green] 934 points and Natural vegetation [Yellow] 4047 points - 1.99999866
Plantation [Green] 934 points and Built-up [Magenta] 338 points - 2.00000000
Waterbody [Blue] 1629 points and Plantation [Green] 934 points - 2.00000000
Waterbody [Blue] 1629 points and Agricultural Land [Sea Green] 564 points - 2.00000000
Plantation [Green] 934 points and Bare Land [Coral] 5200 points - 2.00000000
Waterbody [Blue] 1629 points and Built-up [Magenta] 338 points - 2.00000000
Waterbody [Blue] 1629 points and Bare Land [Coral] 5200 points - 2.00000000
Waterbody [Blue] 1629 points and Natural Vegetation [Yellow] 4047 points - 2.00000000

Input File: FLAASH_2020
ROI Name: (Jeffries-Matusita, Transformed Divergence)

Waterbody [Blue] 1459 points:
Bare Land [Coral] 1520 points: (2.00000000 2.00000000)
Plantation [Green] 1110 points: (2.00000000 2.00000000)
Natural Vegetation [Yellow] 1755 points: (2.00000000 2.00000000)
Built-up [Red] 439 points: (2.00000000 2.00000000)
Agricultural Land [Sea Green] 521 points: (2.00000000 2.00000000)

Bare Land [Coral] 1520 points:
Waterbody [Blue] 1459 points: (2.00000000 2.00000000)
Plantation [Green] 1110 points: (1.99999998 2.00000000)
Natural Vegetation [Yellow] 1755 points: (1.99808895 2.00000000)
Built-up [Red] 439 points: (1.97088214 1.99333613)
Agricultural Land [Sea Green] 521 points: (1.99998036 2.00000000)

Plantation [Green] 1110 points:
Waterbody [Blue] 1459 points: (2.00000000 2.00000000)
Bare Land [Coral] 1520 points: (1.99999998 2.00000000)
Natural Vegetation [Yellow] 1755 points: (1.99997176 2.00000000)
Built-up [Red] 439 points: (1.99999999 2.00000000)
Agricultural Land [Sea Green] 521 points: (1.99997817 2.00000000)

Natural Vegetation [Yellow] 1755 points:
Waterbody [Blue] 1459 points: (2.00000000 2.00000000)

Bare Land [Coral] 1520 points: (1.99808895 2.00000000)
Plantation [Green] 1110 points: (1.99997176 2.00000000)
Built-up [Red] 439 points: (1.99221285 1.99998641)
Agricultural Land [Sea Green] 521 points: (1.98083433 1.99997086)

Built-up [Red] 439 points:
Waterbody [Blue] 1459 points: (2.00000000 2.00000000)
Bare Land [Coral] 1520 points: (1.97088214 1.99333613)
Plantation [Green] 1110 points: (1.99999999 2.00000000)
Natural Vegetation [Yellow] 1755 points: (1.99221285 1.99998641)
Agricultural Land [Sea Green] 521 points: (1.99797429 2.00000000)

Agricultural Land [Sea Green] 521 points:
Waterbody [Blue] 1459 points: (2.00000000 2.00000000)
Bare Land [Coral] 1520 points: (1.99998036 2.00000000)
Plantation [Green] 1110 points: (1.99997817 2.00000000)
Natural Vegetation [Yellow] 1755 points: (1.98083433 1.99997086)
Built-up [Red] 439 points: (1.99797429 2.00000000)

Pair Separation (least to most);

Bare Land [Coral] 1520 points and Built-up [Red] 439 points - 1.97088214
Natural Vegetation [Yellow] 1755 points and Agricultural Land [Sea Green] 521 points - 1.98083433
Natural Vegetation [Yellow] 1755 points and Built-up [Red] 439 points - 1.99221285
Built-up [Red] 439 points and Agricultural Land [Sea Green] 521 points - 1.99797429
Bare Land [Coral] 1520 points and Natural Vegetation [Yellow] 1755 points - 1.99808895
Plantation [Green] 1110 points and Natural Vegetation [Yellow] 1755 points - 1.99997176
Plantation [Green] 1110 points and Agricultural Land [Sea Green] 521 points - 1.99997817
Bare Land [Coral] 1520 points and Agricultural Land [Sea Green] 521 points - 1.99998036
Bare Land [Coral] 1520 points and Plantation [Green] 1110 points - 1.99999998
Plantation [Green] 1110 points and Built-up [Red] 439 points - 1.99999999
Waterbody [Blue] 1459 points and Natural Vegetation [Yellow] 1755 points - 2.00000000
Waterbody [Blue] 1459 points and Built-up [Red] 439 points - 2.00000000
Waterbody [Blue] 1459 points and Agricultural Land [Sea Green] 521 points - 2.00000000
Waterbody [Blue] 1459 points and Plantation [Green] 1110 points - 2.00000000
Waterbody [Blue] 1459 points and Bare Land [Coral] 1520 points - 2.00000000